A Sliding Mode-Based Amplitude- and Rate-Saturated Controller and Its Application to Wind Turbine Systems

ネハル, モハメド, カメス, モハメド, バイオミ

https://doi.org/10.15017/4060160

A Sliding Mode-Based Amplitude- and Rate-Saturated Controller and Its Application to Wind Turbine Systems

by
Nehal Mohamed Khames Mohamed Baiomy

Acknowledgements

This research work would have never been completed without a lot of help from many people. Before thanking them, I would to thank Allah who gave me the chance to be surrounded by such people. I have passed by many difficult moments during this work, and I would not have been able to overcome them it except with the support of Allah. It was my honor to be a member of the academic staff at Cairo University, and now, my honor raised after I had participated at Kyushu University for a while of my life.

First of all, I would like to thank my previous supervisor at Kyushu University, Professor Ryo Kikuuwe, for his guidance and advice during my research. I highly appreciate the time and effort that he devoted to help me in completing my Ph.D. study, even after his moving to Hiroshima University. He was and still my scientific advisor and an inspirational teacher who opened my mind for new viewpoints during the research.

At the same time, I sincerely thank Professor Motoji Yamamoto for accepting me to complete my research under his supervision during the last two years at Kyushu University. I highly appreciate his academic support for my research and I am grateful for his kind guidance and comments during my periodic presentations with him.

I would like to thank Professor Kenji Tahara, and Professor Yasutaka Nakashima for their valuable suggestions and comments through my periodic presentations of my work. I also would like to thank all my previous and current colleagues in Control Engineering Laboratory, especially Dr. Iwatani, Dr. Aung, and Mr. Gyuho, for their friendly talks and discussions. I also cannot forget to thank Ms. Mizuho Nagatomi and Ms. Ayako Kashiwagi for their help in many administrative issues during my study in Kyushu University.

I want to express my gratitude to the Egyptian government and to the Egyptian ministry of higher education for their financial support during my study in Japan.

Finally, I am deeply thankful to my family in Egypt, especially to my parents and my brother for their support and warm words, and I cannot describe the gratitude I have for my husband, Ahmed, and my daughter, Rokaya, for their encouragement and love throughout my Ph.D. study.

Contents

List of figures

List of tables

Nomenclature

List of symbols

$\alpha_{\{\cdot\}}$	Amplitude limitation
$\beta_{\{\cdot\}}$	Rate-of-change limitation
$\mathbb{R}$	Set of real numbers
$\mathbb{C}_-$	The open left-half of the complex plane
$\mathrm{Eig}(\cdot)$	The set of all eigenvalues of a matrix
$*$	The transpose of its symmetric block
$\otimes$	The Kronecker product
$\boldsymbol{A}_d(\gamma)$	A matrix equivalent to $(\boldsymbol{A} - \boldsymbol{b}\boldsymbol{c}^T/\gamma)$
$\boldsymbol{T}$	Transformation matrix
$\mathrm{tr}(\cdot)$	Trace of a matrix
$\det[\cdot]$	Determinant of a matrix
$G[\boldsymbol{A}]$	The bialternate sum of $\boldsymbol{A}$ with itself
$\boldsymbol{M}$	Mass matrix
$\boldsymbol{F}$	Vector of nonlinear terms
$\boldsymbol{Q}$	Vector of displacements
$\boldsymbol{U}$	Vector of the input of the wind turbine plant
$\boldsymbol{\Xi}$	Vector of the input disturbances
θ	The displacement of the rotor shaft (rad)
ϕ	The drivetrain torsional displacement(rad)
$\widehat{u}$	The actual collective pitch control signal (rad)
ξ	The horizontal wind speed (m/s)
ω	The angular velocity of the rotor shaft (rad/s)
ν	The drivetrain torsional rate of change (rad/s)
$\boldsymbol{f}(\cdot)$	A function of proper dimensions
ξ_m	The measured wind speed
$\tilde{\xi}$	The measurement error between ξ and ξ_m
ω_g	The angular velocity of the generator shaft (rpm)
ω_{gr}	The rated speed of the generator shaft (rpm)

List of abbreviations

FAST	Fatigue, Aerodynamics, Structures, and Turbulence
LMI	Linear matrix inequality
CPC	Collective pitch control
GSPI	Gain-scheduling proportional integral
DAC	Disturbance accommodation control
LTI	Linear time invariant
DOF	Degree of freedom
MIMO	Multi-input multi-output

Chapter 1

Introduction

Due to safety reasons and hardware restrictions, systems' actuators such as pumps, valves, and compressors have movement limitations and threshold capacity. For example, the liquid level in a tank is not the only bounded quantity, but also the liquid level cannot change arbitrarily fast. These limitations protect the controlled plants from drastic commands and physical wear, such as in aerodynamics systems [3–10]. If these limitations are not handled and respected through the control method, it may cause unexpected behavior or performance degradation ended by crashes. Flight accidents have been recorded [11] in which the extreme pitching-action caused circling and instability that ended by incident. On another side, a study of a wind turbine system [12] shows that a reduction in the oscillations' amplitude of the generated torque significantly improves the lifetime of the mechanical parts, and consequently, it improves the maintenance cost of such systems.

The behavior of closed-loop systems under limitations on both of the actuator signal's amplitude and the actuator signal's rate-of-change is the main interest of this dissertation. A constraint on the actuator signal's amplitude, unfortunately, converts a linear controlled plant into a nonlinear one, and imposing constraints on the actuator signal's rate-of-change further complicates the stability problem, as has been studied in [1, 13–18]. A significant problem raised in those studies is the trade-off between the stability region and the closed-loop performance [1, 14], where a low-gain control action is a good solution to prevent the actuator from being saturated. However, it does not allow the controlled plant to work at high performance, especially in the presence of uncertainties or external disturbances.

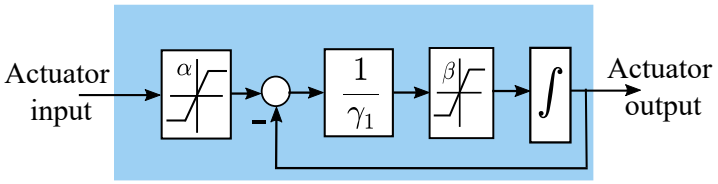

Figure 1.1: Actuator model with amplitude- and rate-limitations.

1.1 Control techniques producing signals with limited amplitudes and limited rate-of-change

Considering that a first-order system is one possible representation of the actuator system, one of the most common ways to implement amplitude- and rate-limitations to such systems is the nested saturated implementation [1, 3, 13–16, 18–20], as shown in Fig 1.1. The following various contexts are existing techniques to deal with such limitations.

1.1.1 Optimal control

Optimal control [21–23] is a control technique in which the control law is selected to satisfy some conditions or to optimize between some control objectives. These objectives and conditions could be expressed by inequality constraints, which are solved together to obtain the controller's parameters. Regarding the aforementioned amplitude- and rate-limitations, the optimal control is applied in some studies [18, 24–26] to deal with these limitations. It is not straight forward to directly consider these limitations via inequality constraints, thus the generalized sector condition [27, 28] has been employed in some work to describe the nonlinearities imposed by the saturation functions and to reduce the conservatism of estimating the stability region.

1.1.2 Anti-windup technique

Anti-windup [17, 20, 29, 30] is another technique used with systems subjected to actuator limitations. The main role of the anti-windup technique is to compensate an existing controller, which has been designed to work in the absence of saturation. The anti-windup loops only become active if saturation occurs, while the existing controller is mainly designed to improve the system performance when there is no saturation. The anti-windup technique could be a common solution for the problem of only the existing limitation on the actuator signal's amplitude [31], while it is rarely presented to

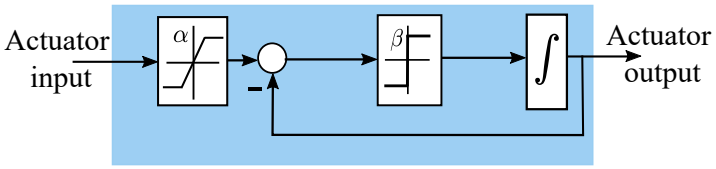

Figure 1.2: Actuator model with amplitude- and rate-limitations consisting of an "ideal rate limiter", i.e., $\gamma_1 = 0$.

solve the problem of existing limitations on both of the amplitude and rate-of-change. Regarding the problem of both limitations, a controller structure with anti-windup loops is introduced in [17], where a linear output compensator is introduced to suppress the disturbance effects. One drawback of the anti-windup technique is that the gains of the anti-windup loops are additional parameters that need to be tuned appropriately.

1.1.3 Model predictive control

Model predictive control is a control technique that produces a control action with certain constraints. Model predictive control technique [32–34] predicts the future outputs over a specific prediction horizon, where a cost function is optimized on-line at each sampling interval-time via a quadratic-programming algorithm [35,36]. Although a long horizon results in better optimal performance, the first value in the predicted control horizon is only applied, and then, the on-line optimization is repeated for the next time interval. Due to the time needed in the on-line optimization, the model predictive control is usually implemented for a relatively slow process, while there are difficulties to be applied to a fast process [37].

1.2 Sliding mode control and its feature to produce a control signal with limited amplitude and limited rate-of-change

Sliding mode control [38,39] is a nonlinear control technique known by its insensitivity to the disturbances and its robustness against systems' uncertainties. This technique uses a set-valued control action to force the controlled system into a sliding surface of known behavior. The boundedness of the set-valued function and the sliding nature of the sliding mode control are the motivation in this dissertation to employ the sliding

mode technique with the considered system in this dissertation, where the produced control signal is already bounded and this boundary can be chosen within the limitations of the actuator system. Sliding-mode control schemes have been proposed [40] to deal with only the problem of exiting amplitude limitation [41–45], in which a low-gain approach is used to reduce the control action of the linear component, while the discontinuous component is decided by the maximum amplitude of system's uncertainty. Meanwhile, dealing with the amplitude and the rate limitations together under the approach of sliding mode control has not been studied yet, as far as the author aware. It is expected that the sliding mode technique would be helpful to analyze and reduce the nonlinearities of the actuator limitations and it would allow the system's state to slide into a linear surface, which is easy to be designed.

Now, let us approach the cases where the time constant (i.e., γ_1 in Fig 1.1) of such actuators is negligible. The saturation block that limits the rate-of-change can be replaced by a set-valued function, which may be referred to as an ideal rate limiter [13, 14, 46]. The set-valued function $\mathrm{sgn}(\cdot)$ can be seen as an almost-everywhere pointwise limit of the saturation function $\mathrm{sat}(\cdot)$ as follows:

$$\mathrm{sgn}(x) = \lim_{\varepsilon \searrow 0} \mathrm{sat}_1(x/\varepsilon) \quad \forall x \neq 0 \tag{1.1}$$

where the saturation function and the set-valued function are defined respectively as follows:

$$\mathrm{sat}_\alpha(x) \triangleq \begin{cases} \alpha x/|x| & \text{if } |x| > \alpha \\ x & \text{if } |x| \leq \alpha, \end{cases} \tag{1.2}$$

$$\mathrm{sgn}(x) \triangleq \begin{cases} [-1, 1] & \text{if } |x| = 0 \\ x/|x| & \text{if } |x| > 0. \end{cases} \tag{1.3}$$

This can be easily proven by considering the definitions of $\mathrm{sgn}(x)$ and $\mathrm{sat}(x)$ for $x \neq 0$ as follows:

$$\begin{aligned} \lim_{\varepsilon \searrow 0} \mathrm{sat}_1(x/\varepsilon) &= \lim_{\varepsilon \searrow 0} \frac{x/\varepsilon}{\max(1, |x|/\varepsilon)} = \lim_{\varepsilon \searrow 0} \frac{x}{\max(\varepsilon, |x|)} \\ &= x/|x| = \mathrm{sgn}(x), \quad \forall x \neq 0. \end{aligned} \tag{1.4}$$

Regarding the implementation of Fig 1.2, which comprises an ideal rate-limiter, this dissertation is going to adopt a new sliding-mode technique to deal with the limitations mentioned above. The set-valued function of the sliding mode controller limits the control signal's rate-of-change, while the control signal's amplitude is limited by a saturation function, implemented inside the set-valued function. A controller with nested structure of set-valued functions shows its ultimate finite-time convergence to the origin, as discussed by Miranda-Villatoro et al. [47]. In this dissertation, the amplitude signal cannot be limited by a set-valued function instead of a saturation

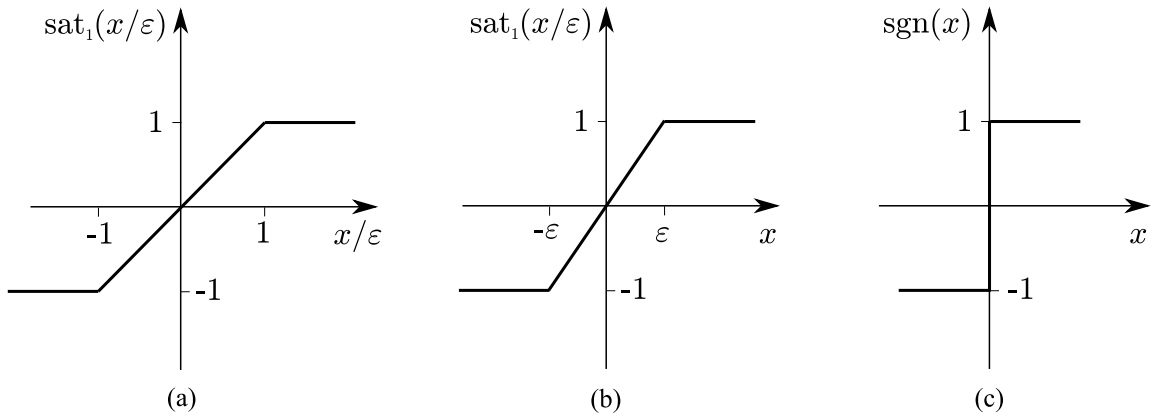

Figure 1.3: Graph (a) is the saturation function $\text{sat}_1(x/\varepsilon)$, graph (b) is an equivalent function of that in graph (a), and graph (c) is the signum function $\text{sgn}(x)$.

function, because the infinite-slope of the set-valued function does not match with the bounded rate-of-change as Remark 2.4.2 shows later on.

Through the analysis of such configuration of nested sgn-sat functions, Chapter 2 suggests that the control law could include a variable parameter to overcome the trade-off between the stability and the rejection of disturbances. This parameter is recommended to be changeable according to the state and magnitude of the disturbances. This parameter is designed to be inversely proportional to the control action. It holds at high values when the state is far from the origin, and consequently, it facilitates a large region of attraction. Meanwhile, this nonlinear parameter holds at low values after the state comes near the origin to consequently produce a high-gain control action, which is a classical method used to reduce the effects of disturbances. Although there is still lack in the theoretical analysis of the proposed controller with respect to time-varying parameters, the results of the simulations in this dissertation show its effectiveness to resolve and relax the trade-off problem between enlarging the region of attraction, respecting the limitations of the actuator, and attenuating the affects of disturbances.

1.3 Major Achievements

The objective of this dissertation is to propose a new control scheme with simple implementation to be applied to systems that need a control signal with limited amplitude and limited rate-of-change. Corresponding to that objective, the major achievements can be summarized as follows:

1.3.1 New amplitude- and rate-saturated controller (Chapter 2)

Based on the idea of the ideal rate limiter, Chapter 2 proposes a new nonlinear controller applicable to single-input linear systems under bounded disturbance. The controller provides control signals satisfying specified amplitude and rate-of-change limitations. This feature is realized by its sliding mode-like structure comprising a set-valued function. The controller also employs a state-dependent parameter to broaden the region of attraction and to shrink the terminal attractor. In addition, a discrete-time implementation of the proposed controller has been developed based on a model-based implicit discretization scheme. Numerical examples show the validity of the proposed controller.

1.3.2 Parameter selection procedure for the proposed controller (Chapter 3)

Chapter 3 presents a selection procedure to obtain parameter values of the proposed amplitude- and rate-saturated controller. The proposed selection procedure involves a set of linear matrix inequalities [48] and also includes iterative computation. The effectiveness of the proposed selection procedure is shown through a comparison with the parameter-tuning guideline of Chapter 2.

1.3.3 Extending the proposed controller to wind turbine systems (Chapter 4)

Chapter 4 proposes a new collective pitch controller appropriate for wind turbine systems to maintain the generator speed constant in the region above the rated wind speed. This controller is built on the controller of chapter 2 to satisfy the amplitude and rate limitations imposed by the hardware of the pitch actuator system. The control gain inversely correlates with the magnitude of the state and disturbances, so that low-gain control action is produced when there is a significant variation in the wind speed. The low-gain action here is to avoid performance degradation, which may happen due to the limitations of the pitch actuator. Moreover, the controller produces a high-gain action when the system state is near the origin to reject the wind speed variations and to regulate the generator speed. The proposed controller is validated by applying it to a three-bladed horizontal-axis wind turbine emulated by a software simulator (FAST). The proposed controller is compared with a gain-scheduling proportional-integral controller and a linear feedback controller.

1.4 Organization

The rest of this dissertation is organized as follows. Chapter 2 proposes a new nonlinear controller applicable to single-input linear systems under bounded disturbance. Chapter 3 proposes a selection procedure to obtain parameter values of the proposed amplitude- and rate-saturated controller. Chapter 4 proposes a real application that can utilize the proposed controller to work efficiently in the presence of hardware limitations. Finally, Chapter 5 provides concluding remarks and some ideas for future work.

Chapter 2

An amplitude- and rate-saturated controller for linear plants

2.1 Introduction

The main interests of previous studies on systems under amplitude- and rate-saturated controllers are to avoid the instability and to realize smooth behaviors. There have been two control approaches to deal with such systems. The first approach [1,13,14] is to model the actuator dynamics as a nested saturation system, in which the amplitude and the rate-of-change of the control signal are saturated. Most of the studies that applied this approach employed Linear Matrix Inequality-based conditions to select the suitable linear feedback gains that maintain stability. The second approach [15–18] is to construct a nonlinear controller providing control signals that already satisfy the amplitude and rate limitations, which are imposed by the actuators.

Regarding the first approach, Gomes da Silva et al. [14] proposed a state feedback controller for such linear systems with actuator limitations. They clarified the trade-off between the closed-loop performance and the size of the region of attraction, and they proposed an algorithm based optimization problem to obtain the controller parameters. Palmeira et al. [1] also introduced a state feedback controller, in which the control signal is sampled by a non-periodic sampling interval. In order to obtain the controller parameters, they introduced two optimization problems based on two scenarios; one aims to maximize the region of attraction, and the other aims to maximize the sampling interval permissible for stability. It should be noted that the existence of external disturbance was not taken into account in [1, 14].

[0]The content of this chapter is partially published in [49], namely, N. Baiomy, R. Kikuuwe. An amplitude- and rate-saturated controller for linear systems. Asian Journal of Control, vol. 21, no. 6, 2019.

Regarding the second approach, Stoorvogel and Saberi [15] presented a nonlinear state feedback controller that produces a control signal with limited amplitude and limited rate-of-change. They employed observer-based measurement feedback to reject the disturbance effects. Gomes da Silva et al. [16] introduced a nonlinear control scheme involving two anti-windup loops, which require additional parameters to be tuned appropriately. This controller has been improved by Bender and Gomes da Silva [17] to take the existence of disturbance into account, where the disturbance tolerance and the system output magnitude are treated in a framework of an optimization problem under LMI constraints.

In this chapter, the second approach is followed, where a new controller is proposed to provide a limited control signal in both its amplitude and its rate-of-change. This controller has a structure in which the saturation function and the signum function are used in a nested way. This structure is similar to the one called an ideal rate limiter [13, 14, 46], and it does not include anti-windup loops. One of the main features of the new controller is that it involves a nonlinear function to suppress the effect of disturbance without affecting its convergence behavior. More specifically, this nonlinear function imposes low gain when the state is far from the origin and imposes high gain when the state is near the origin. Another feature of the proposed controller lies in its discrete-time implementation, which is derived based on the implicit Euler method to avoid chattering raised by the discontinuous (or more strictly, set-valued) function.

The remainder of this chapter is organized as follows. Section 2.2 presents the problem formulation in the continuous-time and shows two previous approaches for linear systems subjected to amplitude- and a rate-saturated control signal. In Section 2.3, the idea of using the signum function is analyzed to produce rate-saturated control signals. Section 2.4 introduces a new control scheme with a designed nonlinear function to improve its convergence behavior and its insensitivity against the disturbance near the origin. A new discrete-time algorithm is also proposed in Section 2.4. Section 2.5 shows illustrative numerical examples of the proposed controller. Finally, a summary is provided in Section 2.6.

2.2 Linear plants subjected to actuator limitations

Here, a linear controlled plant is considered with the following form:

$$\dot{\boldsymbol{x}} = \boldsymbol{A}\boldsymbol{x} + \boldsymbol{b}(u + \zeta) \tag{2.1}$$

where $\boldsymbol{x} \in \mathbb{R}^n$ is the state vector, $u \in \mathbb{R}$ is the control input, and $\zeta \in \mathbb{R}$ is the unknown perturbation. It is assumed that there exists $L_m > 0$ with which the perturbation ζ satisfies $|\zeta| \leq L_m$ for all $t > 0$. It is also assumed that the input signal u needs to

satisfy

$$|u| \leq \alpha \quad \text{and} \quad |\dot{u}| \leq \beta \tag{2.2}$$

where α and β are positive scalars, and $L_m < \alpha$. For the convenience of further derivation, another positive constant L is used so that it satisfies $L_m < L < \alpha$. The matrices $\boldsymbol{A} \in \mathbb{R}^{n\times n}$ and $\boldsymbol{b} \in \mathbb{R}^n$ are constant, and the pair $(\boldsymbol{A}, \boldsymbol{b})$ is controllable.

To model the control input restrictions of (2.2), many studies [1, 3, 13–16, 18–20], employ the following differential equation:

$$\dot{u} = -\mathrm{sat}_\beta \left(\frac{1}{\gamma_1} \left(u + \mathrm{sat}_\alpha(\sigma(\boldsymbol{x})/\gamma) \right) \right). \tag{2.3}$$

Here, $\sigma(\boldsymbol{x})$ is a scalar function of the state vector $\boldsymbol{x}$, and the scalars $\{\gamma, \gamma_1\}$ are positive constants. This differential equation has been used for the model of the hardware limitation of actuators [1, 13] and for controllers that have amplitude and rate-of-change limitations [18].

When (2.3) is viewed as an actuator model, as shown in Fig. 2.1.(a), the constant γ_1 can be seen as a model parameter that is determined by the hardware and as the time constant of the first-order lag. In this case, $\sigma(\boldsymbol{x})/\gamma$ and u are the input and the output of the actuator model, respectively. Bateman and Lin [13] employed this actuator model and derived conditions for the controller parameters to achieve the stability in the presence and in the absence of disturbances. Other research work [1,46] focused on the enlargement of the domain of attraction.

When (2.3) is viewed as a controller, as shown in Fig. 2.1.(b), the actuator is considered as a part of the linear plant that accepts the control input satisfying (2.2). The extreme case where $\gamma_1 \searrow 0$ is considered by Stoovrogel and Saberi [15], where (2.3) reduces to

$$\dot{u} \in -\beta \mathrm{sgn} \left(u + \mathrm{sat}_\alpha(\sigma(\boldsymbol{x})/\gamma) \right), \tag{2.4}$$

as shown in Fig. 2.1(c). Note that the controller of this extreme case is effective only if the time constant γ_1 of the actuator is sufficiently close to zero. As is formally pointed out in [13,14,46], (2.4) can be seen as an ideal amplitude and rate limitation operator.

2.3 Analysis of the sgn-sat controller

By combining the controlled plant (2.1) with the control law (2.4), the following system is obtained:

$$\dot{\boldsymbol{\chi}} \in \begin{bmatrix} \boldsymbol{A}\boldsymbol{x} + \boldsymbol{b}(u + \zeta) \\ -\beta \mathrm{sgn} \left(u + \mathrm{sat}_\alpha \left(\boldsymbol{c}^T \boldsymbol{x}/\gamma \right) \right) \end{bmatrix} \tag{2.5}$$

$$|\zeta| \leq L_m < L < \alpha \tag{2.6}$$

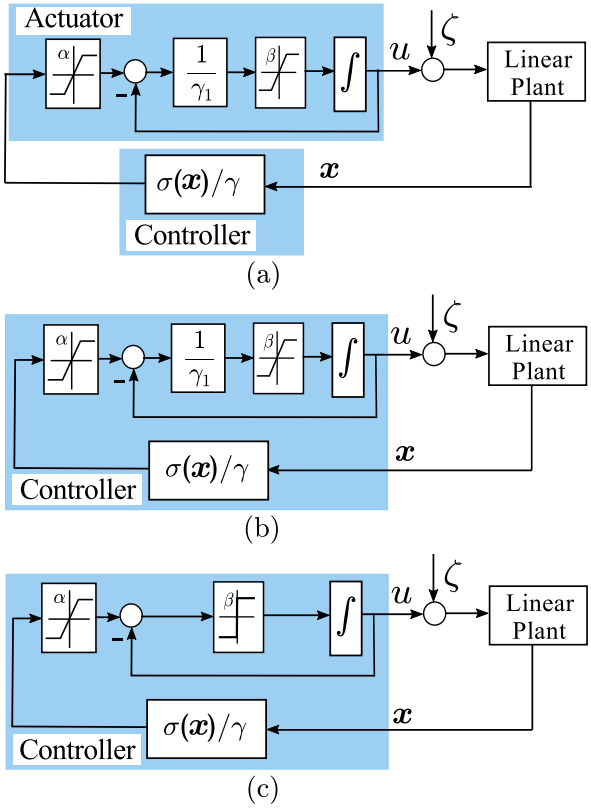

Figure 2.1: Some control structures involving amplitude and rate-of-change limitations. (a) System with amplitude- and rate-limited actuator. (b) System with amplitude- and rate-limited controller. (c) System with controller consisting of an "ideal rate limiter," which is an extreme case of (b), i.e., $\gamma_1 = 0$.

where $\{\alpha, \beta, \gamma\} \subset \mathbb{R}^+$, $\boldsymbol{A} \in \mathbb{R}^{n\times n}$, $\boldsymbol{b} \in \mathbb{R}^n$, $\boldsymbol{c} \in \mathbb{R}^n$ and

$$\boldsymbol{\chi} \triangleq [\boldsymbol{x}^T, u]^T \in \mathbb{R}^{n+1} \tag{2.7}$$

$$\boldsymbol{c}^T\boldsymbol{b} > 0. \tag{2.8}$$

Let us define

$$\sigma \triangleq \boldsymbol{c}^T\boldsymbol{x},\ \eta \triangleq \boldsymbol{c}^T\boldsymbol{A}\boldsymbol{x}/(\boldsymbol{c}^T\boldsymbol{b}),\ \kappa \triangleq \boldsymbol{c}^T\boldsymbol{b},\ \hat{\beta} \triangleq \beta/(\boldsymbol{c}^T\boldsymbol{b}). \tag{2.9}$$

Then, we can consider a subsystem of the system (2.5)(2.6) as follows:

$$\dot{\boldsymbol{\xi}} \in \begin{bmatrix} \kappa(\eta + u + \zeta) \\ \phi(\boldsymbol{x}, u, \zeta) \\ -\kappa\hat{\beta}\mathrm{sgn}\left(s(\boldsymbol{\xi})\right) \end{bmatrix} \tag{2.10}$$

$$|\zeta| \leq L_m < L < \alpha \tag{2.11}$$

where

$$\boldsymbol{\xi} \triangleq [\sigma, \eta, u]^T \in \mathbb{R}^3 \tag{2.12}$$

$$s(\boldsymbol{\xi}) \triangleq u + \mathrm{sat}_\alpha\left(\sigma/\gamma\right) \tag{2.13}$$

and $\phi(\boldsymbol{x}, u, \zeta)$ is a linear function of $\{\boldsymbol{x}, u, \zeta\}$. The subsystem (2.10)(2.11) is obtained by projecting the system (2.5)(2.6) to the subspace $\mathbb{R}^3$ with the following operation:

$$\boldsymbol{\xi} = \begin{bmatrix} \boldsymbol{M} & \boldsymbol{o}_2 \\ \boldsymbol{o}_n^T & 1 \end{bmatrix} \boldsymbol{\chi} = \begin{bmatrix} \boldsymbol{M}\boldsymbol{x} \\ u \end{bmatrix} \in \mathbb{R}^3 \tag{2.14}$$

where

$$\boldsymbol{M} \triangleq \begin{bmatrix} \boldsymbol{c}^T \\ \boldsymbol{c}^T\boldsymbol{A}/(\boldsymbol{c}^T\boldsymbol{b}) \end{bmatrix} \in \mathbb{R}^{2\times n}. \tag{2.15}$$

For the convenience of further discussion, let us define the following subsets of the sub-state space $\mathbb{R}^3$:

$$\boldsymbol{\mathcal{D}} \triangleq \left\{ \boldsymbol{\xi} \in \mathbb{R}^3 \middle| \ |\eta| < \alpha - L \right\} \tag{2.16}$$

$$\boldsymbol{\mathcal{F}} \triangleq \left\{ \boldsymbol{\xi} \in \mathbb{R}^3 \middle| \ |\eta + u| < \hat{\beta}\gamma - L \right\} \tag{2.17}$$

$$\boldsymbol{\mathcal{S}} \triangleq \left\{ \boldsymbol{\xi} \in \mathbb{R}^3 \middle| \ s(\boldsymbol{\xi}) = 0 \right\} \tag{2.18}$$

$$\boldsymbol{\mathcal{S}}_L \triangleq \left\{ \boldsymbol{\xi} \in \boldsymbol{\mathcal{S}} \middle| \ |\sigma| < \alpha\gamma \right\} \tag{2.19}$$

$$\boldsymbol{\mathcal{S}}_C \triangleq \left\{ \boldsymbol{\xi} \in \boldsymbol{\mathcal{S}} \middle| \ |\sigma| > \alpha\gamma \right\}, \tag{2.20}$$

which are illustrated in Fig. 2.2. The following operators; $\widehat{\boldsymbol{\mathcal{E}}} : 2^{\mathbb{R}^3} \to 2^{\mathbb{R}^{n+1}}$ and $\boldsymbol{\mathcal{P}} : 2^{\mathbb{R}^{n+1}} \to 2^{\mathbb{R}^3}$ are defined as follows:

$$\widehat{\boldsymbol{\mathcal{E}}}(\boldsymbol{\mathcal{X}}) \triangleq \left\{ \begin{bmatrix} \boldsymbol{x} \\ u \end{bmatrix} \in \mathbb{R}^{n+1} \middle| \begin{bmatrix} \boldsymbol{M}\boldsymbol{x} \\ u \end{bmatrix} \in \boldsymbol{\mathcal{X}} \right\} \tag{2.21}$$

$$\boldsymbol{\mathcal{P}}(\widehat{\boldsymbol{\mathcal{X}}}) \triangleq \left\{ \begin{bmatrix} \boldsymbol{M}\boldsymbol{x} \\ u \end{bmatrix} \in \mathbb{R}^3 \middle| \begin{bmatrix} \boldsymbol{x} \\ u \end{bmatrix} \in \widehat{\boldsymbol{\mathcal{X}}} \right\}, \tag{2.22}$$

which are to make correspondence between a subset of the total state space $\mathbb{R}^{n+1}$ and a subset of the sub-state space $\mathbb{R}^3$. Throughout this chapter, a calligraphic symbol

with or without a hat denotes a subset of $\mathbb{R}^{n+1}$ or $\mathbb{R}^3$, respectively. In this chapter, the symbols $\mathrm{cl}(\boldsymbol{\mathcal{X}})$ and $\overline{\boldsymbol{\mathcal{X}}}$ denote the closure and the complementary set, respectively, of a set $\boldsymbol{\mathcal{X}}$. The interior and the boundary of a set $\boldsymbol{\mathcal{X}}$ are denoted by $\mathrm{Int}(\boldsymbol{\mathcal{X}})$ and $\partial\boldsymbol{\mathcal{X}}$, respectively. The set of all subsets of a set $\boldsymbol{\mathcal{X}}$ is denoted by $2^{\boldsymbol{\mathcal{X}}}$. For brevity, $\mathrm{Eig}(\boldsymbol{X})$ denotes the set of all eigenvalues of a matrix $\boldsymbol{X}$.

Now, let us show that the sliding mode takes place at a portion of $\boldsymbol{\mathcal{S}}$.

Theorem 2.3.1. *Let us consider the system (2.5)(2.6). Then, the sliding mode takes place at the portion $\widehat{\boldsymbol{\mathcal{E}}}(\boldsymbol{\mathcal{S}}_C \cup (\boldsymbol{\mathcal{S}}_L \cap \boldsymbol{\mathcal{F}}))$ of the surface $\widehat{\boldsymbol{\mathcal{E}}}(\boldsymbol{\mathcal{S}})$, on which $s(\boldsymbol{\xi}) = 0$ is satisfied.*

Proof. Let us consider the following function:

$$V_s(s) \triangleq |s|. \tag{2.23}$$

One can see that, for a $\boldsymbol{\xi}_s \in \boldsymbol{\mathcal{S}}$, if there exists a $\lambda > 0$ that satisfies

$$\dot{V}_s(s(\boldsymbol{\xi})) \leq -\lambda \tag{2.24}$$

in the intersection of an open neighborhood of $\boldsymbol{\xi}_s \in \boldsymbol{\mathcal{S}}$ and the subset $\overline{S}$, where $s(\boldsymbol{\xi}) \neq 0$, we can say that the sliding mode takes place at $\boldsymbol{\xi}_s \in \boldsymbol{\mathcal{S}}$. The following proof shows that such a $\lambda > 0$ exists for every $\boldsymbol{\xi} \in \boldsymbol{\mathcal{S}}_C \cup (\boldsymbol{\mathcal{S}}_L \cap \boldsymbol{\mathcal{F}})$.

From (2.13), we can obtain the following:

$$\dot{V}_s(s(\boldsymbol{\xi})) = \begin{cases} -\beta & \text{if } |\sigma| > \alpha\gamma \wedge s(\boldsymbol{\xi}) \neq 0 \\ -\beta\left(1 - \mathrm{sgn}(s(\boldsymbol{\xi}))\dfrac{\dot{\sigma}}{\beta\gamma}\right) & \text{if } |\sigma| < \alpha\gamma \wedge s(\boldsymbol{\xi}) \neq 0. \end{cases} \tag{2.25}$$

This means that, if $|\sigma| > \alpha\gamma$ and $s(\boldsymbol{\xi}) \neq 0$, (2.24) is satisfied with $\lambda = \beta$ and thus the sliding mode takes place on the set $\boldsymbol{\mathcal{S}}_C$, which is the portion of $\boldsymbol{\mathcal{S}}$ that lies in the region $|\sigma| > \alpha\gamma$.

Meanwhile, if $|\sigma| < \alpha\gamma$, $s(\boldsymbol{\xi}) \neq 0$ and also $\boldsymbol{\xi} \in \boldsymbol{\mathcal{F}}$ are satisfied, (2.25) implies that the following is satisfied:

$$\begin{aligned} \dot{V}_s(s(\boldsymbol{\xi})) &= -\beta\left(1 - \mathrm{sgn}(s(\boldsymbol{\xi}))\frac{\dot{\sigma}}{\beta\gamma}\right) \\ &\leq -\beta\left(1 - \frac{|\eta + u + \zeta|}{\hat{\beta}\gamma}\right) \\ &\leq -\beta\left(\frac{\hat{\beta}\gamma - |\eta + u| - L_m}{\hat{\beta}\gamma}\right) \\ &\leq -\kappa(L - L_m)/\gamma, \end{aligned} \tag{2.26}$$

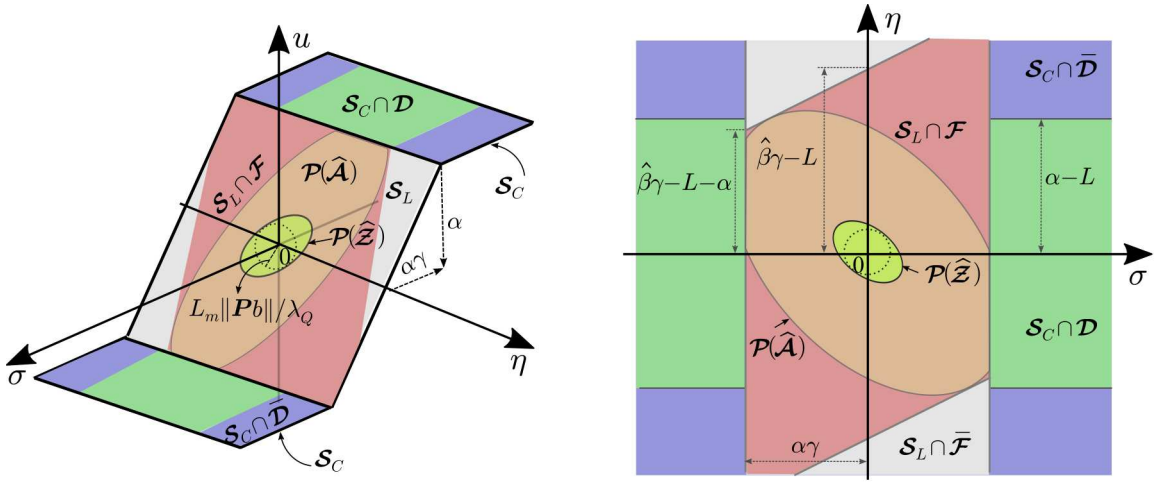

Figure 2.2: Subsets of the sub-state space $\mathbb{R}^3$. (a) The switching surface $\boldsymbol{\mathcal{S}}$ and its subsets. (b) The projection of some subsets on the σ-η plane.

where the following the fact is used:

$$\hat{\beta}\gamma > |\eta + u + \zeta| \quad \forall \boldsymbol{\xi} \in \boldsymbol{\mathcal{F}}. \tag{2.27}$$

This means that (2.24) is also satisfied in this case and thus the sliding mode also takes place on the set $\boldsymbol{\mathcal{S}}_L \cap \boldsymbol{\mathcal{F}}$. Therefore, we can see that the subsystem (2.10)(2.11) is in the sliding mode on the patch $\boldsymbol{\mathcal{S}}_C \cup (\boldsymbol{\mathcal{S}}_L \cap \boldsymbol{\mathcal{F}})$ of the switching surface $\boldsymbol{\mathcal{S}}$. This implies that the total system (2.5)(2.6) is in the sliding mode on the patch $\widehat{\boldsymbol{\mathcal{E}}}(\boldsymbol{\mathcal{S}}_C \cup (\boldsymbol{\mathcal{S}}_L \cap \boldsymbol{\mathcal{F}}))$ of the surface $\widehat{\boldsymbol{\mathcal{E}}}(\boldsymbol{\mathcal{S}})$. This completes the proof. □

This theorem indicates that, once the state ξ reaches the manifold $\boldsymbol{\mathcal{S}}$, the state may escape from $\boldsymbol{\mathcal{S}}$ only from the portion $\boldsymbol{\mathcal{S}}_L \cap \overline{\boldsymbol{\mathcal{F}}}$. Considering that $u = -\sigma/\gamma$ is satisfied on $\boldsymbol{\mathcal{S}}_L$, the subset $\boldsymbol{\mathcal{S}}_L \cap \boldsymbol{\mathcal{F}}$ can be written as follows:

$$\boldsymbol{\mathcal{S}}_L \cap \boldsymbol{\mathcal{F}} = \left\{ \boldsymbol{\xi} \in \boldsymbol{\mathcal{S}}_L \,\middle|\, |\eta - \sigma/\gamma| < \hat{\beta}\gamma - L \right\}. \tag{2.28}$$

After reaching the set $\boldsymbol{\mathcal{S}}_C$, the state $\boldsymbol{\xi}$ moves toward $\boldsymbol{\mathcal{S}}_L$ as long as it stays in $\boldsymbol{\mathcal{S}}_C \cap \boldsymbol{\mathcal{D}}$. The following theorem formally states this fact:

Theorem 2.3.2. *Let us consider the system (2.5)(2.6) and assume that* $\boldsymbol{\chi} \in \widehat{\boldsymbol{\mathcal{E}}}(\boldsymbol{\mathcal{S}}_C \cap \boldsymbol{\mathcal{D}})$ *at* $t = t_0$. *Then, the state* $\boldsymbol{\chi}$ *reaches* $\widehat{\boldsymbol{\mathcal{E}}}(\mathrm{cl}(\boldsymbol{\mathcal{S}}_L))$ *or* $\widehat{\boldsymbol{\mathcal{E}}}(\mathrm{cl}(\boldsymbol{\mathcal{S}}_C \cap \overline{\boldsymbol{\mathcal{D}}}))$ *in finite time.*

Proof. When $\boldsymbol{\xi} \in \boldsymbol{\mathcal{S}}_C \cap \boldsymbol{\mathcal{D}}$, the following is satisfied:

$$u = -\alpha \mathrm{sgn}(\sigma) \ \wedge \ |\sigma| \geq \alpha\gamma \ \wedge \ |\eta| < \alpha - L, \tag{2.29}$$

which leads to the following:

$$\begin{aligned} d|\sigma|/dt &= \mathrm{sgn}(\sigma)\dot{\sigma} \\ &= -\kappa \mathrm{sgn}(\sigma)(\alpha \mathrm{sgn}(\sigma) - \eta - \zeta) \\ &\leq -\kappa(\alpha - |\eta| - L_m) \\ &< -\kappa(L - L_m). \end{aligned} \tag{2.30}$$

With the use of the comparison lemma [50, Lemma 3.4], one can obtain the following from (2.30):

$$\boldsymbol{\xi}(t) \in \boldsymbol{\mathcal{S}}_C \cap \boldsymbol{\mathcal{D}} \quad \forall t \in (t_0, t_1) \Rightarrow \ |\sigma(t_1)| < |\sigma(t_0)| - \kappa(L - L_m)(t_1 - t_0). \tag{2.31}$$

In $\boldsymbol{\mathcal{S}}_C \cap \boldsymbol{\mathcal{D}}$, $|\sigma|$ is lower-bounded by $\alpha\gamma$. Therefore, if we set

$$t_1 \triangleq t_0 + \frac{|\sigma(t_0)| - \alpha\gamma}{\kappa(L - L_m)}, \tag{2.32}$$

we have the following:

$$\exists t_m \in (t_0, t_1) \text{ s.t. } \left((\boldsymbol{\xi}(t) \in \boldsymbol{\mathcal{S}}_C \cap \boldsymbol{\mathcal{D}} \ \forall t \in (t_0, t_m)) \wedge \left(\boldsymbol{\xi}(t_m) \in \overline{\boldsymbol{\mathcal{S}}_C \cap \boldsymbol{\mathcal{D}}} \right) \right). \tag{2.33}$$

This means that, at such a time instant t_m shown in (2.33), the state $\boldsymbol{\xi}$ is outside the set $\boldsymbol{\mathcal{S}}_C \cap \boldsymbol{\mathcal{D}}$. Because the sliding mode takes place on $\boldsymbol{\mathcal{S}}_C \cap \boldsymbol{\mathcal{D}}$, the state does not move directly from $\boldsymbol{\mathcal{S}}_C \cap \boldsymbol{\mathcal{D}}$ into $\overline{\boldsymbol{\mathcal{S}}}$. Therefore, possible transitions at the time t_m is only into $\mathrm{cl}(\boldsymbol{\mathcal{S}}_L)$ and $\mathrm{cl}(\boldsymbol{\mathcal{S}}_C \cap \overline{\boldsymbol{\mathcal{D}}})$. This completes the proof. □

After the state $\boldsymbol{\xi}$ reaches the set $\boldsymbol{\mathcal{S}}_L$ (i.e., the state χ reaches the set $\widehat{\boldsymbol{\mathcal{E}}}(\boldsymbol{\mathcal{S}}_L)$), the system is linear. As long as the system state $\boldsymbol{\chi}$ stays in $\widehat{\boldsymbol{\mathcal{E}}}(\boldsymbol{\mathcal{S}}_L \cap \boldsymbol{\mathcal{F}})$ (i.e., the condition (2.27) is satisfied), one can prove that the state is attracted to a neighborhood of the origin through the following Theorem:

Theorem 2.3.3. *With the system (2.5)(2.6), there exists a set $\widehat{\boldsymbol{\mathcal{Z}}} \subset \widehat{\boldsymbol{\mathcal{E}}}(\boldsymbol{\mathcal{S}}_L \cap \boldsymbol{\mathcal{F}})$ that includes the origin and is asymptotically stable if L_m is small enough and if $\boldsymbol{A} - \boldsymbol{b}\boldsymbol{c}^T/\gamma$ is Hurwitz.*

Proof. When $\boldsymbol{\xi} \in \boldsymbol{\mathcal{S}}_L$, the system (2.5)(2.6) reduces to the following linear system:

$$\dot{\boldsymbol{x}} = (\boldsymbol{A} - \boldsymbol{b}\boldsymbol{c}^T/\gamma)\boldsymbol{x} + \boldsymbol{b}\zeta \tag{2.34}$$

$$u = -\boldsymbol{c}^T\boldsymbol{x}/\gamma. \tag{2.35}$$

If $\boldsymbol{A}-\boldsymbol{b}\boldsymbol{c}^T/\gamma$ is Hurwitz, for every positive definite matrix $\boldsymbol{Q}\in\mathbb{R}^{n\times n}$, there exists a positive definite matrix $\boldsymbol{P}\in\mathbb{R}^{n\times n}$ that satisfies

$$\boldsymbol{P}(\boldsymbol{A}-\boldsymbol{b}\boldsymbol{c}^T/\gamma)+(\boldsymbol{A}-\boldsymbol{b}\boldsymbol{c}^T/\gamma)^T\boldsymbol{P}=-2\boldsymbol{Q}. \tag{2.36}$$

With such $\boldsymbol{Q}$ and $\boldsymbol{P}$, let us define the following function:

$$V_q(\boldsymbol{x})\triangleq \boldsymbol{x}^T\boldsymbol{P}\boldsymbol{x}/2. \tag{2.37}$$

Then, one can find that

$$\begin{aligned}\dot{V}_q(\boldsymbol{x})&=-\boldsymbol{x}^T\boldsymbol{Q}\boldsymbol{x}+\boldsymbol{x}^T\boldsymbol{P}\boldsymbol{b}\zeta\\&\leq-\lambda_{\boldsymbol{Q}}\|\boldsymbol{x}\|^2+L_m\|\boldsymbol{x}\|\|\boldsymbol{P}\boldsymbol{b}\|\end{aligned} \tag{2.38}$$

where $\lambda_{\boldsymbol{Q}}$ stands for the minimum eigenvalue of $\boldsymbol{Q}$. This means that $\dot{V}_q(\boldsymbol{x})<0$ is satisfied if

$$\|\boldsymbol{x}\|>L_m\|\boldsymbol{P}\boldsymbol{b}\|/\lambda_{\boldsymbol{Q}}. \tag{2.39}$$

Thus, the following quantity can be defined:

$$\rho_a\triangleq\max_{\substack{\boldsymbol{x}\in\mathbb{R}^n\\\|\boldsymbol{x}\|\leq\|\boldsymbol{P}\boldsymbol{b}\|/\lambda_{\boldsymbol{Q}}}}V_q(\boldsymbol{x})=\max_{\substack{\boldsymbol{x}\in\mathbb{R}^n\\\|\boldsymbol{x}\|\leq L_m\|\boldsymbol{P}\boldsymbol{b}\|/\lambda_{\boldsymbol{Q}}}}\frac{V_q(\boldsymbol{x})}{L_m^2}, \tag{2.40}$$

which does not depend on L_m. Based on this, let us define the followings:

$$\widehat{\boldsymbol{\mathcal{Z}}}\triangleq\{\boldsymbol{\chi}\in\boldsymbol{\mathcal{S}}_L\mid V_q(\boldsymbol{x})<L_m^2\rho_a\wedge V_s(s(\boldsymbol{\xi}))=0\}. \tag{2.41}$$

Let us assume that $\widehat{\boldsymbol{\mathcal{Z}}}\subset\mathrm{Int}(\widehat{\boldsymbol{\mathcal{E}}}(\boldsymbol{\mathcal{S}}_L\cap\boldsymbol{\mathcal{F}}))$. Then, there exists an open neighborhood $\widehat{\boldsymbol{\mathcal{N}}}$ of $\widehat{\boldsymbol{\mathcal{Z}}}$ that is small enough to satisfy $\widehat{\boldsymbol{\mathcal{N}}}\cap\widehat{\boldsymbol{\mathcal{E}}}(\boldsymbol{\mathcal{S}}_L\backslash\boldsymbol{\mathcal{F}})=\emptyset$. With such an $\widehat{\boldsymbol{\mathcal{N}}}$, we can see that $\dot{V}_q(\boldsymbol{x})$ and $\dot{V}_s(s(\boldsymbol{\xi}))$ are bounded as

$$\dot{V}_q(\boldsymbol{x})<a_1\ \wedge\ \dot{V}_s(s(\boldsymbol{\xi}))<-a_2\ \ \forall\boldsymbol{\chi}\in\widehat{\boldsymbol{\mathcal{N}}}\backslash\widehat{\boldsymbol{\mathcal{E}}}(\boldsymbol{\mathcal{S}}_L) \tag{2.42}$$

$$\dot{V}_q(\boldsymbol{x})<0\ \wedge\ \dot{V}_s(s(\boldsymbol{\xi}))=0\quad\forall\boldsymbol{\chi}\in\widehat{\boldsymbol{\mathcal{N}}}\cap\widehat{\boldsymbol{\mathcal{E}}}(\boldsymbol{\mathcal{S}}_L) \tag{2.43}$$

where a_1 and a_2 are positive scalars. Therefore, if one set

$$V_a(\boldsymbol{\chi})\triangleq\max(0,V_q(\boldsymbol{x})-L_m^2\rho_a)+\frac{a_1}{a_2}V_s(s(\boldsymbol{\xi})), \tag{2.44}$$

we can see that $V_a(\boldsymbol{\chi})=0$ is satisfied for all $\boldsymbol{\chi}\in\widehat{\boldsymbol{\mathcal{Z}}}$ and $\dot{V}_a(\boldsymbol{\chi})<0$ is satisfied for all $\boldsymbol{\chi}\in\widehat{\boldsymbol{\mathcal{N}}}\backslash\widehat{\boldsymbol{\mathcal{Z}}}$. Thus, $\widehat{\boldsymbol{\mathcal{Z}}}$ is asymptotically stable in a local sense if $\widehat{\boldsymbol{\mathcal{Z}}}\subset\mathrm{Int}(\widehat{\boldsymbol{\mathcal{E}}}(\boldsymbol{\mathcal{S}}_L\cap\boldsymbol{\mathcal{F}}))$. The definition (2.41) implies that $\widehat{\boldsymbol{\mathcal{Z}}}\subset\mathrm{Int}(\widehat{\boldsymbol{\mathcal{E}}}(\boldsymbol{\mathcal{S}}_L\cap\boldsymbol{\mathcal{F}}))$ is satisfied if L_m is small enough. This completes the proof. □

With respect to the terminal attractor $\widehat{\boldsymbol{\mathcal{Z}}}$, a subset of the region of attraction can be given as follows:

$$\widehat{\boldsymbol{\mathcal{A}}} \triangleq \left\{ \boldsymbol{\chi} \in \widehat{\boldsymbol{\mathcal{E}}}(\boldsymbol{\mathcal{S}}_L) \,|V_q(\boldsymbol{x}) < \rho_b \right\} \tag{2.45}$$

where

$$\rho_b \triangleq \min_{\substack{\boldsymbol{\chi}\in\mathbb{R}^{n+1} \\ \boldsymbol{\chi}\in\widehat{\boldsymbol{\mathcal{E}}}(\boldsymbol{\mathcal{S}}_L\cap(\partial\boldsymbol{\mathcal{F}}))}} V_q(\boldsymbol{x}). \tag{2.46}$$

If the set $\widehat{\boldsymbol{\mathcal{A}}}$ shares its boundary with the set $\widehat{\boldsymbol{\mathcal{E}}}(\boldsymbol{\mathcal{S}}_L \cap \boldsymbol{\mathcal{F}})$, then the state reaches the terminal attractor $\widehat{\boldsymbol{\mathcal{Z}}}$, as long as it stays in $\widehat{\boldsymbol{\mathcal{E}}}(\boldsymbol{\mathcal{S}}_L \cap \boldsymbol{\mathcal{F}})$.

In conclusions, as long as $\boldsymbol{\chi}$ is in the portion $\widehat{\boldsymbol{\mathcal{E}}}(\boldsymbol{\mathcal{S}}_C \cap \boldsymbol{\mathcal{D}})$, it is attracted to the subset $\widehat{\boldsymbol{\mathcal{E}}}(\boldsymbol{\mathcal{S}}_L)$. Once $\boldsymbol{\chi}$ reaches $\widehat{\boldsymbol{\mathcal{A}}}$, which is a subset of $\widehat{\boldsymbol{\mathcal{E}}}(\boldsymbol{\mathcal{S}}_L \cap \boldsymbol{\mathcal{F}})$, the state asymptotically approaches the terminal attractor $\widehat{\boldsymbol{\mathcal{Z}}}$. It should be noted that a smaller γ results in a smaller terminal attractor $\widehat{\boldsymbol{\mathcal{Z}}}$ because it is a subset of $\widehat{\boldsymbol{\mathcal{E}}}(\boldsymbol{\mathcal{S}}_L \cap \boldsymbol{\mathcal{F}})$, of which the width is $\alpha\gamma$. It however results in a smaller size of the linear sliding patch $\widehat{\boldsymbol{\mathcal{E}}}(\boldsymbol{\mathcal{S}}_L \cap \boldsymbol{\mathcal{F}})$, which includes a subset of the region of attraction $\widehat{\boldsymbol{\mathcal{A}}}$. Therefore, one can conclude that γ should be large when the state is far from the origin and should be small when the state is close to the origin.

2.4 Proposed controller

Now, a new controller algorithm based on the discussion in Section 2.3 is proposed. The proposed controller is built on the controller (2.4) but the parameter γ is determined by a particular function of the state variables $\boldsymbol{x}$ and u. This nonlinear function γ is chosen to decrease the size of the terminal attractor $\widehat{\boldsymbol{\mathcal{Z}}}$ and to increase the size of the linear sliding patch $\widehat{\boldsymbol{\mathcal{E}}}(\boldsymbol{\mathcal{S}}_L \cap \boldsymbol{\mathcal{F}})$.

2.4.1 Continuous-time representation

For the application to the controlled plant (2.1), a new controller is presented as follows:

$$\dot{u} \in -\beta \mathrm{sgn}\left(u + \mathrm{sat}_\alpha(\boldsymbol{c}^T\boldsymbol{x}/\gamma(\boldsymbol{x},u))\right) \tag{2.47}$$

where

$$\gamma(\boldsymbol{x},u) \triangleq \min\left(\gamma_c, \frac{|\boldsymbol{c}^T\boldsymbol{A}\boldsymbol{x}| + \boldsymbol{c}^T\boldsymbol{b}|u| + \boldsymbol{c}^T\boldsymbol{b}L}{\beta}\right). \tag{2.48}$$

Here, u is the control signal amplitude, γ_c is a positive constant representing an upperbound of $\gamma(\boldsymbol{x},u)$, L is a positive constant that is greater than the expected

disturbance (i.e., $L > |\zeta|$), and $\boldsymbol{c} \in \mathbb{R}^n$ is a vector chosen so that it satisfies $\boldsymbol{c}^T\boldsymbol{b} > 0$. It is assumed that the maximum control signal amplitude α is greater than L, i.e.,

$$|\zeta| < L < \alpha. \tag{2.49}$$

The choice of the nonlinear function $\gamma(\boldsymbol{x}, u)$ is motivated by the proof of Theorem 2.3.1, which shows that

$$\gamma > \frac{|\boldsymbol{c}^T\boldsymbol{A}\boldsymbol{x} + \boldsymbol{c}^T\boldsymbol{b}u + \boldsymbol{c}^T\boldsymbol{b}\zeta|}{\beta} \tag{2.50}$$

needs to hold true to realize the sliding mode. To satisfy this condition, one choice is to set γ as follows:

$$\gamma = \frac{|\boldsymbol{c}^T\boldsymbol{A}\boldsymbol{x}| + \boldsymbol{c}^T\boldsymbol{b}|u| + \boldsymbol{c}^T\boldsymbol{b}L}{\beta}. \tag{2.51}$$

Here, γ needs to be prevented from becoming excessively large because a very large γ means a very low control gain. Considering these points, we can see that the definition (2.48) of $\gamma(\boldsymbol{x}, u)$ is a natural choice, in which an upperbound γ_c is set.

With the nonlinear function $\gamma(\boldsymbol{x}, u)$, the stability proofs in Section 2.3 do not strictly hold because it will inject additional terms proportional to $\dot{\gamma}$ to the derivatives of $V_s(s(\boldsymbol{\xi}))$ and $V_q(\boldsymbol{x})$. They are still valid if $\dot{\gamma}$ is small enough, although it is still unclear in what regions of the state space $|\dot{\gamma}|$ can be said to be small enough. One approach to this problem might be to use the fact that the upperbound of $\dot{\gamma}$ can be given as a function of the state vector $\boldsymbol{\chi}$. Leaving this problem as an open problem, usefulness of the controller is supported through some numerical examples in Section 2.5.

2.4.2 Parameter tuning guideline

This section shows an approach to design the vector $\boldsymbol{c} \in \mathbb{R}^n$ and the parameter $\gamma_c > 0$, which comprise all parameters that need to be designed. Here, the problem to choose $\boldsymbol{c}$ and γ_c is considered so that the eigenvalues of the matrix $\boldsymbol{A} - \boldsymbol{b}\boldsymbol{c}^T/\gamma$ is within a given region $\mathcal{R}$ in the complex plane for all $\gamma \in (0, \gamma_c]$. The region $\mathcal{R}$ can be given according to required response characteristics, such as damping ratio and settling time, of applications.

Let us define

$$\boldsymbol{A}_d(\gamma) \triangleq \boldsymbol{A} - \boldsymbol{b}\boldsymbol{c}^T/\gamma. \tag{2.52}$$

Then, one can see that, as $\gamma \searrow 0$, one of the eigenvalues of the matrix $\boldsymbol{A}_d(\gamma)$ goes to $-\infty$, while the others remain finite because it has been assumed that $\boldsymbol{c}^T\boldsymbol{b} > 0$ in the

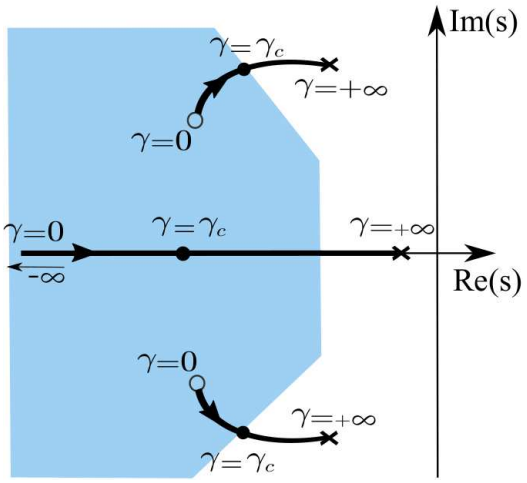

Figure 2.3: Illustrative graph for the region $\mathcal{R}$ and the loci of $\mathrm{Eig}(\boldsymbol{A}_d(\gamma))$.

condition (2.8). Thus, the vector $\boldsymbol{c}$ needs to be designed so that $\lim_{\gamma \searrow 0} \mathrm{Eig}(\boldsymbol{A}_d(\gamma)) \subset \mathcal{R}$. For this purpose, the following theorem is useful:

Theorem 2.4.1 (a special case of Theorem 2 in [51]). *Let us define the following matrices:*

$$\bar{\boldsymbol{A}} = \begin{bmatrix} \bar{\boldsymbol{A}}_{11} & \bar{\boldsymbol{a}}_{12} \\ \bar{\boldsymbol{a}}_{21}^T & \bar{a}_{22} \end{bmatrix}, \quad \bar{\boldsymbol{b}} = \begin{bmatrix} \boldsymbol{o}_{n-1} \\ 1 \end{bmatrix}, \quad \bar{\boldsymbol{c}} = \begin{bmatrix} \bar{\boldsymbol{c}}_1{}^T & 1 \end{bmatrix}^T \tag{2.53}$$

where $\bar{\boldsymbol{A}}_{11} \in \mathbb{R}^{(n-1)\times(n-1)}$, $\{\bar{\boldsymbol{a}}_{21}, \bar{\boldsymbol{a}}_{12}, \bar{c}_1\} \subset \mathbb{R}^{n-1}$, *and* $\bar{a}_{22} \in \mathbb{R}$. *Let us assume that* $\gamma > 0$ *and that the pair* $(\bar{\boldsymbol{A}}, \bar{\boldsymbol{b}})$ *is controllable. Let us define the following matrix:*

$$\bar{\boldsymbol{A}}_c(\gamma) = \bar{\boldsymbol{A}} - \bar{\boldsymbol{b}}\bar{\boldsymbol{c}}^T/\gamma. \tag{2.54}$$

Then, as $\gamma \searrow 0$, *one of the eigenvalues of* $\bar{\boldsymbol{A}}_c(\gamma)$ *goes to* $-\infty$ *and the other* $(n-1)$ *eigenvalues converge to the eigenvalues of* $\bar{\boldsymbol{A}}_{11} - \bar{\boldsymbol{a}}_{12}\bar{\boldsymbol{c}}_1^T \in \mathbb{R}^{(n-1)\times(n-1)}$.

With this theorem, a pole placement problem of an $n \times n$ system with one infinitely fast pole can be reduced to another pole placement problem of an $(n-1) \times (n-1)$ system. This theorem can be used to set the eigenvalues of $\lim_{\gamma \searrow 0} \boldsymbol{A}_d(\gamma)$ to specified locations $\{q_i, \cdots, q_{n-1}\}$, which should be located in $\mathcal{R}$. To apply this theorem to system (2.1), let us define a matrix $\boldsymbol{T} \in \mathbb{R}^{n\times n}$ so that $\boldsymbol{T}\boldsymbol{b} = [\boldsymbol{o}_{n-1}^T, 1]^T$ is satisfied. Once we obtain the vector $\bar{\boldsymbol{c}}_1 \in \mathbb{R}^{n-1}$ using Theorem 2.4.1, the vector $\boldsymbol{c}$ can be chosen as follows:

$$\boldsymbol{c} = \boldsymbol{T}^T \begin{bmatrix} \bar{\boldsymbol{c}}_1{}^T & 1 \end{bmatrix}^T. \tag{2.55}$$

Now, let us discuss the choice of γ_c, which is the upperbound of the nonlinear function $\gamma(\boldsymbol{x}, u)$. Recalling that $\mathrm{Eig}(\boldsymbol{A}_d(\gamma)) \subset \mathcal{R}$ should be satisfied for all $\gamma \in (0, \gamma_c]$, the maximum of such values of γ can be found by drawing the loci of $\mathrm{Eig}(\boldsymbol{A}_d(\gamma))$ with γ increasing from zero and by searching for the critical value of γ with which at least one of $\mathrm{Eig}(\boldsymbol{A}_d(\gamma))$ crosses the boundary of $\mathcal{R}$. Fig. 2.3 is an illustrative graph to show $\mathrm{Eig}(\boldsymbol{A}_d(\gamma))$ as a function of γ and to show the selection of γ_c according to the region $\mathcal{R}$.

In conclusion, the following procedure is for choosing the vector c and the upperbound γ_c:

1. Set a region $\mathcal{R}$ in the complex plane and the desired eigenvalue $\{q_1, \cdots, q_{n-1}\}$ in $\mathcal{R}$ according to required response characteristics of the application.

2. Find an invertible matrix $\boldsymbol{T} \in \mathbb{R}^{n\times n}$ with which

$$\boldsymbol{T}\boldsymbol{b} = \begin{bmatrix} \boldsymbol{o}_{n-1} \\ 1 \end{bmatrix} \tag{2.56}$$

   is satisfied.

3. Calculate the matrix $\bar{\boldsymbol{A}}_{11} \in \mathbb{R}^{(n-1)\times(n-1)}$ and the vector $\bar{\boldsymbol{a}}_{12} \in \mathbb{R}^{n-1}$ as follows:

$$\begin{bmatrix} \bar{\boldsymbol{A}}_{11} & \bar{\boldsymbol{a}}_{12} \\ \bar{\boldsymbol{a}}_{21}^T & \bar{a}_{22} \end{bmatrix} := \boldsymbol{T}\boldsymbol{A}\boldsymbol{T}^{-1}. \tag{2.57}$$

4. Solve the pole placement problem to choose the vector $\bar{\boldsymbol{c}}_1 \in \mathbb{R}^{n-1}$ so that $\mathrm{Eig}(\bar{\boldsymbol{A}}_{11} - \bar{\boldsymbol{a}}_{12}\bar{\boldsymbol{c}}_1^T) = \{q_1, \cdots, q_{n-1}\}$, and set $\boldsymbol{c} = \boldsymbol{T}^T[\bar{\boldsymbol{c}}_1{}^T, 1]^T$.

5. Draw the loci of $\mathrm{Eig}(\boldsymbol{A}_d(\gamma))$ with γ increasing from zero, and find the critical value of γ_c at which at least one of the loci crosses the boundary of $\mathcal{R}$.

Note that the step 4 is to adjust $\mathrm{Eig}(\boldsymbol{A}_d(\gamma))$ at $\gamma = 0$ and that the step 5 is to adjust $\mathrm{Eig}(\boldsymbol{A}_d(\gamma))$ at $\gamma \in (0, \gamma_c]$.

2.4.3 Discrete-time implementation

This section presents a discrete-time algorithm of the proposed controller for its implementation to digital controllers. Since the proposed continuous-time controller (2.47)(2.48) involves the set-valued function $\mathrm{sgn}(\cdot)$, inappropriate discretization prevents the exact sliding mode and causes chattering [52, 53]. Here, the approach called an implicit method [54, 55] is employed. The idea of the implicit method is to resolve the set-valuedness of the controller's equation by viewing the mutual dependence between the control input and the system state as an algebraic constraint. This approach

utilizes the model of the controlled plant as a predictor of the system state that is achieved by a given control input.

Let us start from the implicit Euler discretization of the controller (2.47)(2.48) as follows:

$$\frac{u_k - u_{k-1}}{h} \in -\beta \mathrm{sgn}\left(u_k + \mathrm{sat}_\alpha\left(\frac{\sigma_k}{\gamma_k}\right)\right) \tag{2.58}$$

$$\sigma_k = \boldsymbol{c}^T \boldsymbol{x}_k \tag{2.59}$$

$$\gamma_k = \min\left(\gamma_c, \frac{|\boldsymbol{c}^T \boldsymbol{A}\boldsymbol{x}_{k-1}| + \boldsymbol{c}^T\boldsymbol{b}|u_{k-1}| + \boldsymbol{c}^T\boldsymbol{b}L}{\beta}\right), \tag{2.60}$$

in which h denotes the sampling interval. Now, the system state $\boldsymbol{x}$ at time step k needs to be predicted by the nominal model of the controlled plant, thus the following "predictor" is used:

$$\frac{\hat{\boldsymbol{x}}_k - \boldsymbol{x}_{k-1}}{h} = \boldsymbol{A}\boldsymbol{x}_{k-1} + \boldsymbol{b}u_k. \tag{2.61}$$

This "predictor" equation is obtained by neglecting the perturbation ζ in the system model (2.1). Substituting $\boldsymbol{x}_k$ in (2.59) by the predicted value $\hat{\boldsymbol{x}}_k$, the predicted value of σ_k is obtained as follows:

$$\hat{\sigma}_k = \boldsymbol{c}^T(\boldsymbol{I} + h\boldsymbol{A})x_{k-1} + \boldsymbol{c}^T\boldsymbol{b}hu_k \tag{2.62}$$

Let us define $w_{k-1} \triangleq \boldsymbol{c}^T(\boldsymbol{I} + h\boldsymbol{A})\boldsymbol{x}_{k-1}$ so that $\hat{\sigma}_k$ is rewritten as follows:

$$\hat{\sigma}_k = w_{k-1} + \boldsymbol{c}^T\boldsymbol{b}hu_k. \tag{2.63}$$

Then, substituting σ_k in (2.58) by $\hat{\sigma}_k$ in (2.63) yields the following:

$$u_k \in u_{k-1} - h\beta \mathrm{sgn}\left(u_k + \mathrm{sat}_\alpha\left(\frac{w_{k-1} + \boldsymbol{c}^T\boldsymbol{b}hu_k}{\gamma_k}\right)\right), \tag{2.64}$$

in which u_k appears in both of the right- and left-hand sides. To solve (2.64) with respect to u_k, the following lemmas are introduced.

Lemma 2.4.1. *For any y, $z \in \mathbb{R}$ and $a > 0$, the following is satisfied:*

$$y \in a\mathrm{sgn}(z - y) \iff y = \mathrm{sat}_a(z). \tag{2.65}$$

Proof. See [56, Sec.II]. □

Lemma 2.4.2. *For any $y \in \mathbb{R}$ and $a, b, c, d > 0$, the following is satisfied:*

$$\mathrm{sgn}\left(y + a + \mathrm{sat}_b\left(\frac{y+c}{d}\right)\right) = \mathrm{sgn}\left(y + a + \mathrm{sat}_b\left(\frac{c-a}{1+d}\right)\right) \tag{2.66}$$

Proof. Let us define the following function:

$$\phi(y) \triangleq y + a + \mathrm{sat}_b\left(\frac{y+c}{d}\right). \tag{2.67}$$

It is obvious that the function ϕ is strictly monotonically increasing function and it is unbounded. Thus, it is clear that there is a unique real value Y that satisfies $\phi(Y) = 0$, and that such a Y satisfies $\mathrm{sgn}(\phi(y)) = \mathrm{sgn}(y - Y)$ is satisfied. Then, one can see that the real value Y can be obtained by solving $\phi(Y) = 0$ as follows. First, if $|Y + c|/d \leq b$, $\phi(Y) = 0$ reduces to $Y + a + (Y + c)/d = 0$, which is equivalent to:

$$Y = -a - \frac{c-a}{1+d}. \tag{2.68}$$

Second, if $(Y + c)/d > b$, $\phi(Y) = 0$ reduces to $Y + a + b = 0$, which is equivalent to:

$$Y = -a - b. \tag{2.69}$$

Third, if $(Y + c)/d < -b$, $\phi(Y) = 0$ reduces to $Y + a - b = 0$, which is equivalent to:

$$Y = -a + b. \tag{2.70}$$

By combining these three cases (2.68),(2.69), and(2.70), one can obtain the solution Y as follows:

$$Y = -a - \mathrm{sat}_b\left(\frac{c-a}{1+d}\right). \tag{2.71}$$

Therefore, the left-hand side of (2.66) is equal to $\mathrm{sgn}(y - Y)$ with Y defined in (2.71), and it is equal to the right-hand side of (2.66). This completes the proof. □

Using Lemmas 2.4.1 and 2.4.2, one can obtain the following theorem:

Theorem 2.4.2. *With any $y \in \mathbb{R}$ and $a, b, c, d > 0$ the following is satisfied:*

$$y \in -f\mathrm{sgn}\left(y + a + \mathrm{sat}_b\left(\frac{y+c}{d}\right)\right) \iff y = -\mathrm{sat}_f\left(a + \mathrm{sat}_b\left(\frac{c-a}{1+d}\right)\right). \tag{2.72}$$

Now, Theorem 2.4.2 is used to solve (2.64) with respect to u_k as follows:

$$u_k = u_{k-1} - \mathrm{sat}_{h\beta}\left(u_{k-1} + \mathrm{sat}_{\alpha}\left(\frac{w_{k-1}}{\gamma_k + \boldsymbol{c}^T\boldsymbol{b}h}\right)\right). \tag{2.73}$$

Here, one can see that the set-valuedness in (2.64) is resolved as in (2.73). In conclusion, the discrete-time controller, which realizes the controller (2.47)(2.48), can be given as follows:

$$w_{k-1} := \boldsymbol{c}^T(\boldsymbol{I} + h\boldsymbol{A})x_{k-1} \tag{2.74}$$

$$\gamma_k := \min\left(\gamma_c, \frac{|\boldsymbol{c}^T\boldsymbol{A}x_{k-1}| + \boldsymbol{c}^T\boldsymbol{b}|u_{k-1}| + \boldsymbol{c}^T\boldsymbol{b}L}{\beta}\right) \tag{2.75}$$

$$u_k := u_{k-1} - \mathrm{sat}_{h\beta}\left(u_{k-1} + \mathrm{sat}_{\alpha}\left(\frac{w_{k-1}}{\gamma_k + \boldsymbol{c}^T\boldsymbol{b}h}\right)\right). \tag{2.76}$$

Remark 2.4.1. *In case where the rate-of-change of the control signal is not limited (i.e., $\beta = \infty$), the nonlinear function γ_k holds at zero. In this case, the controller (2.74)(2.75)(2.76) reduces to the following simpler controller,*

$$w_{k-1} = \boldsymbol{c}^T(\boldsymbol{I} + h\boldsymbol{A})x_{k-1} \tag{2.77}$$

$$u_k = -\mathrm{sat}_{\alpha}(w_{k-1}/(\boldsymbol{c}^T\boldsymbol{b}h)), \tag{2.78}$$

which is an implicit implementation of the conventional sliding mode controller $u = -\alpha\mathrm{sgn}(\boldsymbol{c}^T\boldsymbol{x})$ combined with the nominal plant model (2.61).

Remark 2.4.2. *By setting $\beta < \infty$ and holding $\gamma = 0$, the controller (2.47)(2.48) reduces to*

$$\dot{u} \in -\beta\mathrm{sgn}(u + \alpha\mathrm{sgn}(\boldsymbol{c}^T\boldsymbol{x})) \tag{2.79}$$

for all $\boldsymbol{x}$ satisfying $\boldsymbol{c}^T\boldsymbol{x} \neq 0$. In order to deal with the case of $c^Tx = 0$, a nested signum structure needs rigorous re-definition of the set-valued mapping sgn. *A similar nested signum structure appears in the work of Miranda-Villatoro et al. [47], who also used the implicit discretization scheme [54, 55]. This chapter does not discuss the extreme case of $\gamma = 0$ because $\gamma > 0$ is always satisfied in the proposed controller.*

2.5 Examples

In this section, the proposed controller is applied to some numerical examples. The simulations are performed with MATLAB software in the discrete time.

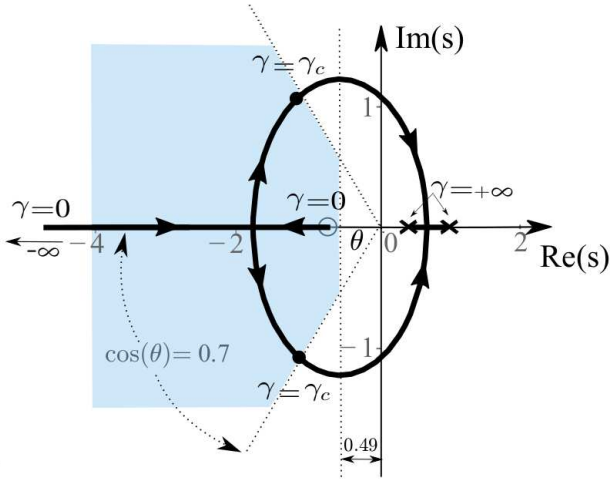

Figure 2.4: Example 1: The region $\mathcal{R}$ and the loci of $\mathrm{Eig}(\boldsymbol{A}_d(\gamma))$.

2.5.1 Example 1

Here, an example reported in [13, 46] employs the controlled plant (2.1) with the following matrices:

$$\boldsymbol{A} = \begin{bmatrix} 0 & -0.5 \\ 1 & 1.5 \end{bmatrix}, \quad \boldsymbol{b} = \begin{bmatrix} 0 \\ -1 \end{bmatrix} \tag{2.80}$$

where the pair $(\boldsymbol{A}, \boldsymbol{b})$ is controllable. Let us consider that this controlled plant is subjected to disturbance and parameter uncertainty as in the following form:

$$\dot{\boldsymbol{x}} = (\boldsymbol{A} + \Delta\boldsymbol{A})\boldsymbol{x} + \boldsymbol{b}(u + \zeta) \tag{2.81}$$

where

$$\Delta\boldsymbol{A} = \begin{bmatrix} 0 & -0.05 \\ 0 & 0.1 \end{bmatrix}, \quad \zeta = 0.1\sin(t). \tag{2.82}$$

The control input u is under the restriction of $|u| \leq 1$ and $|\dot{u}| \leq 2.5$, and the initial states are $\boldsymbol{x}_0 = [0, 0.4]^T$ and $u_0 = 0$. The requirement is to set the 2% settling time to be less than or equal to 8 s and the damping ratio to be greater than or equal to 0.7.

The discrete-time algorithm (2.74)(2.75)(2.76) is applied with the sampling interval $h = 0.01$, and $L = 0.125$. The parameters $\boldsymbol{c}$ and γ_c are obtained based on the design procedure in Section 2.4.2 as follows:

1. Set $\mathcal{R}$ as shown in Fig. 2.4, i.e., $\mathcal{R} = \{s \in \mathbb{C} \,|\, \Re(s) \leq -\ln(0.02)/8 \wedge \cos(\arg(s)) \leq -0.7\}$, and set $q_1 = -0.5$ so that it resides in $\mathcal{R}$.
2. Set $\boldsymbol{T} = -\boldsymbol{I}$ in order to realize $\boldsymbol{Tb} = [0, 1]^T$.
3. From (2.57), we can find that $\bar{\boldsymbol{A}}_{11} = 0$ and $\bar{\boldsymbol{a}}_{12} = -0.5$.
4. By solving $\bar{\boldsymbol{A}}_{11} - \bar{\boldsymbol{a}}_{12}\bar{\boldsymbol{c}}_1^T = q_1$, $\bar{\boldsymbol{c}}_1 = -1$, and thus, $\boldsymbol{c} = [1, -1]^T$.
5. By drawing the loci of $\mathrm{Eig}(\boldsymbol{A} - \boldsymbol{bc}^T/\gamma)$ as shown in Fig. 2.4, we can find that $\gamma_c = 1/3.62 = 0.277$.

Fig. 2.5(a) shows the results of simulation under $\zeta = 0.1\sin(t)$ and $\Delta\boldsymbol{A} = 0$. Here, one can see that the use of the small constant $\gamma \equiv 0.6\gamma_c$ results in the instability. In contrast, the use of the nonlinear function $\gamma(\boldsymbol{x}, u)$ provides best convergent behavior in spite of the fact that the value of $\gamma(\boldsymbol{x}, u)$ eventually becomes smaller than $0.6\gamma_c$. It should be noted that the decrease of $\gamma(\boldsymbol{x}, u)$ takes place after the state comes close to the origin. This decreasing leads to better disturbance rejection than the case with the larger constant $\gamma \equiv \gamma_c$. Fig. 2.6 shows more details about the state trajectory in σ-η plane under using $\gamma(\boldsymbol{x}, u)$, where the initial state lies in the portion $(\boldsymbol{\mathcal{S}}_C \cap \boldsymbol{\mathcal{D}})$. As long as the state trajectory stays in $(\boldsymbol{\mathcal{S}}_C \cap \boldsymbol{\mathcal{D}})$, it reaches the linear portion $\boldsymbol{\mathcal{S}}_L$ in finite time as proven in Theorem 2.3.2. After that, the trajectory catches the wider sliding patch $\boldsymbol{\mathcal{S}}_L \cap \boldsymbol{\mathcal{F}}$ (the light-coral region), i.e., $\gamma(\boldsymbol{x}, u)$ at its maximum γ_c, and then, the state moves towards the neighborhood of the origin inside a smaller sliding patch (the red region), i.e., $\gamma(\boldsymbol{x}, u) = 0.105$.

Fig. 2.5(b) shows the results of simulation under ζ and $\Delta\boldsymbol{A}$ indicated in (2.82). The state still smoothly converges to the neighborhood of the origin with the nonlinear function $\gamma(\boldsymbol{x}, u)$, although the constant γ values produce larger errors and overshoots. It should be noted that the nonlinear function $\gamma(\boldsymbol{x}, u)$ results in smaller terminal error than the larger constant $\gamma \equiv \gamma_c$ and smaller overshoots than the smaller constant $\gamma \equiv 0.9\gamma_c$. It is also interesting to see that, although the constant $\gamma \equiv 0.8\gamma_c$ results in the instability, the proposed $\gamma(\boldsymbol{x}, u)$, which eventually falls far below $0.8\gamma_c$, maintains the stability with good convergence.

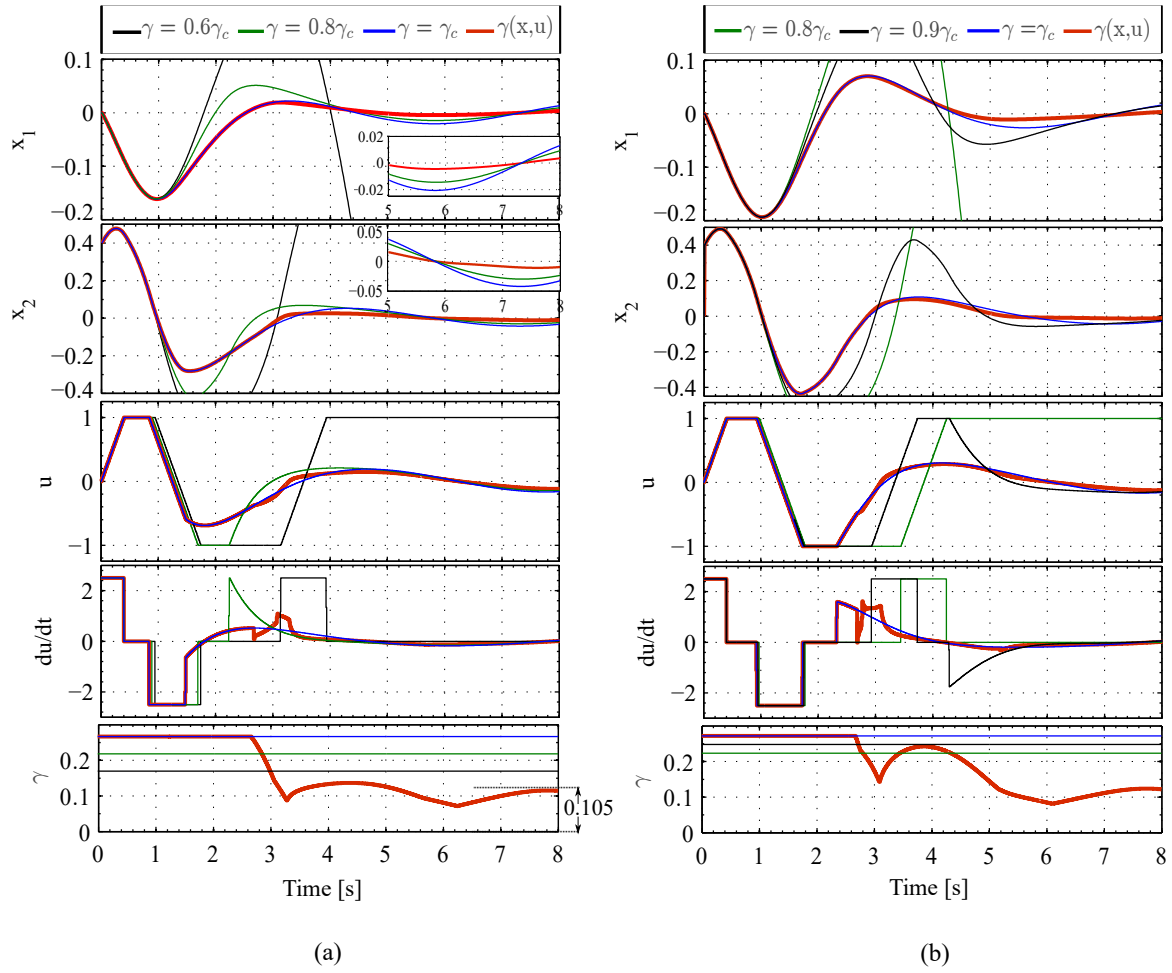

Figure 2.5: (a) Results of Example 1 with $\zeta = 0.1\sin(t)$ and $\Delta\boldsymbol{A} = 0$. (b) Results of Example 1 with ζ and $\Delta\boldsymbol{A}$ indicated in (2.82).

2.5.2 Example 2

As an example of a third-order system, the controlled plant (2.1) is considered with the following controllable pair of matrices:

$$\boldsymbol{A} = \begin{bmatrix} 0 & 0 & 1 \\ 172.6 & -2.73 & 1.237 \\ -195 & 2.538 & -1.589 \end{bmatrix}, \quad \boldsymbol{b} = \begin{bmatrix} 0 \\ 0 \\ -1.0698 \end{bmatrix}. \tag{2.83}$$

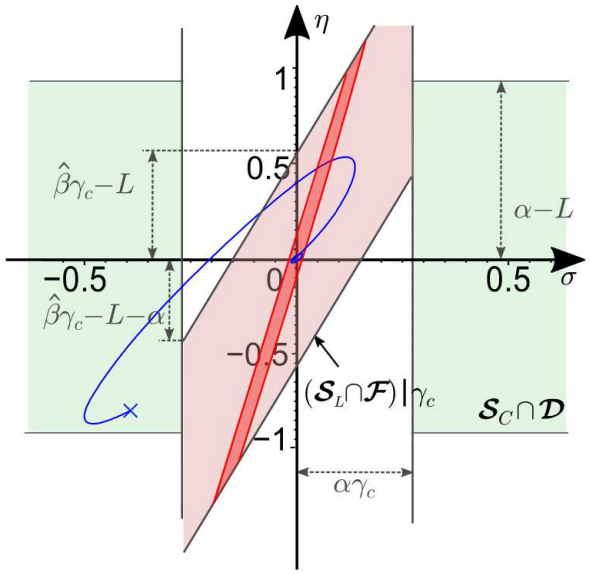

Figure 2.6: Example 1: The state trajectory (blue) in σ-η plane in case that $\zeta = 0.1\sin(t)$ and $\Delta\boldsymbol{A} = 0$. The light-coral region is $(\boldsymbol{\mathcal{S}} \cap \boldsymbol{\mathcal{F}})$ at $\gamma(\boldsymbol{x}, u) \equiv \gamma_c$, while the red region is $(\boldsymbol{\mathcal{S}} \cap \boldsymbol{\mathcal{F}})$ at $\gamma(\boldsymbol{x}, u) \equiv 0.105$.

Let us consider that this controlled plant is subjected to disturbance and parameter uncertainty as in the following form:

$$\dot{\boldsymbol{x}} = (\boldsymbol{A} + \Delta\boldsymbol{A})\boldsymbol{x} + \boldsymbol{b}(u + \zeta) \tag{2.84}$$

where

$$\Delta\boldsymbol{A} = \begin{bmatrix} 0 & 0 & 0.1 \\ -3 & 0.1 & -0.5 \\ -2 & -0.2 & 0.1 \end{bmatrix}. \tag{2.85}$$

The disturbance ζ is equal to $0.0184\sin(t)$ from 0 to 7 s, and after that, it changes into $\zeta = 0.0184\sin(2t)$. The control signal amplitude and its rate-of-change are set to be subject to the following limitations: $|u| \leq 1.5$ and $|\dot{u}| \leq 0.139$. The initial states are set as $\boldsymbol{x}_0 = [0.0, 0.1, 0.01]^T$ and $u_0 = 0.05$. The requirement is to set the eigenvalues of the overall system on the left side of the line $\Re(s) = -1.9$ and also it is required to set $\{q_1, q_2\} = \{-1.92 + 13.8j, -1.92 - 13.8j\}$.

In the use of the algorithm (2.74)(2.75)(2.76), $h = 0.01$ and $L = 0.019$. The parameters $\boldsymbol{c}$ and γ_c are obtained through the design procedure in Section 2.4.2 as follows:

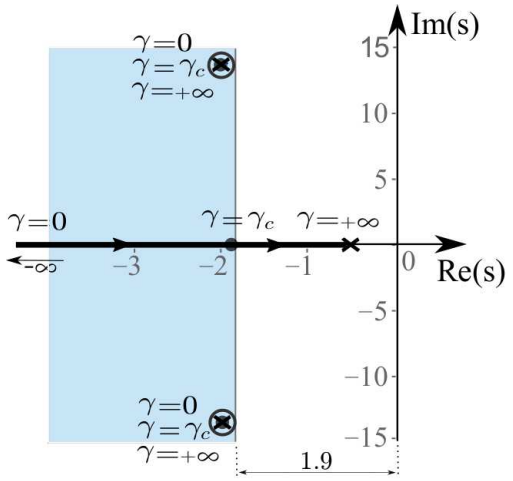

Figure 2.7: Example 2: The region $\mathcal{R}$ and the loci of $\mathrm{Eig}(\boldsymbol{A}_d(\gamma))$.

1. Set $\mathcal{R}$ as shown in Fig. 2.7, i.e., $\mathcal{R} = \{s \in \mathbb{C} \,|\, \Re(s) < -1.9\}$, and set $\{q_1, q_2\} = \{-1.92 + 13.8j, -1.92 - 13.8j\}$ so that they reside in $\mathcal{R}$.

2. To realize $\boldsymbol{Tb} = [0, 1]^T$, set

$$\boldsymbol{T} = \begin{bmatrix} -1 & 0 & 0 \\ 0 & -1 & 0 \\ 0 & 0 & -0.9348 \end{bmatrix}. \tag{2.86}$$

3. From (2.57), we can find that: $\bar{\boldsymbol{A}}_{11} = \begin{bmatrix} 0 & 0 \\ 172.6 & -2.73 \end{bmatrix}$ and $\bar{\boldsymbol{a}}_{12} = \begin{bmatrix} 1.0698 \\ 1.3233 \end{bmatrix}$.

4. By solving the pole placement problem to put $\mathrm{Eig}(\bar{\boldsymbol{A}}_{11} - \bar{\boldsymbol{a}}_{12}\bar{\boldsymbol{c}}_1^T)$ at $\{q_1, q_2\}$, it is found that $\bar{\boldsymbol{c}}_1 = [-0.1177, 1.0549]^T$, and thus, $\boldsymbol{c} = [0.2681, -1.0556, -0.9348]^T$.

5. By drawing the loci of $\mathrm{Eig}(\boldsymbol{A} - \boldsymbol{bc}^T/\gamma)$ as shown in Fig. 2.7, we can find that $\gamma_c = 1/1.44 = 0.69$.

Fig. 2.8(a) shows the simulation results of Example 2 under the existence of ζ. It is clearly seen that the convergence is much faster with $\gamma(\boldsymbol{x}, u)$ than with the smaller constant $\gamma \equiv 0.2\gamma_c$ in spite of the fact that $\gamma(\boldsymbol{x}, u)$ goes below $0.2\gamma_c$. Fig. 2.8(a) also shows that the system with $\gamma(\boldsymbol{x}, u)$ is less sensitive to the disturbance than that with the larger constant $\gamma \equiv \gamma_c$.

Fig. 2.8(b) shows the simulation results of Example 2 under the existence of both ζ and $\Delta\boldsymbol{A}$. The states with $\gamma(\boldsymbol{x}, u)$ converge faster than those with $\gamma \equiv 0.2\gamma_c$, and are less sensitive to the disturbance than those with $\gamma \equiv \gamma_c$.

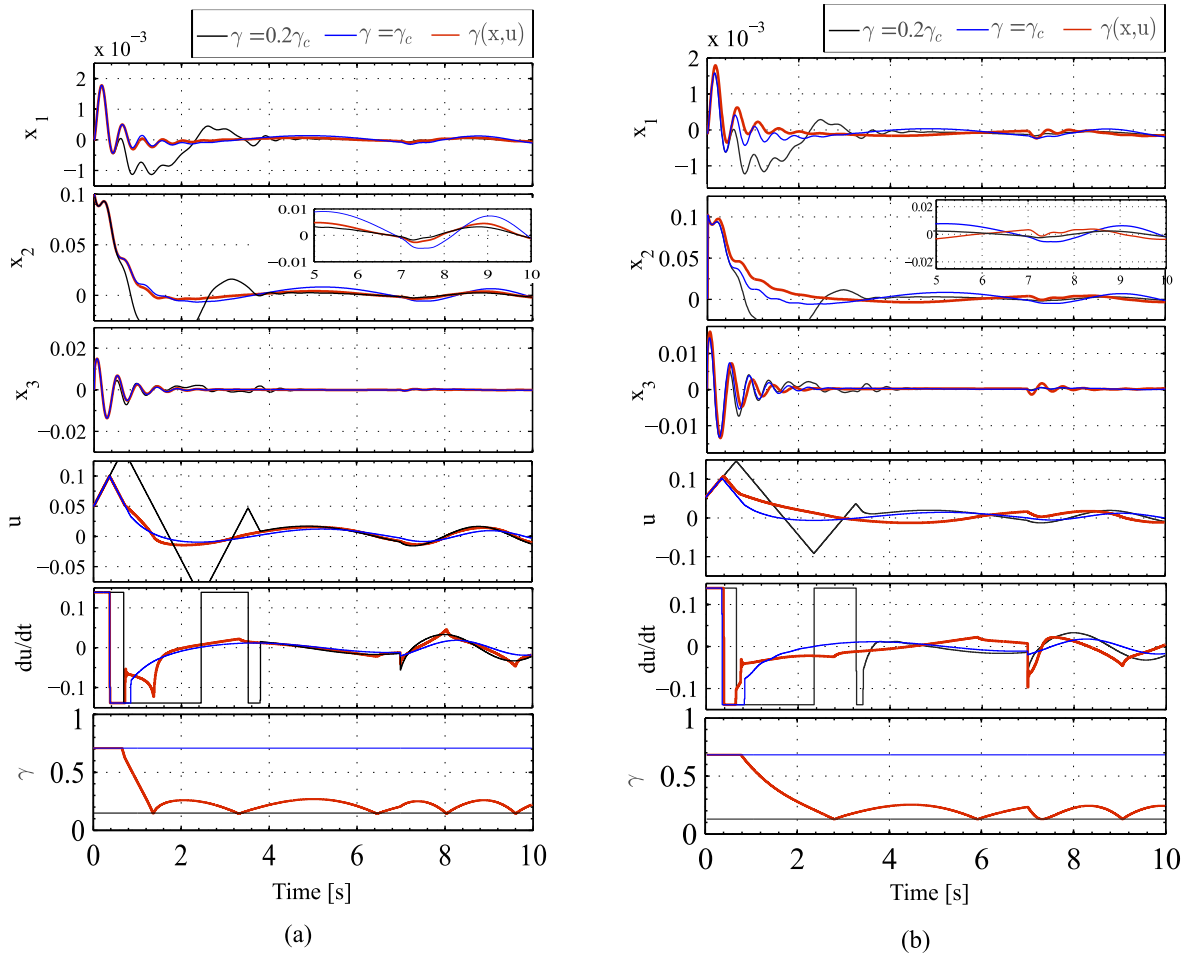

Figure 2.8: (a) Results of Example 2 with $\Delta \boldsymbol{A} = 0$, $\zeta = 0.0184\sin(t)$ from 0 to 7 s, and $\zeta = 0.0184\sin(2t)$ after 7 s. (b) Results of Example 2 with $\Delta \boldsymbol{A}$ indicated in (2.85) and ζ of the same setting as in (b).

2.5.3 Example 3

In this example, the proposed controller is compared with a previous discrete-time controller introduced by Palmeira et al. [1]. The plant considered in [1] is as follows.

$$\dot{\boldsymbol{x}} = \boldsymbol{A}\boldsymbol{x} + \boldsymbol{b}u_a + \boldsymbol{b}\zeta \tag{2.87}$$

$$\dot{u}_a = \mathrm{sat}_\beta\left(\frac{1}{\gamma_1}\left(-u_a + \mathrm{sat}_\alpha(u)\right)\right) \tag{2.88}$$

$$\zeta = 0.1\sin(t), \tag{2.89}$$

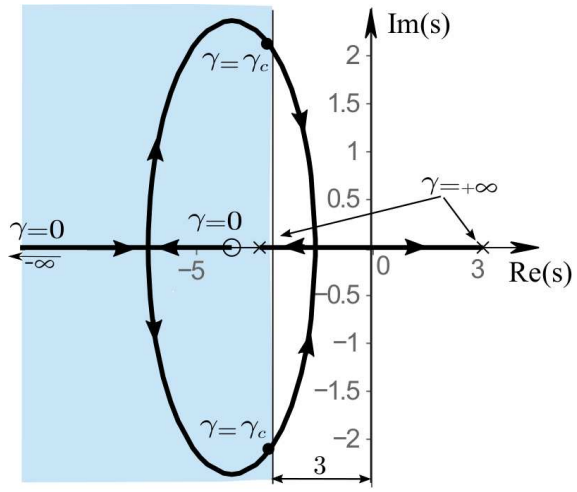

Figure 2.9: Example 3: The region $\mathcal{R}$ and the loci of $\mathrm{Eig}(\boldsymbol{A}_d(\gamma))$.

with the following controllable pair of matrices:

$$\boldsymbol{A} = \begin{bmatrix} 0 & 1 \\ 10 & -0.1 \end{bmatrix}, \quad \boldsymbol{b} = \begin{bmatrix} 0 \\ 1 \end{bmatrix}. \tag{2.90}$$

Here, (2.88) is regarded as an actuator having dynamics with the time constant γ_1 as in Fig. 2.1(a). The actuator provides the input u_a to the plant (2.87) and the control command u needs to be provided by the controller. The initial states are set as $\boldsymbol{x}_0 = [0.01, -0.24]^T$, and $u_{a0} = 1.2$. The actuator parameters are set as $\gamma_1 = 0.05$, $\alpha = 1$ and $\beta = 10$.

Palmeira et al.'s [1] controller is obtained by solving an optimization problem that maximizes the region of attraction with a given sampling interval $h \in [0.01, 0.07]$, without considering the existence of disturbance ζ. The obtained controller is written as follows:

$$u = \begin{bmatrix} -6.318 & -1.966 & 0.502 \end{bmatrix} \begin{bmatrix} \boldsymbol{x} \\ u_a \end{bmatrix}. \tag{2.91}$$

The proposed controller is applied to this example with neglecting the actuator dynamics (2.88). The requirements are assumed to place the eigenvalues of the overall system in the region $\Re(s) < -3$ and $\{q_1\} = \{-4\}$. By setting $h = 0.01$ and $L = 0.11$ to satisfy $|\zeta| < L$ and by using the proposed tuning guideline, the vector $\boldsymbol{c}$ and γ_c are obtained in the following procedure:

1. Set $\mathcal{R}$ as shown in Fig. 2.9, i.e., $\mathcal{R} = \{s \in \mathbb{C} \,|\, \Re(s) < -3\}$, and set $\{q_1\} = \{-4\}$ so that it resides in $\mathcal{R}$.

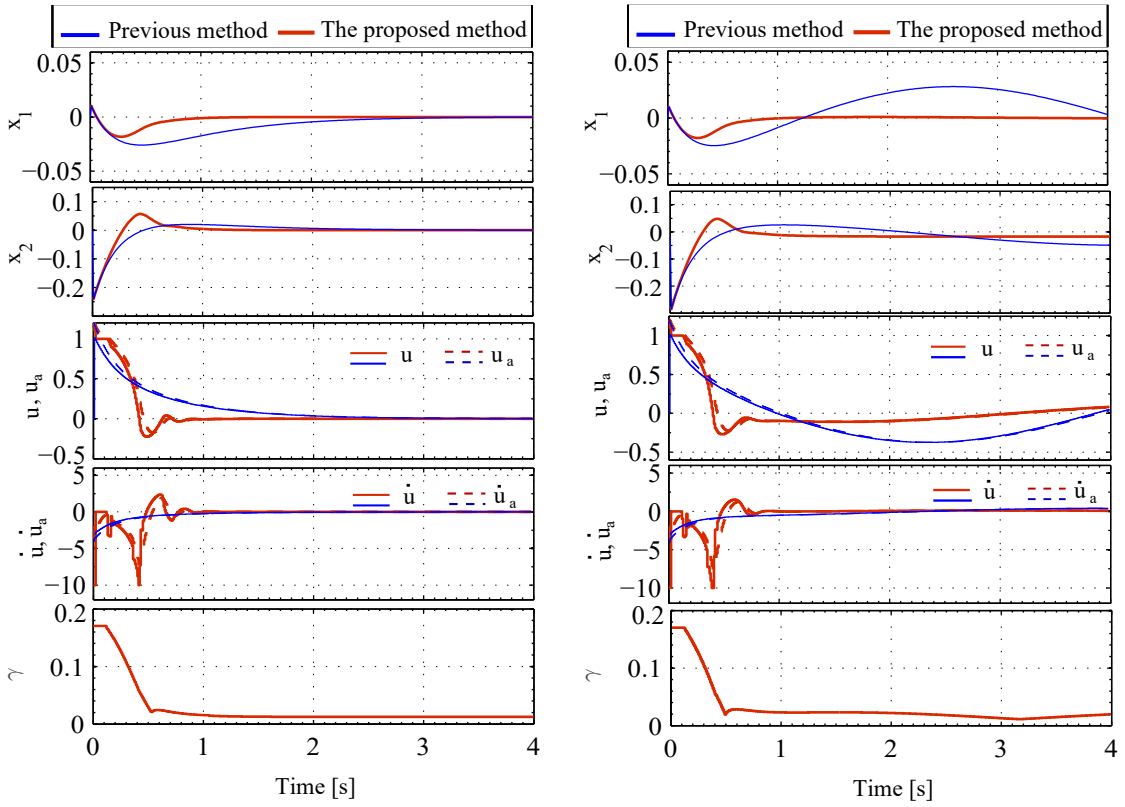

Figure 2.10: (a) Results of Example 3 with no disturbance, i.e., $\zeta = 0$. The red lines represent the results of the proposed controller. The blue lines represent the results of Palmeira et al.'s [1] controller. (b) Results of Example 3 with ζ indicated in (2.89). The red lines represent the results of the proposed controller. The blue lines represent the results of Palmeira et al.'s [1] controller.

2. To realize $\boldsymbol{T}\boldsymbol{b} = [0, 1]^T$, set $\boldsymbol{T} = \boldsymbol{I}$.

3. From (2.57), It is found that: $\bar{\boldsymbol{A}}_{11} = 0$, and $\bar{\boldsymbol{a}}_{12} = 1$.

4. By solving the pole placement problem to put $\mathrm{Eig}(\bar{\boldsymbol{A}}_{11} - \bar{\boldsymbol{a}}_{12}\bar{\boldsymbol{c}}_1^T)$ at $\{q_1\}$, It is found that $\bar{\boldsymbol{c}}_1 = 4$, and thus, $\boldsymbol{c} = [4, 1]^T$.

5. By drawing the loci of $\mathrm{Eig}(\boldsymbol{A} - \boldsymbol{b}\boldsymbol{c}^T/\gamma)$ as shown in Fig. 2.9, one can obtain $\gamma_c = 0.17$.

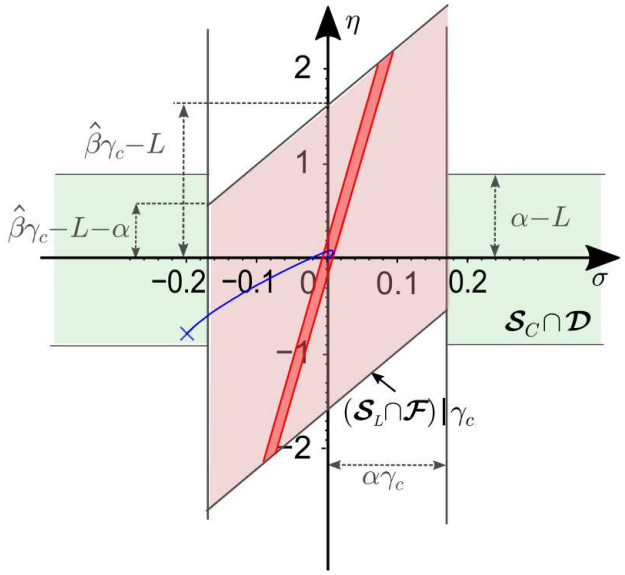

Figure 2.11: Example 3: The state trajectory (blue) in σ-η plane in case that $\zeta = 0.1\sin(t)$ and $\Delta\boldsymbol{A} = 0$. The light-coral region is $(\boldsymbol{\mathcal{S}} \cap \boldsymbol{\mathcal{F}})$ at $\gamma(\boldsymbol{x}, u) \equiv \gamma_c$, while the red region is $(\boldsymbol{\mathcal{S}} \cap \boldsymbol{\mathcal{F}})$ at $\gamma(\boldsymbol{x}, u) = 0.023$.

Fig. 2.10(a) and Fig. 2.10(b) compare the proposed controller with the previous controller introduced in [1]. Fig. 2.10(a) shows the results under no disturbance ($\zeta \equiv 0$), where the both controllers realize smooth convergence. Fig. 2.10(b) shows the results with non-vanishing disturbance $\zeta = 0.1\sin(t)$, where the proposed controller shows much better performance against the disturbance than the previous one. Fig. 2.11 shows the state trajectory in σ-η plane when the system is subjected to $\zeta = 0.1\sin(t)$. Here, the initial state lies in the portion $(\boldsymbol{\mathcal{S}}_C \cap \boldsymbol{\mathcal{D}})$, and the state trajectory moves towards the wider sliding patch $\boldsymbol{\mathcal{S}}_L \cap \boldsymbol{\mathcal{F}}$, i.e., $\gamma(\boldsymbol{x}, u)$ at its maximum γ_c. After that, the state trajectory stays at a neighborhood of the origin inside a smaller sliding patch, i.e., $\gamma(\boldsymbol{x}, u) = 0.023$.

The graphs in Fig. 2.10(a) and Fig. 2.10(b) show that there exists a significant lag between the actuator signals $\{u_a, \dot{u}_a\}$ and the controller signal $\{u, \dot{u}\}$, which is caused by the actuator dynamics (2.88). We can see that the proposed controller provides smooth and accurate convergence even under this lag.

2.6 Summary

This chapter has proposed a sliding mode-like controller that produces control signal with limitations on both its amplitude and its rate-of-change. This chapter is motivated by the idea of the ideal rate limiter, which involves the nested signum (sgn) function, while a saturation (sat) function has been used to produce limited control signal amplitude. The analysis of this sng-sat type controller shows that the closed-loop system reduces to a linear system in the sliding mode. Based on the analysis, a nonlinear parameter has been proposed so that the value of this parameter reduces when the state approaches the origin, and it contributes the reduction of the size of the terminal attractor. A tuning guideline for other controller parameters is also presented, which places the poles of the system in a given region in the complex plane. A discrete-time implementation of the proposed controller is also presented. This implementation does not produce chattering, which could be caused by other discretization schemes. The discrete-time implementation has been applied to three various systems to clarify the efficacy of the proposed controller and the influence of using the nonlinear function $\gamma(\boldsymbol{x}, u)$.

Chapter 3

Parameter Selection Procedure

3.1 Introduction

The controller proposed in Chapter 2 has two groups of parameters, i.e., the vector $\boldsymbol{c}$ and a positive scalar γ_c. Roughly speaking, the vector $\boldsymbol{c}$ governs the feedback gain for the case where the state is sufficiently close to the origin, and γ_c governs how far the region of attraction can be enlarged when the state is far from the origin. The previous chapter also proposed a tuning guideline for $\boldsymbol{c}$ and γ_c. Drawbacks of that previous procedure are that the vector $\boldsymbol{c}$ is chosen only based on the pole placement problem [58, 59] and that the reduction of the feedback gain is not explicitly intended. Moreover, the desired poles need to be given in advance. In addition, the tuning procedure of the parameter γ_c is not well sophisticated in that it requires the user to draw the loci of eigenvalues in the complex plane.

This chapter proposes a new design procedure for the proposed controller of Chapter 2. The new procedure explicitly attempts to realize low-gain control action, for enlarging the region of attraction, by reducing the norm of the vector $\boldsymbol{c}$. This chapter also employs a method to obtain γ_c without drawing the loci of eigenvalues, which is now incorporated in an automatic iterative algorithm. The proposed procedure is an iterative method in which a set of linear matrix inequalities (LMIs) [48] needs to be satisfied.

This chapter is organized as follows. Section 3.2 presents the proposed selection procedure in which the procedure of selecting $\boldsymbol{c}$ is explained in Section 3.2.2, while the procedure of selecting γ_c is explained in Sections 3.2.3 and 3.2.4. In Section 3.3, numerical examples illustrate the efficacy of the proposed method. Section 3.4 provides

[0]The content of this chapter is partially published in [57], namely, N. Baiomy and R. Kikuuwe. Parameter selection procedure for an amplitude- and rate-saturated controller. International Journal of Control, Automation and Systems, vol. 17, no. 4, pp. 926-935, 2019.

the summary of this chapter.

3.2 New parameter selection scheme

3.2.1 Design objectives

In the previous chapter, the controller (2.47)(2.48) was motivated by a consideration on the controller (2.47) with a fixed γ value. The behavior of the plant (2.1) combined with the controller (2.47) with a fixed γ is illustrated by using a three-dimensional subspace of the state space as shown in Fig. 2.2. The previous chapter has shown that the sliding mode takes place on the portion $\boldsymbol{\mathcal{S}}_C \cup (\boldsymbol{\mathcal{S}}_L \cap \boldsymbol{\mathcal{F}})$ of the switching surface. It has also be shown that the sliding mode on the linear portion $\boldsymbol{\mathcal{S}}_L \cap \boldsymbol{\mathcal{F}}$ requires the following condition:

$$\frac{|\boldsymbol{c}^T\boldsymbol{A}\boldsymbol{x} + \boldsymbol{c}^T\boldsymbol{b}u| + \boldsymbol{c}^T\boldsymbol{b}L}{\beta} < \gamma. \tag{3.1}$$

This shows that increasing γ enlarges the region in which the condition (3.1) is satisfied. Meanwhile, it has been shown that increasing γ enlarges the size of the finite-time attractor (indicated by the yellow ellipse in Fig. 2.2), which is a part of the linear portion $\boldsymbol{\mathcal{S}}_L$.

In Fig. 2.2(b), one can see that enlarging the linear region $\boldsymbol{\mathcal{S}}_L \cap \boldsymbol{\mathcal{F}}$ requires a smaller norm of the vector $\boldsymbol{c}$ and a larger value of γ. It is also required that the $\mathrm{Eig}(\boldsymbol{A} - \boldsymbol{b}\boldsymbol{c}^T/\gamma(\boldsymbol{x}, u))$ maintain inside a given desired region $\mathcal{R} \subset \mathbb{C}$ for all $\gamma(\boldsymbol{x}, u) \in [\gamma_{\min}, \gamma_c]$, where $\mathcal{R}$ is a subset of the left half-plane of the complex plane, and $\gamma_{\min}$ is the lowerbound of $\gamma(\boldsymbol{x}, u)$ defined as follows:

$$\gamma_{\min} \triangleq \boldsymbol{c}^T\boldsymbol{b}L/\beta, \tag{3.2}$$

in which $\boldsymbol{b}$ satisfies

$$\boldsymbol{b} = \begin{bmatrix} \boldsymbol{o}_{n-1} \\ 1 \end{bmatrix} \tag{3.3}$$

as has been introduced in Chapter 2.

Based on the above requirements, the design objectives are organized as follows:

- **Objective 1**: the vector norm $\|\boldsymbol{c}\|$ should be small,
- **Objective 2**: the eigenvalues of the matrix $\boldsymbol{A} - \boldsymbol{b}\boldsymbol{c}^T/\gamma$ should be located in the set $\mathcal{R}$ for all $\gamma \in [\gamma_{\min}, \gamma_c]$, and

- **Objective 3**: the upperbound γ_c should be large.

In the parameter tuning guideline of Chapter 2, the desired locations of $\lim_{\gamma \searrow 0} \mathrm{Eig}(\boldsymbol{A} - \boldsymbol{b}\boldsymbol{c}^T/\gamma)$ are given and the vector $\boldsymbol{c}$ is obtained by solving a pole placement problem without considering a smaller norm of $\boldsymbol{c}$ (i.e., see Theorem 2.4.1). Now, an LMI-based parameter selection procedure is introduced to obtain $\boldsymbol{c}$ with a small norm considering that the desired locations of $\lim_{\gamma \searrow 0} \mathrm{Eig}(\boldsymbol{A} - \boldsymbol{b}\boldsymbol{c}^T/\gamma)$ are not given.

3.2.2 The selection procedure of $\boldsymbol{c}$

When $\gamma(\boldsymbol{x}, u) = \gamma_{\min}$ and $\zeta = 0$, the plant (2.1) combined with the controller (2.47)(2.48) reduces to a linear system described as follows:

$$\dot{\boldsymbol{x}} = \boldsymbol{A}\boldsymbol{x} + \boldsymbol{b}u \tag{3.4}$$

$$u = -\boldsymbol{c}^T\boldsymbol{x}/\gamma_{\min}. \tag{3.5}$$

Objective 1 states that the norm of $\boldsymbol{c}$ should be set small. To take this point into account, let us consider the following cost function:

$$J \triangleq \int_0^\infty (\boldsymbol{x}^T\boldsymbol{Q}\boldsymbol{x} + \gamma_{\min}^2 R u^2)dt \tag{3.6}$$

where $\boldsymbol{Q} \in \mathbb{R}^{n\times n}$ is a positive definite matrix and $R \in \mathbb{R}$ is a positive constant. Because of (3.5), the cost function can be rewritten as follows:

$$J = \int_0^\infty \boldsymbol{x}^T(\boldsymbol{Q} + \boldsymbol{c}R\boldsymbol{c}^T)\boldsymbol{x}dt. \tag{3.7}$$

This cost function becomes small when both $\boldsymbol{x}$ and $\boldsymbol{c}$ are kept small. This feature justifies the inclusion of $\gamma_{\min}^2$ in the definition (3.6) of the cost function J.

Now, let us introduce the following lemma:

Lemma 3.2.1. *With the linear system (3.4)(3.5) with initial state $\boldsymbol{x}_0$, the cost function J defined in (3.6) is upperbounded as $J < \boldsymbol{x}_0^T\boldsymbol{P}\boldsymbol{x}_0$ if there exists a symmetric matrix $\boldsymbol{P} \in \mathbb{R}^{n\times n}$ that satisfies*

$$\boldsymbol{P} > 0 \tag{3.8}$$

$$\boldsymbol{P}(\boldsymbol{A} - \boldsymbol{b}\boldsymbol{c}^T/\gamma_{\min}) + (\boldsymbol{A} - \boldsymbol{b}\boldsymbol{c}^T/\gamma_{\min})^T\boldsymbol{P} + \boldsymbol{c}R\boldsymbol{c}^T + \boldsymbol{Q} < 0. \tag{3.9}$$

Proof. From the system (3.4)(3.5), we have the following differential equation:

$$\dot{\boldsymbol{x}} = (\boldsymbol{A} - \boldsymbol{b}\boldsymbol{c}^T/\gamma_{\min})\boldsymbol{x}, \quad \boldsymbol{x}(0) = \boldsymbol{x}_0. \tag{3.10}$$

Here, one can see that if positive definite matrices $\boldsymbol{P} \in \mathbb{R}^{n\times n}$, $\boldsymbol{Q} \in \mathbb{R}^{n\times n}$ and a positive scalar R satisfy (3.9), the followings are satisfied:

$$\frac{d}{dt}(\boldsymbol{x}^T\boldsymbol{P}\boldsymbol{x}) < -\boldsymbol{x}^T(\boldsymbol{Q}+\boldsymbol{c}R\boldsymbol{c}^T)x \tag{3.11}$$

$$\lim_{t\to\infty} \boldsymbol{x}^T\boldsymbol{P}\boldsymbol{x} = 0. \tag{3.12}$$

Therefore, one can see that

$$\begin{aligned} J &= \int_0^\infty \boldsymbol{x}^T(\boldsymbol{Q}+\boldsymbol{c}R\boldsymbol{c}^T)\boldsymbol{x}dt \\ &< \int_0^\infty -\frac{d}{dt}(\boldsymbol{x}^T\boldsymbol{P}\boldsymbol{x})dt = -\boldsymbol{x}^T\boldsymbol{P}\boldsymbol{x}\Big|_{t=0}^{t=\infty} = \boldsymbol{x}_0^T\boldsymbol{P}\boldsymbol{x}_0. \end{aligned} \tag{3.13}$$

This implies that, if there exists a symmetric matrix $\boldsymbol{P} \in \mathbb{R}^{n\times n}$ that satisfies (3.8) and (3.9), the cost function J is upperbounded by $J < \boldsymbol{x}_0^T\boldsymbol{P}\boldsymbol{x}_0$ where $\boldsymbol{x}_0$ is the initial value of $\boldsymbol{x}$. □

Now, for a given pair $\{\boldsymbol{Q}, R\}$, we are searching for $\{\boldsymbol{c}, \boldsymbol{P}, \gamma_{\min}\}$ that provides a small $\boldsymbol{x}_0^T\boldsymbol{P}\boldsymbol{x}_0$ under the inequality constraints (3.8)(3.9). One difficulty here is that the inequality (3.9) is nonlinear and cannot be transformed into an LMI because of the products of $\boldsymbol{c}$, $\boldsymbol{P}$, and $\gamma_{\min}^{-1}$. In addition, $\boldsymbol{c}$ and $\gamma_{\min}$ are constrained by (3.2), which implies that $\boldsymbol{c}$ is partitioned as

$$\boldsymbol{c} = [\boldsymbol{c}_1^T, c_2]^T. \tag{3.14}$$

Here, $\boldsymbol{c}_1 \in \mathbb{R}^{n-1}$ and $c_2 \triangleq \gamma_{\min}\beta/L$. Therefore, if one assumes that $\gamma_{\min}$ is given, the inequality (3.9) can be seen as a nonlinear matrix inequality with respect to an unknown vector-matrix pair $\{\boldsymbol{c}_1, \boldsymbol{P}\}$.

For the convenience of derivation, $\boldsymbol{A}$, $\boldsymbol{Q}$ and $\boldsymbol{P}$ are partitioned as follows:

$$\boldsymbol{A} = \begin{bmatrix} \boldsymbol{A}_{11} & \boldsymbol{A}_{12} \\ \boldsymbol{A}_{21} & A_{22} \end{bmatrix}, \quad \boldsymbol{Q} = \begin{bmatrix} \boldsymbol{Q}_1 & \boldsymbol{Q}_2 \\ * & Q_3 \end{bmatrix}, \quad \boldsymbol{P} = \begin{bmatrix} \boldsymbol{P}_{11} & \gamma_{\min}\tilde{\boldsymbol{P}}_{12} \\ * & \gamma_{\min}\tilde{P}_{22} \end{bmatrix} \tag{3.15}$$

where $\{\boldsymbol{A}_{11}, \boldsymbol{Q}_1, \boldsymbol{P}_{11}\} \subset \mathbb{R}^{(n-1)\times(n-1)}$, $\{\boldsymbol{A}_{12}, \boldsymbol{A}_{21}^T, \boldsymbol{Q}_2, \tilde{\boldsymbol{P}}_{12}\} \subset \mathbb{R}^{n-1}$, $\{A_{22}, Q_3, \tilde{P}_{22}\} \subset \mathbb{R}$, and the symbol $*$ inside a matrix stands for the transpose of its symmetric element. Then, the inequalities (3.8)(3.9) are rewritten as the following partitioned forms:

$$\begin{bmatrix} \boldsymbol{P}_{11} & \gamma_{\min}\tilde{\boldsymbol{P}}_{12} \\ * & \gamma_{\min}\tilde{P}_{22} \end{bmatrix} > 0 \tag{3.16}$$

$$\begin{bmatrix} \boldsymbol{L}_1 & \boldsymbol{L}_2 \\ * & L_3 \end{bmatrix} + \gamma_{\min}\begin{bmatrix} \bar{\boldsymbol{L}}_1 & \bar{\boldsymbol{L}}_2 \\ * & \bar{L}_3 \end{bmatrix} < 0 \tag{3.17}$$

where

$$\boldsymbol{L}_1 \triangleq \boldsymbol{P}_{11}\boldsymbol{A}_{11} + \boldsymbol{A}_{11}^T\boldsymbol{P}_{11} - \tilde{\boldsymbol{P}}_{12}\boldsymbol{c}_1^T - \boldsymbol{c}_1\tilde{\boldsymbol{P}}_{12}^T + \boldsymbol{c}_1 R\boldsymbol{c}_1^T + \boldsymbol{Q}_1 \tag{3.18}$$

$$\boldsymbol{L}_2 \triangleq \boldsymbol{P}_{11}\boldsymbol{A}_{12} - c_2\tilde{\boldsymbol{P}}_{12} - \boldsymbol{c}_1\tilde{P}_{22} + c_2 R\boldsymbol{c}_1 + \boldsymbol{Q}_2 \tag{3.19}$$

$$L_3 \triangleq -2c_2\tilde{P}_{22} + c_2^2 R + Q_3, \tag{3.20}$$

and

$$\bar{\boldsymbol{L}}_1 \triangleq \tilde{\boldsymbol{P}}_{12}\boldsymbol{A}_{21} + \boldsymbol{A}_{21}^T\tilde{\boldsymbol{P}}_{12}^T \tag{3.21}$$

$$\bar{\boldsymbol{L}}_2 \triangleq \tilde{\boldsymbol{P}}_{12}A_{22} + \boldsymbol{A}_{11}^T\tilde{\boldsymbol{P}}_{12} + \boldsymbol{A}_{21}^T\tilde{P}_{22} \tag{3.22}$$

$$\bar{L}_3 \triangleq \tilde{\boldsymbol{P}}_{12}^T\boldsymbol{A}_{12} + \tilde{P}_{22}A_{22} + \boldsymbol{A}_{12}^T\tilde{\boldsymbol{P}}_{12} + A_{22}\tilde{P}_{22}. \tag{3.23}$$

Let us consider using

$$\begin{bmatrix} \boldsymbol{L}_1 & \boldsymbol{L}_2 \\ * & L_3 \end{bmatrix} \leq 0 \tag{3.24}$$

as an approximation of (3.17). We can search for a quartet $\{\boldsymbol{c}_1, \boldsymbol{P}_{11}, \tilde{\boldsymbol{P}}_{12}, \tilde{P}_{22}\}$ satisfying the approximation (3.24), and then check whether the found quartet $\{\boldsymbol{c}_1, \boldsymbol{P}_{11}, \tilde{\boldsymbol{P}}_{12}, \tilde{P}_{22}\}$ satisfies the original inequalities (3.16)(3.17).

Now, let us decompose the inequality (3.24) into three inequalities using the following lemma, which is a slightly modified version of Lemma 1 in [60, 61]:

Lemma 3.2.2. *: For square matrices $\boldsymbol{M}_1$ and $\boldsymbol{M}_3$ and a matrix $\boldsymbol{M}_2$ with appropriate dimensions, the inequality*

$$\begin{bmatrix} \boldsymbol{M}_1 & \boldsymbol{M}_2 \\ \boldsymbol{M}_2^T & \boldsymbol{M}_3 \end{bmatrix} \leq 0 \tag{3.25}$$

holds true if there exist positive scalars δ_1 and δ_2 such that the following inequalities hold true:

$$\boldsymbol{M}_1 + \delta_1\boldsymbol{I} \leq 0 \tag{3.26}$$

$$\begin{bmatrix} -\frac{\delta_1}{\delta_2}\boldsymbol{I} & \boldsymbol{M}_2 \\ * & -\boldsymbol{I} \end{bmatrix} \leq 0 \tag{3.27}$$

$$\boldsymbol{M}_3 + \delta_2^{-1}\boldsymbol{I} \leq 0. \tag{3.28}$$

Proof. The matrix inequality (3.27) implies that

$$-\delta_1\boldsymbol{I} + \boldsymbol{M}_2(\delta_2\boldsymbol{I})\boldsymbol{M}_2^T \leq 0, \tag{3.29}$$

and the inequalities (3.26) and (3.28) imply

$$\boldsymbol{M}_1 \leq -\delta_1 \boldsymbol{I} < 0 \tag{3.30}$$

$$0 < -\boldsymbol{M}_3^{-1} \leq \delta_2 \boldsymbol{I}, \tag{3.31}$$

respectively. Therefore, we have

$$\boldsymbol{M}_1 - \boldsymbol{M}_2 \boldsymbol{M}_3^{-1} \boldsymbol{M}_2^T \leq 0. \tag{3.32}$$

Because $\boldsymbol{M}_3$ is negative definite and invertible due to (3.31), (3.32) implies (3.25) (see the Section "Schur complements for nonstrict inequalities" in [62, Chapter 2]). □

Then, the inequality (3.24) is satisfied if there exist $\delta_1 > 0$ and $\delta_2 > 0$ satisfying the following three inequalities:

$$\boldsymbol{L}_1 + \delta_1 \boldsymbol{I} \leq 0 \tag{3.33}$$

$$\begin{bmatrix} -\dfrac{\delta_1}{\delta_2}\boldsymbol{I} & \boldsymbol{L}_2 \\ * & -1 \end{bmatrix} \leq 0 \tag{3.34}$$

$$L_3 + 1/\delta_2 \leq 0. \tag{3.35}$$

Here, we can notice that (3.35) is a linear scalar inequality with respect to $\tilde{P}_{22}$, while (3.33) and (3.34) are nonlinear with respect to $\{\boldsymbol{c}_1, \boldsymbol{P}_{11}, \tilde{\boldsymbol{P}}_{12}, \tilde{P}_{22}\}$ due to the terms $\boldsymbol{c}_1 \tilde{\boldsymbol{P}}_{12}^T$, $\boldsymbol{c}_1 R \boldsymbol{c}_1^T$ and $\boldsymbol{c}_1 \tilde{P}_{22}$. The inequality (3.34), however, can be seen as linear with respect to $\{\boldsymbol{c}_1, \boldsymbol{P}_{11}, \tilde{\boldsymbol{P}}_{12}\}$, if we use $\tilde{P}_{22}$ obtained by (3.35).

Regarding the inequality (3.33), let us employ an approach presented in [60, 61] to relax it into the following matrix inequality:

$$\boldsymbol{L}_1 + \delta_1 \boldsymbol{I} + (\tilde{\boldsymbol{P}}_{12} - \boldsymbol{P}_{120}) R^{-1} (\tilde{\boldsymbol{P}}_{12} - \boldsymbol{P}_{120})^T \leq 0 \tag{3.36}$$

where $\boldsymbol{P}_{120} \in \mathbb{R}^{n-1}$ is given. Due to the fact that $R > 0$, the second term in the left-hand side of (3.36) is positive definite, and thus (3.36) is a sufficient condition of (3.33). Through a tedious but straightforward derivations, one can see that (3.36) is equivalent to the following LMI:

$$\begin{bmatrix} \Sigma_1 & \tilde{\boldsymbol{P}}_{12} R^{-1} - \boldsymbol{c}_1 \\ * & -R^{-1} \end{bmatrix} \leq 0 \tag{3.37}$$

where

$$\begin{aligned} \Sigma_1 \triangleq\ & \boldsymbol{P}_{11} \boldsymbol{A}_{11} + \boldsymbol{A}_{11}^T \boldsymbol{P}_{11} + \boldsymbol{Q}_1 + \delta_1 \boldsymbol{I} \\ & + \boldsymbol{P}_{120} R^{-1} \boldsymbol{P}_{120}^T - \tilde{\boldsymbol{P}}_{12} R^{-1} \boldsymbol{P}_{120}^T - \boldsymbol{P}_{120} R^{-1} \tilde{\boldsymbol{P}}_{12}^T \end{aligned} \tag{3.38}$$

because the left-hand side of (3.36) is the Schur complement of $-R^{-1}$ in the left-hand side of (3.37) [62, Chapter 2].

Now, the given vector $\boldsymbol{P}_{120}$ needs to be close to $\tilde{\boldsymbol{P}}_{12}$ to make the inequality (3.37) as less restrictive as the original nonlinear inequality (3.33). Therefore, let us minimize $\mathrm{tr}(\boldsymbol{P}_{11})$ subject to the LMIs (3.34)(3.37), and refine $\boldsymbol{P}_{120}$ by substituting it with the obtained $\tilde{\boldsymbol{P}}_{12}$. To make this iterative loops, there is a need to set an initial value for $\boldsymbol{P}_{120}$. One way to obtain a wild initial guess for the $\boldsymbol{P}_{120}$ is to choose a $\boldsymbol{c}$ with zero norm (extremely small norm) as an initial guess and find $\boldsymbol{P}_{120}$ and $\boldsymbol{P}_{110}$ satisfying

$$\boldsymbol{L}_1|_{\boldsymbol{c}_1=0,\boldsymbol{P}_{11}=\boldsymbol{P}_{110}} + \delta_1 \boldsymbol{I} = 0 \tag{3.39}$$

$$\boldsymbol{L}_2|_{\boldsymbol{c}_1=0,\boldsymbol{P}_{11}=\boldsymbol{P}_{110},\tilde{\boldsymbol{P}}_{12}=\boldsymbol{P}_{120}} = 0. \tag{3.40}$$

They are rewritten as

$$\boldsymbol{P}_{110}(\boldsymbol{A}_{11} - \epsilon \boldsymbol{I}) + (\boldsymbol{A}_{11} - \epsilon \boldsymbol{I})^T \boldsymbol{P}_{110} + \boldsymbol{Q}_1 + \delta_1 \boldsymbol{I} = 0 \tag{3.41}$$

$$\boldsymbol{P}_{110}\boldsymbol{A}_{12} - c_2 \boldsymbol{P}_{120} + \boldsymbol{Q}_2 = 0 \tag{3.42}$$

where ϵ is a small positive scalar and $\boldsymbol{P}_{110} > 0$. Now, (3.41) is easy to be solved because it is a continuous Lyapunov function, while the obtained $\boldsymbol{P}_{110}$ from the solution of (3.41) is used to obtain $\boldsymbol{P}_{120}$ as follows:

$$\boldsymbol{P}_{120} := (\boldsymbol{P}_{110}\boldsymbol{A}_{12} + \boldsymbol{Q}_2)/c_2 \tag{3.43}$$

in which c_2 is a scalar.

We have now the linear inequalities (3.37)(3.34)(3.35) involving given variables, which are $\{\boldsymbol{Q}, R, \delta_1, \delta_2, \gamma_{\min}, \boldsymbol{P}_{120}\}$, where (3.37) and (3.34) are LMIs with respect to $\{\boldsymbol{c}_1, \boldsymbol{P}_{11}, \tilde{\boldsymbol{P}}_{12}\}$, and (3.35) is a linear scalar inequality with respect to $\tilde{P}_{22}$. Because the matrix $\boldsymbol{P}$ determines an upperbound of the cost function J, it is needed to find a quartet $\{\boldsymbol{c}_1, \boldsymbol{P}_{11}, \tilde{\boldsymbol{P}}_{12}, \tilde{P}_{22}\}$ that provides small $\mathrm{tr}(\boldsymbol{P}_{11})$ and $\tilde{P}_{22}$ under the approximated linear inequality constraints (3.37)(3.34)(3.35). After finding such a quartet, we have to check whether it actually satisfies the original inequalities (3.16) (3.17) and the original eigenvalue requirement $\mathrm{Eig}(\boldsymbol{A} - \boldsymbol{b}\boldsymbol{c}^T/\gamma_{\min}) \subset \mathcal{R}$ as mentioned in Objective 2. If it does not, we need to try again with different values of $\{\gamma_{\min}, \delta_1, \delta_2\}$. This procedure is now written as the following algorithm.

Algorithm 1:

- **Step 1:** Select a quartet of positive scalars $\{\delta_1, \delta_2, \gamma_{\min}, R\}$ and a symmetric positive definite matrix $\boldsymbol{Q}$.
- **Step 2:** Set $c_2 := \gamma_{\min}\beta/L$.

- **Step 3:** Find the minimum of $\tilde{P}_{22}$ subject to (3.35). By noting that (3.35) is equivalent to

$$\tilde{P}_{22} \geq \frac{c_2^2 R + Q_3 + \delta_2^{-1}}{2c_2}, \tag{3.44}$$

  the minimum value of $\tilde{P}_{22}$ that satisfies the above inequality is obtained as:

$$\tilde{P}_{22} := \frac{c_2^2 R + Q_3 + \delta_2^{-1}}{2c_2}. \tag{3.45}$$

- **Step 4:** Solve (3.41) with respect to $\boldsymbol{P}_{110}$ and set $\boldsymbol{P}_{120} := (\boldsymbol{P}_{110}\boldsymbol{A}_{12} + \boldsymbol{Q}_2)/c_2$, as an initial guess for $\tilde{\boldsymbol{P}}_{12}$ (see Appendix C).

- **Step 5:** Find the set $\{\boldsymbol{c}_1, \boldsymbol{P}_{11}, \tilde{\boldsymbol{P}}_{12}\}$ that minimizes $\mathrm{tr}(\boldsymbol{P}_{11})$ subject to (3.34) and (3.37), which are LMIs with respect to $\{\boldsymbol{c}_1, \boldsymbol{P}_{11}, \tilde{\boldsymbol{P}}_{12}\}$, with $\boldsymbol{P}_{120}$ obtained in Step 4.

- **Step 6:** Set $\boldsymbol{P}_{120} := \tilde{\boldsymbol{P}}_{12}$ and repeat Step 5 until $\mathrm{tr}(\boldsymbol{P}_{11})$ converges to a certain value.

- **Step 7:** Check whether the conditions (3.16), (3.17), and $\mathrm{Eig}(\boldsymbol{A}-\boldsymbol{b}\boldsymbol{c}^T/\gamma_{\min}) \subset \mathcal{R}$ are satisfied. If not, repeat the algorithm with different values of $\{\delta_1, \delta_2, \gamma_{\min}\}$. If yes, set $\boldsymbol{c} := [\boldsymbol{c}_1^T, c_2]^T$.

It should be noted that, although this algorithm tends to provide small $\mathrm{tr}(\boldsymbol{P}_{11})$ and P_{22}, it is not a minimization algorithm in a strict sense.

With regards to choosing a value of the parameter γ_c, Chapter 2 proposed a method in which the loci of $\mathrm{Eig}(\boldsymbol{A} - \boldsymbol{b}\boldsymbol{c}^T/\gamma(\boldsymbol{x}, u))$ are drawn and the critical value γ_c is found manually. This chapter introduces two new methods to obtain γ_c automatically. One is a general method and it employs an iterative computation to locate $\mathrm{Eig}(\boldsymbol{A}-\boldsymbol{b}\boldsymbol{c}^T/\gamma(\boldsymbol{x}, u))$ inside a specific region in the left half of the complex plane. The second is used when there is no specific requirements on the loci of $\mathrm{Eig}(\boldsymbol{A}-\boldsymbol{b}\boldsymbol{c}^T/\gamma(\boldsymbol{x}, u))$ inside the left half of the complex plane.

3.2.3 Selection procedure of γ_c: Method A

Regarding Objective 2 and Objective 3, detailed in Section 3.2.1, Method A is searching for the maximum γ_c with which $\mathrm{Eig}(\boldsymbol{A}_d(\gamma_c))$ are inside $\mathcal{R}$. Let us assume that the region $\mathcal{R}$ is given in the following form:

$$\mathcal{R} = \{s \in \mathbb{C} \,|\, \boldsymbol{N} + s\boldsymbol{M} + \bar{s}\boldsymbol{M}^T < 0\} \tag{3.46}$$

where $\boldsymbol{M}$ and $\boldsymbol{N}$ are real matrices and $\boldsymbol{N} = \boldsymbol{N}^T$. This representation of regions in the complex plane has been proposed by Chilali and Gahinet [63, Definition 2.1]. Some examples for the matrix values of $\boldsymbol{M}$ and $\boldsymbol{N}$ are given as follows:

- for $\mathcal{R} = \{s \in \mathbb{C} \,|\, \cos(\arg(s)) \leq -\cos(\theta)\}$:

$$\boldsymbol{M} = \begin{bmatrix} \sin(\theta) & -\cos(\theta) \\ \cos(\theta) & \sin(\theta) \end{bmatrix}, \quad \boldsymbol{N} = 0_{2\times 2}, \tag{3.47}$$

- for $\mathcal{R} = \{s \in \mathbb{C} \,|\, \Re(s) \leq -\alpha_r\}$:

$$\boldsymbol{M} = 1, \quad \boldsymbol{N} = 2\alpha_r, \tag{3.48}$$

- for $\mathcal{R} = \{s \in \mathbb{C} \,|\, \Re(s) \leq -\alpha_r \wedge \cos(\arg(s)) \leq -\cos(\theta)\}$:

$$\boldsymbol{M} = \begin{bmatrix} \sin(\theta) & -\cos(\theta) & 0 \\ \cos(\theta) & \sin(\theta) & 0 \\ 0 & 0 & 1 \end{bmatrix}, \quad \boldsymbol{N} = \begin{bmatrix} \boldsymbol{o}_{2\times 2} & 0 \\ 0 & 2\alpha_r \end{bmatrix}. \tag{3.49}$$

From [63, 64], it can be seen that $\mathrm{Eig}(\boldsymbol{A}_d(\gamma)) \subset \mathcal{R}$ if and only if there exists a symmetric positive definite matrix $\boldsymbol{X}$ that satisfies

$$\boldsymbol{N} \otimes \boldsymbol{X} + \boldsymbol{M} \otimes (\boldsymbol{X}\boldsymbol{A}_d(\gamma)) + \boldsymbol{M}^T \otimes (\boldsymbol{A}_d^T(\gamma)\boldsymbol{X}) < 0 \tag{3.50}$$

where $\otimes$ denotes the Kronecker product. Here, we have to note that the inequality (3.50) is an LMI with respect to $\boldsymbol{X}$ for a fixed γ. In order to obtain γ_c with which (3.50) is satisfied for all $\gamma \in [\gamma_{\min}, \gamma_c]$, let us employ an iterative loop searching for $\boldsymbol{X} > 0$ that satisfies (3.50) at every single loop with a given incremental value of γ. Starting with $\gamma \equiv \gamma_{\min}$, the value of γ is gradually increased and the loop is repeated as long as we can find $\boldsymbol{X} > 0$ that satisfies (3.50). Once we fail to find such $\boldsymbol{X}$, the repeated loop is broken and the critical value of γ is chosen as γ_c.

3.2.4 Selection procedure of γ_c: Method B

The following method is introduced to directly obtain the upperbound γ_c without iterative computation. This method is only valid in case where the desired region $\mathcal{R}$ coincides with the whole left half of the complex plane $\mathbb{C}_-$.

Fuller [65, Section 13] has studied systems' stability under variable parameters, where a system is known to be stable for certain values of this parameter, and the problem is to find how far these parameter can be changed without losing the stability. For such a case, Fuller has introduced two necessary conditions with which the system

is within the stability region. Fuller called these conditions by "a critical criteria", which is derived from his theorem [65, Theorem 9] to check the Hurwitzness of a matrix via calculating the bialternate sum of the same matrix itself.

In the same light, the condition $\mathrm{Eig}(\boldsymbol{A}-\boldsymbol{b}\boldsymbol{c}^T/\gamma_{\min}) \subset \mathcal{R}$ in Algorithm 1 (i.e., Step 7) shows that the matrix $\boldsymbol{A}_d(\gamma)$ defined in (2.52) is already Hurwitz when $\gamma \equiv \gamma_{\min}$, and the problem here is to find the critical value of γ that keeps the Hurwitzness of $\boldsymbol{A}_d(\gamma)$. Fuller's Theorem 9 [65] and Fuller' derivation in Section Critical Criteria [65, Section 13] can be merged and written in the following theorem:

Theorem 3.2.1. *An n-dimensional square matrix $\boldsymbol{X}$ is Hurwitz if and only if the following two conditions are satisfied:*

$$(-1)^n \det[\boldsymbol{X}] > 0 \tag{3.51}$$

$$(-1)^{n(n-1)/2} \det[G[\boldsymbol{X}]] > 0 \tag{3.52}$$

where $G[\boldsymbol{X}]$ is an $n(n-1)/2$-dimensional square matrix defined as follows:

$$G[\boldsymbol{X}] = \boldsymbol{X} \otimes \boldsymbol{I}_{n\times n} + \boldsymbol{I}_{n\times n} \otimes \boldsymbol{X}. \tag{3.53}$$

Proof. See [65, Section 13]. □

Here, it should be noted that $G[\boldsymbol{X}]$ is often referred to as the bialternate sum of $\boldsymbol{X}$ with itself. Following this theorem, one can obtain the following corollary:

Corollary 3.2.1. *With the square matrix $\boldsymbol{A}_d(\gamma)$ defined in (2.52), let us assume that it is already Hurwitz with $\gamma = \gamma_{\min}$. Then, $\boldsymbol{A}_d(\gamma)$ is Hurwitz if $\gamma_{\min} \leq \gamma \leq \min(\gamma_{c1}, \gamma_{c2})$ where γ_{c1} and γ_{c2} are the values of γ with which*

$$(-1)^n \det[\boldsymbol{A}_d(\gamma)] = 0 \tag{3.54}$$

$$(-1)^{n(n-1)/2} \det[G[\boldsymbol{A}_d(\gamma)]] = 0, \tag{3.55}$$

are satisfied, respectively.

Following this Corollary, it is founded that the upper limit of γ, which is defined by γ_c in this dissertation, is obtained as follows:

$$\gamma_c \equiv \min(\gamma_{c1}, \gamma_{c2}). \tag{3.56}$$

The next sections will show how to obtain γ_{c1} and γ_{c2} that respectively satisfy the conditions (3.54) and (3.55).

3.2.5 Fuller's first condition of Hurwitzness

Now, let us obtain the value of γ that satisfies the first condition (3.54). Considering the partition forms of $\boldsymbol{A}$ and $\boldsymbol{c}$ in (3.15) and (3.14), respectively, let us partition $\boldsymbol{A}_d(\gamma)$ as follows:

$$\boldsymbol{A}_d(\gamma) = \begin{bmatrix} \boldsymbol{A}_{11} & \boldsymbol{A}_{12} \\ \boldsymbol{A}_{21} - \boldsymbol{c}_1^T/\gamma & A_{22} - c_2/\gamma \end{bmatrix}. \tag{3.57}$$

Following the properties of matrices' determinant [66, Section 2.4], one can see that

$$\det[\boldsymbol{A}_d(\gamma)] \equiv \gamma^{-1} \det\left[\begin{bmatrix} \boldsymbol{A}_{11} & \boldsymbol{A}_{12} \\ -\boldsymbol{c}_1^T & -c_2 \end{bmatrix} + \gamma \begin{bmatrix} 0 & 0 \\ \boldsymbol{A}_{21} & A_{22} \end{bmatrix}\right] \tag{3.58}$$

$$\equiv \gamma^{-1} \det[\boldsymbol{E}_1 + \gamma \boldsymbol{F}_1], \tag{3.59}$$

in which

$$\boldsymbol{E}_1 = \begin{bmatrix} \boldsymbol{A}_{11} & \boldsymbol{A}_{12} \\ -\boldsymbol{c}_1^T & -c_2 \end{bmatrix}, \quad \boldsymbol{F}_1 = \begin{bmatrix} 0 & 0 \\ \boldsymbol{A}_{21} & A_{22} \end{bmatrix}. \tag{3.60}$$

Because $\boldsymbol{c}$ is designed so that $\boldsymbol{c}^T\boldsymbol{b} > 0$, the matrix $\boldsymbol{A}_d(\gamma)$ is Hurwitz when $\gamma \searrow 0$. Thus, condition (3.51) implies that:

$$\lim_{\gamma \searrow 0} \; (-1)^n \gamma^{-1} \det[\boldsymbol{E}_1 + \gamma \boldsymbol{F}_1] > 0, \tag{3.61}$$

which reduces to

$$(-1)^n \det[\boldsymbol{E}_1] > 0. \tag{3.62}$$

Now, let us rewrite the condition (3.54) as follows:

$$(-1)^n \gamma^{-1} \det[\boldsymbol{E}_1(\boldsymbol{I} + \gamma \boldsymbol{F}_1 \boldsymbol{E}_1^{-1})] = 0 \tag{3.63}$$

which is reduced to

$$\det[\boldsymbol{I} + \gamma \boldsymbol{F}_1 \boldsymbol{E}_1^{-1}] = 0 \tag{3.64}$$

because of (3.62). By defining λ_{m1} as the minimum real eigenvalue of $(\boldsymbol{F}_1\boldsymbol{E}_1^{-1})$, the critical value γ_{c1} that satisfy (3.54) is obtained as follows:

$$\gamma_{c1} = \begin{cases} \infty & \text{if } \lambda_{m1} > 0 \\ -1/\lambda_{m1} & \text{if } \lambda_{m1} < 0. \end{cases} \tag{3.65}$$

3.2.6 Fuller's second condition of Hurwitzness

Now, let us obtain the critical value of γ that satisfies the second condition (3.55). For simplicity, each element in $G[\boldsymbol{A}_d(\gamma)]$ can be separately calculated as:

$$g_{pq,rs} = \begin{vmatrix} a_{dpr} & a_{dps} \\ \delta_{qr} & \delta_{qs} \end{vmatrix} + \begin{vmatrix} \delta_{pr} & \delta_{ps} \\ a_{dqr} & a_{dqs} \end{vmatrix} \tag{3.66}$$

where a_{dij} denotes the (i,j)-th element of the matrix $\boldsymbol{A}_d(\gamma)$. The labels pq and rs are the label of rows and columns of $G[A_d(\gamma)]$, respectively with the following values; $p = 2, 3, \ldots, n$, $q = 1, 2, \ldots, p-1$, $r = 2, 3, \ldots, n$ and $s = 1, 2, \ldots, r-1$ (i.e., when n=3, the elements of the first raw are $\{g_{21,21}, g_{21,31}, g_{21,32}\}$, the elements of the second raw are $\{g_{31,21}, g_{31,31}, g_{31,32}\}$ and the elements of the last raw are $\{g_{32,21}, g_{32,31}, g_{32,32}\}$). The operator δ_{ij} stands for the Kronecker delta, which is defined as follows:

$$\delta_{ij} \triangleq \begin{cases} 0 & \text{if } i \neq j \\ 1 & \text{if } i = j. \end{cases} \tag{3.67}$$

Through a tedious but straightforward derivations, one can determine $\det[G[\boldsymbol{A}_d(\gamma)]]$ as follows:

$$\det[G[\boldsymbol{A}_d(\gamma)]] = \gamma^{-l} \det[\boldsymbol{E}_2 + \gamma \boldsymbol{F}_2] \tag{3.68}$$

where $l = -(n-1)$, and each element of the matrices $\boldsymbol{E}_2$ and $\boldsymbol{F}_2$ can be respectively obtained as follows:

$$e_{pq,rs} = \begin{cases} \begin{vmatrix} a_{pr} & a_{ps} \\ \delta_{qr} & \delta_{qs} \end{vmatrix} + \begin{vmatrix} \delta_{pr} & \delta_{ps} \\ a_{qr} & a_{qs} \end{vmatrix} & \text{if } p \leq n_1, \text{or } q > n_1 \\ \begin{vmatrix} \bar{c}_{pr} & \bar{c}_{ps} \\ \delta_{qr} & \delta_{qs} \end{vmatrix} & \text{otherwise} \end{cases} \tag{3.69}$$

$$f_{pq,rs} = \begin{cases} 0 & \text{if } p \leq n_1, \text{or } q > n_1 \\ \begin{vmatrix} a_{pr} & a_{ps} \\ \delta_{qr} & \delta_{qs} \end{vmatrix} + \begin{vmatrix} \delta_{pr} & \delta_{ps} \\ a_{qr} & a_{qs} \end{vmatrix} & \text{otherwise ,} \end{cases} \tag{3.70}$$

in which a_{ij} denotes the (i,j)-th element of the matrix $\boldsymbol{A}$, and $\bar{c}_{ij}$ denotes the (i,j)-th element of the matrix $\bar{\boldsymbol{c}}$, which is defined as $\bar{\boldsymbol{c}} \triangleq -[\boldsymbol{o}_{n-1}^T, 1]^T \boldsymbol{c}^T$. The configuration (3.68) is similar to the one that have been developed by Sen and Datta [67], while the definitions of $\boldsymbol{E}_2$ and $\boldsymbol{F}_2$ here are different due to the configuration of the matrix $\boldsymbol{A}_d(\gamma)$. As an illustrative example for the calculation of $G[\boldsymbol{A}_d(\gamma)]$, $\boldsymbol{E}_2$ and $\boldsymbol{F}_2$, let us consider a matrix with $n = 3$, and $\boldsymbol{c}^T \equiv [c_{11}, c_{12}, c_2]$. Then, $G[\boldsymbol{A}_d(\gamma)]$ is calculated as follows:

$$G[\boldsymbol{A}_d(\gamma)] = \begin{bmatrix} a_{11} + a_{22} & a_{23} & -a_{13} \\ a_{32} - c_{12}/\gamma & a_{11} + a_{33} - c_2/\gamma & a_{12} \\ -a_{31} + c_{11}/\gamma & a_{21} & a_{22} + a_{33} - c_2/\gamma \end{bmatrix}, \tag{3.71}$$

and $\boldsymbol{E}$ and $\boldsymbol{F}$ are calculated as follows:

$$\boldsymbol{E}_2 = \begin{bmatrix} a_{11}+a_{22} & a_{23} & -a_{13} \\ -c_{12} & -c_2 & 0 \\ c_{11} & 0 & -c_2 \end{bmatrix} \tag{3.72}$$

$$\boldsymbol{F}_2 = \begin{bmatrix} 0 & 0 & 0 \\ a_{32} & a_{11}+a_{33} & a_{12} \\ -a_{31} & a_{21} & a_{22}+a_{33} \end{bmatrix}. \tag{3.73}$$

Because the matrix $\boldsymbol{A}_d(\gamma)$ is Hurwitz when $\gamma \searrow 0$, where $\boldsymbol{c}^T\boldsymbol{b} > 0$, the condition (3.52) implies that:

$$\lim_{\gamma \searrow 0} \; (-1)^{n(n-1)/2}\gamma^{-l} \det[\boldsymbol{E}_2 + \gamma \boldsymbol{F}_2] > 0, \tag{3.74}$$

which reduces to

$$(-1)^{n(n-1)/2} \det[\boldsymbol{E}_2] > 0. \tag{3.75}$$

Now, let us rewrite (3.55) as follows:

$$(-1)^{n(n-1)/2}\gamma^{-l} \det[\boldsymbol{E}_2(\boldsymbol{I} + \gamma \boldsymbol{F}_2\boldsymbol{E}_2^{-1})] = 0, \tag{3.76}$$

which is reduced to

$$\det[\boldsymbol{I} + \gamma \boldsymbol{F}_2\boldsymbol{E}_2^{-1}] = 0 \tag{3.77}$$

because of (3.75) and $\gamma^{-l} > 0$. By defining λ_{m2} as the minimum real eigenvalue of $(\boldsymbol{F}_2\boldsymbol{E}_2^{-1})$, the critical bound γ_{c2} that satisfy (3.55) is obtained as follows:

$$\gamma_{c2} = \begin{cases} \infty & \text{if } \lambda_{m2} > 0 \\ -1/\lambda_{m2} & \text{if } \lambda_{m2} < 0, \end{cases} \tag{3.78}$$

Finally, γ_c is obtained as follows:

$$\gamma_c \equiv \min(\gamma_{c1}, \gamma_{c2}). \tag{3.79}$$

3.2.7 The complete selection procedure of $\{\boldsymbol{c}, \gamma_c\}$

After proposing the aforementioned methods to obtain the controller parameters $\{\boldsymbol{c}, \gamma_c\}$, one can see that the obtained γ_c by any of Method A or Method B depends on the vector $\boldsymbol{c}$. This implies that we may find $\boldsymbol{c}$ and γ_c with a smaller norm of $\boldsymbol{c}/\gamma_c$ by searching wider ranges of the sets $\{\delta_1, \delta_2, \gamma_{\min}\}$. Therefore, the complete selection procedure to obtain the controller parameters is shown in the flowchart of Fig. 3.1, which includes some nested iterative loops. It should again be noted that, as Algorithm 1 is not a strict minimization algorithm, the overall selection procedure in Fig. 3.1 is not a strict optimization procedure either.

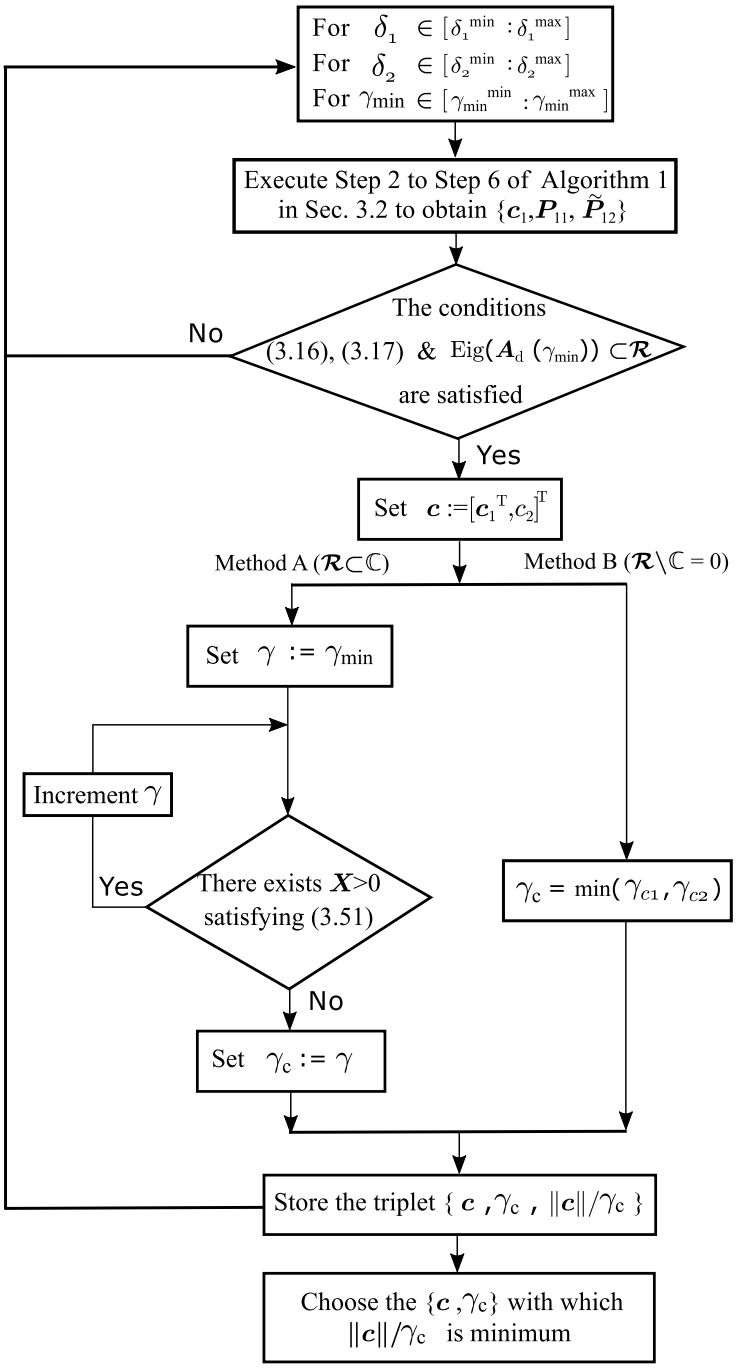

Figure 3.1: The overall flowchart of the proposed selection procedure.

Remark 3.2.1. *This chapter presents a modification version of the selection procedure proposed by Baiomy and Kikuuwe [68]. The main modification lies in the procedure to obtain γ_c, where γ_c is obtained via repeated loop containing an inequality constraints as shown in Method A or by directly solving mathematical equations as in Method B, while the method in [68] obtains γ_c by drawing the loci of all the eigenvalues of the system with different values of γ, similar to the method proposed in Chapter 2. This modification allows the realization of the outer iterative loop of the flowchart in Fig. 3.1, which automatically searches for smaller norm of $\boldsymbol{c}/\gamma_c$ within given ranges of inputs. The selection procedure of this Chapter includes a condition to examine that* $\mathrm{Eig}(\boldsymbol{A} - \boldsymbol{b}\boldsymbol{c}^T/\gamma_{\min}) \subset \mathcal{R}$*, while in [68], it only guarantees the Hurwitzness of the matrix* $(\boldsymbol{A} - \boldsymbol{b}\boldsymbol{c}^T/\gamma_{\min})$.

3.3 Examples

3.3.1 Example 1

A third-order system proposed in [35] is considered here with a sinusoidal disturbance as follows:

$$\dot{\boldsymbol{x}} = \begin{bmatrix} -0.2 & 1 & 0 \\ 0 & -0.2 & 1 \\ 0 & 0 & -0.2 \end{bmatrix} \boldsymbol{x} + \begin{bmatrix} 0 \\ 0 \\ -1 \end{bmatrix} (u + \zeta) \tag{3.80}$$

$$\zeta = 0.01 \sin(t). \tag{3.81}$$

The control input u is under the limitations of $|u| \leq 0.6$ and $|\dot{u}| \leq 0.3$. The initial states are $\boldsymbol{x}_0 = [-1, -1, 1]^T$ and $u_0 = 0$, and the desired region is given as $\mathcal{R} = \{s \in \mathbb{C} \mid \cos(\arg(s)) \leq -0.7\}$.

In order to have the vector $\boldsymbol{b}$ of the form of (3.3), the transformation matrix $\boldsymbol{T} = -\boldsymbol{I}$ is used to transform the pair $(\boldsymbol{A}, \boldsymbol{b})$ into $(\boldsymbol{A}_T, [0, 0, 1]^T)$, where $\boldsymbol{A}_T = \boldsymbol{T}\boldsymbol{A}\boldsymbol{T}^{-1}$ and $[0, 0, 1]^T = \boldsymbol{T}\boldsymbol{b}$. The inputs of the procedure of Fig. 3.1 are selected as follows; $\delta_1 \in [10^{-5}, 1]$, $\delta_2 \in [0.06, 4]$, $\gamma_{\min} \in [0.01, 0.1]$, $\boldsymbol{A}_T = \boldsymbol{T}\boldsymbol{A}\boldsymbol{T}^{-1}$, $\beta = 0.3$, $L = 0.011$, $R = 1$, and $\boldsymbol{Q} = \boldsymbol{I}$. The obtained controller parameters are $\boldsymbol{c}^T\boldsymbol{T}^{-1} = [0.5568, 1.6346, 3.6734]$ and $\gamma_c = 2.5353$ with $\delta_1 = 10^{-5}$, $\delta_2 = 0.08$, $\gamma_{\min} = 0.1347$, $\tilde{P}_{22} = 3.6742$, $\tilde{\boldsymbol{P}}_{12} = [-0.5569, -1.6350]^T$, and $\boldsymbol{P}_{11} = \begin{bmatrix} 1.7252 & 2.0365 \\ 2.0365 & 6.0020 \end{bmatrix}$. The simulations are performed with the discrete-time algorithm (2.74)(2.75)(2.76) with the sampling interval $h = 0.01$.

The simulation results are shown in Fig. 3.2. Here, we can see that $\gamma(x, u)$ with the designed values of the parameter set $\{\boldsymbol{c}, \gamma_c\}$ realizes accurate convergence. This

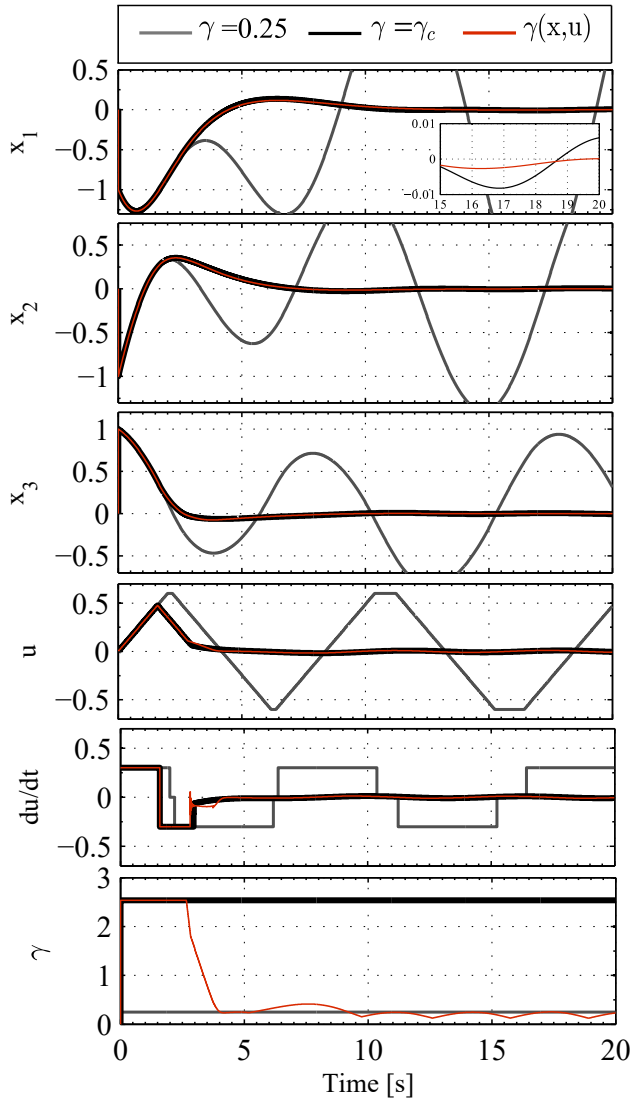

Figure 3.2: Example 1: Simulation results with different values of γ.

figure also includes the results with two constant γ values. The larger γ value realizes convergence but it is less accurate than that of $\gamma(\boldsymbol{x}, u)$, as indicated in the small panel in the graph. The state with the smaller constant γ goes unstable although this smaller constant $\gamma = 0.25$ is larger than $\gamma_{\min}$.

3.3.2 Example 2

Here, the proposed controller is applied to a second order system adopted in [13, 46]. The controlled plant (2.1) is with the following matrices:

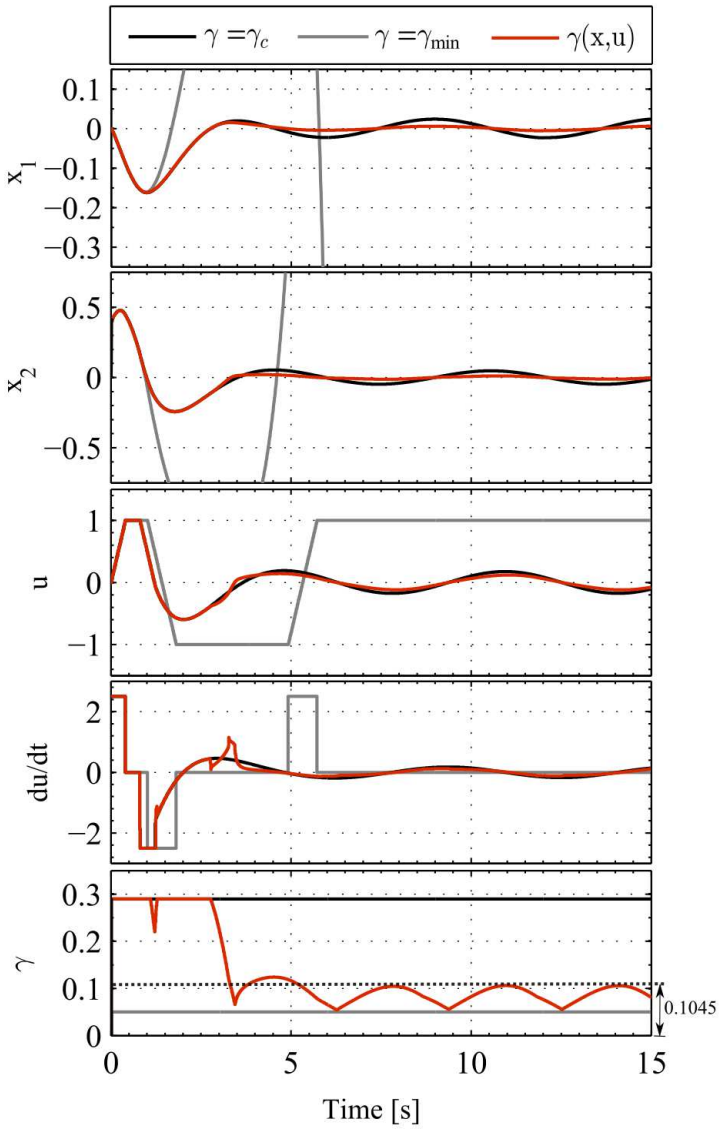

Figure 3.3: Example 2: Simulation results with the initial conditions $\boldsymbol{x}_0 = [0, 0.4]^T$ and $u_0 = 0$ and different values of γ.

$$\boldsymbol{A} = \begin{bmatrix} 0 & -0.5 \\ 1 & 1.5 \end{bmatrix}, \quad \boldsymbol{b} = \begin{bmatrix} 0 \\ -1 \end{bmatrix}, \tag{3.82}$$

and is subjected to the following disturbance:

$$\zeta = 0.1 \sin(t). \tag{3.83}$$

The control input u is limited as $|u| \leq 1$ and $|\dot{u}| \leq 2.5$. The desired region is given as $\mathcal{R} = \{s \in \mathbb{C} \,|\, \Re(s) \leq -0.49 \wedge \cos(\arg(s)) \leq -0.7\}$.

In order to have the vector $\boldsymbol{b}$ of the form of (3.3), we can use the transformation matrix $\boldsymbol{T} = -\boldsymbol{I}$ to transform the pair $(\boldsymbol{A}, \boldsymbol{b})$ into $(\boldsymbol{A}_T, [0,1]^T)$, where $\boldsymbol{A}_T = \boldsymbol{T}\boldsymbol{A}T^{-1}$ and $[0,1]^T = \boldsymbol{T}\boldsymbol{b}$. The inputs of the procedure of Fig. 3.1 are chosen as follows; $\delta_1 \in [10^{-5}, 1]$, $\delta_2 \in [0.01, 4]$, $\gamma_{\min} \in [0.01, 0.1]$, $\boldsymbol{A}_T = \boldsymbol{T}\boldsymbol{A}\boldsymbol{T}^{-1}$, $\beta = 2.5$, $L = 0.125$, $R = 1$, and $\boldsymbol{Q} = \boldsymbol{I}$. The selection procedure in Fig. 3.1 obtains the controller parameters as $\boldsymbol{c}^T\boldsymbol{T}^{-1} = [-0.8499, 1]$ and $\gamma_c = 0.2899$, where $\delta_1 = 10^{-5}$, $\delta_2 = 2.6$, $\gamma_{\min} = 0.05$, $\tilde{P}_{22} = 1.1923$, $\tilde{\boldsymbol{P}}_{12} = 1.0134$, and $\boldsymbol{P}_{11} = 2.3498$.

The simulations are performed with the discrete-time algorithm (2.74)(2.75)(2.76) with the sampling interval $h = 0.01$. To show the efficacy of $\gamma(\boldsymbol{x}, u)$ with the designed parameter set $\{\boldsymbol{c}, \gamma_c\}$, Fig. 3.3 compares the results of $\gamma(\boldsymbol{x}, u)$ and the results of two constant values of γ. Here, the state with $\gamma \equiv \gamma_{\min}$ goes unstable, while that with $\gamma(\boldsymbol{x}, u)$ does not lose the convergence. We also can see that the system with $\gamma(\boldsymbol{x}, u)$ is less sensitive to the disturbance (i.e., has a smaller finite-time attractor) than that with $\gamma \equiv \gamma_c$.

The contraction of the finite-time attractor due to the use of $\gamma(\boldsymbol{x}, u)$ is shown in Fig. 3.4. In this figure, the linear portion $\mathcal{S}_L \cap \mathcal{F}$ is shown with $\gamma \equiv \gamma_c$ (i.e., the light-coral region), and with $\gamma \equiv 0.1045$ (i.e., the red region), which is an upperbound of γ after $t > 5$, indicated in Fig. 3.3. We can see that the system state with $\gamma(\boldsymbol{x}, u)$, which is the blue-thin trajectory, goes inside the contracted finite-time attractor (i.e., inside the red region), while the state with the constant $\gamma \equiv \gamma_c$, which is the gray-thick trajectory, goes to the larger finite-time attractor (i.e., the yellow ellipsoidal region).

Regarding this example, the previous parameter tuning method in Chapter 2 obtained $\boldsymbol{c}$ and γ_c as indicated in Table 3.1. From Table 3.1, one can see that the proposed method in this chapter provides smaller $\|\boldsymbol{c}\|$ and $\|\boldsymbol{c}\|/\gamma_c$ than that of the previous method. Another point to be noted is that, with $\boldsymbol{c}$ obtained by the proposed method, the slowest pole of $\boldsymbol{A} - \boldsymbol{b}\boldsymbol{c}^T/\gamma_{\min}$ is $-0.50 + 0j$, which is marginally inside $\mathcal{R}$, and $\lim_{\gamma \to 0}(\boldsymbol{A} - \boldsymbol{b}\boldsymbol{c}^T/\gamma)$ is outside $\mathcal{R}$. Meanwhile, with c obtained by the previous method, the poles are in $\mathcal{R}$ even for $\gamma \to 0$. Considering that γ is lowerbounded by $\gamma_{\min}$, the previous method can be said to be unnecessarily conservative for the choice of $\boldsymbol{c}$, resulting in a larger norm of $\boldsymbol{c}$.

Table 3.1: Example 2: Comparison of parameter values obtained by the parameter tuning guideline in Chapter 2 and the proposed selection procedure here.

	Proposed Method (Chapter 3)	Previous Method (Chapter 2)
$\boldsymbol{c}$	$[0.8499, -1]^T$	$[1, -1]^T$
γ_c	0.2899	0.276
$\|\boldsymbol{c}\|/\gamma_c$	4.52	5.12

Fig. 3.5 compares the two parameter sets in Table 1, which are obtained by the proposed and the previous methods. With the initial state $\boldsymbol{x}_0 = [0, 0.4]^T$, these parameter sets realize similar performance to each other. Meanwhile, with the initial state $\boldsymbol{x}_0 = [0, 0.47]^T$, which is at a larger distance from the origin, the parameter set with the previous procedure resulted in unstable behavior, while that of the proposed method maintains the stability. This difference can be attributed to the smaller norm of $\boldsymbol{c}/\gamma_c$

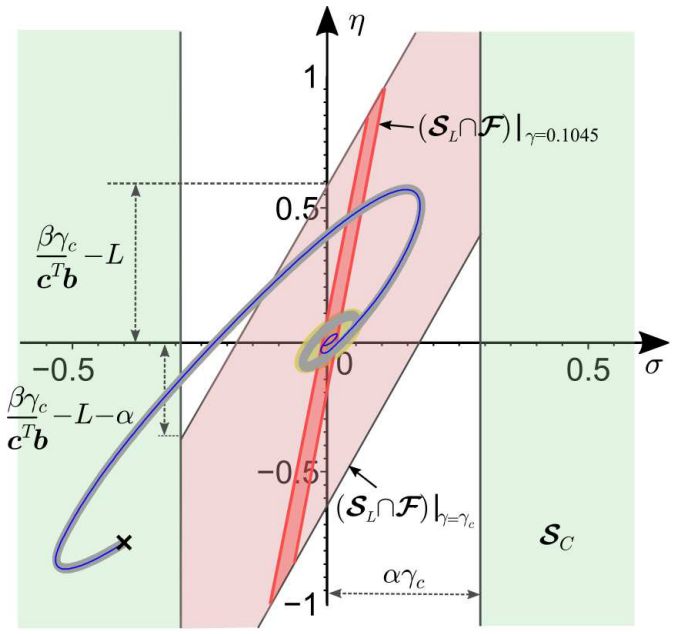

Figure 3.4: Example 2: The state mapping in σ-η plane with the initial condition $\boldsymbol{x}_0 = [0, 0.4]^T$. The blue-thin trajectory is the state trajectory with $\gamma(\boldsymbol{x}, u)$, while the gray-thick one is the state trajectory with $\gamma \equiv \gamma_c$.

realized by the proposed method, which resulted in a larger region of attraction.

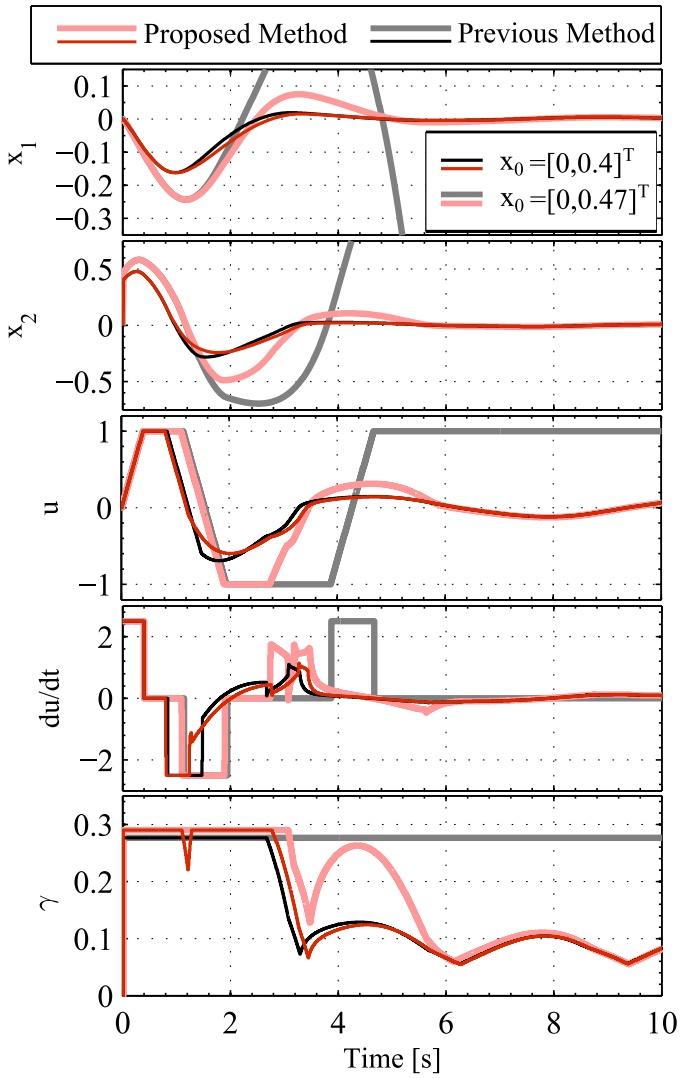

Figure 3.5: Example 2: comparison between the controllers with two parameter sets in Table 1, which are obtained by the proposed and the previous methods, with two different initial states $\boldsymbol{x}_0$.

3.4 Summary

This chapter has proposed a selection procedure for the parameter values of an amplitude- and rate-saturated controller proposed in Chapter 2. The proposed selection procedure explicitly seeks a small norm for the control action to enlarge the region of attraction. It obtains the parameter values through an iterative computation that involves linear matrix inequalities. The simulation results show that the parameter values obtained by the proposed procedure realizes proper performance of the controller, and also results in a larger region of attraction than the previous parameter designing procedure in Chapter 2.

Chapter 4

Application to Wind Turbine Systems

4.1 Introduction

One application needs amplitude- and rate-saturated controller is the wind turbine systems [8,69]. The control techniques of the wind turbine system are growing research area, which concerns with improving the efficiency of the generation process with better power quality and with less maintenance cost [70–72]. The control targets of the variable-speed wind turbine [73, 74] are specified by the operating regions, which are classified according to a power versus wind speed curve shown in Fig 4.1. The wind speed range in that curve is bounded by a cut-in speed at which the turbine starts to produce energy, and a cut-out speed at which the turbine is braked to save its structure from damage. Between the cut-in and cut-out speeds, there is a rated wind speed value at which the designed rated power of the turbine is achieved. In a region called "Region 3", in which the wind speed is above the rated value, the generated power needs to be constant at the rated power to avoid overloading on the generator [75,76]. One method to maintain the generated power constant in Region 3 is to maintain the generator speed via manipulating the angles of the turbine blades [76]. Each blade of them has limitations on its angle and its angle rate-of-change. The control method that would manipulate the blades' angles should be robust enough to regulate the speed of the generator over a wide range of wind speeds [70, 77]. In addition, the control method should respect the limitations of the blade angle to avoid degradation in the turbine performance.

A control scheme that sends identical pitch angle commands to all blades of a turbine is referred to as collective pitch control (CPC). Various CPC methods have been developed to achieve the regulation of the generator speed in Region 3. Gain-

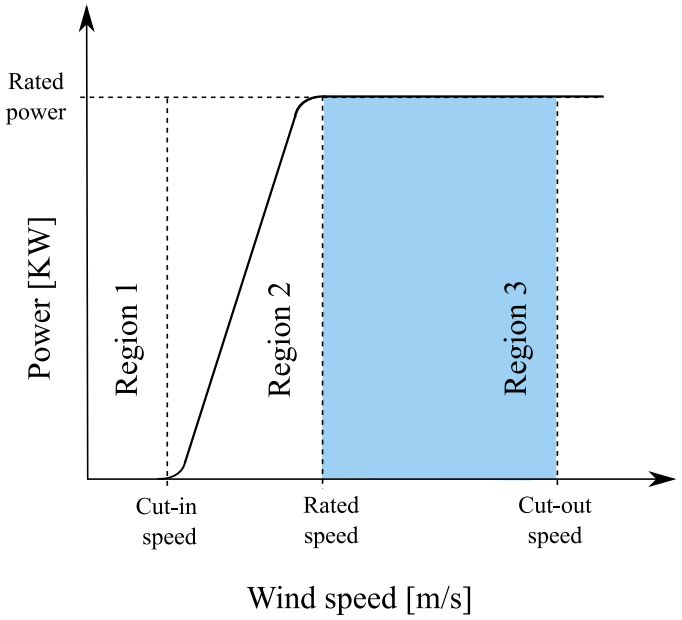

Figure 4.1: Power-versus-wind speed of variable-speed wind turbine.

scheduling proportional integral (GSPI) controller [2, 78] is a conventional controller used with most commercial wind turbines [75]. This conventional control methodology has a difficulty in tuning the controller parameters for a wide range of wind speeds, which continuously change during operation. Disturbance accommodation control (DAC) is another control methodology, which is applied earlier to wind turbine systems [79, 80] to attenuate the effect of wind disturbances. One of its drawbacks is the sensitivity against the unmodeled dynamics of the turbine, which may cause instability in the turbine performance [81].

Some sliding mode control schemes have been proposed [82–84] to cope with the turbine structure nonlinearity and uncertainty. Beltran *et al.* [83] introduced a dynamic sliding-mode controller to maintain the generated speed via controlling the torque of the generator. Their sliding-mode controller employs an adaptive gain, which continuously increases as long as there exists an error between the reference and the actual power of the turbine. The methodology of employing an adaptive gain proportional to the error may be undesirable to be used for controlling the pitch angles of the turbine because, in such a case, the control signal may increase over the limitations of the pitch angles.

In order to circumvent the so-called chattering problem produced by sliding-mode controllers, modified schemes have been developed, in which the sign function is re-

laxed into a saturation function [82, 83], while in another work, higher-order sliding-mode schemes [85] are introduced. Colombo *et al.* [86] have proposed a sliding-mode approach to maintain the generator speed via controlling the pitch angle, and they employed the boundary-layer method to reduce the chattering phenomenon. Although their scheme is designed to deal with several uncertainties in the model, it does not take the amplitude- and rate-limitations of the blade angle into account. As far as the author is aware, there have been no studies employing sliding mode controllers taking into account the limitations on the blade angles and their rate-of-change.

This chapter proposes a new CPC scheme based on the proposed controller in Chapter 2. The proposed CPC scheme respects the hardware limitation of the pitch actuators, and it involves a nonlinear function in order to change the control gain according to the state and the magnitude of the disturbance. This nonlinear function facilitates a wider region of attraction when there are significant variations in the wind speed and also facilitates a proper regulation of the generator speed when the variations are small. The chattering is eliminated by a model-based implicit method [54, 55] employed in the discrete-time implementation of the controller.

The controller is based on a standardized linearlized modeling scheme for the inherently nonlinear wind turbine dynamics, which is provided by a well-established wind turbine simulator ("Fatigue, Aerodynamics, Structures, and Turbulence") [87]. The validation of the proposed controller is shown through a comparative study with two conventional control methods; a gain-scheduling proportional integral controller [2], and a linear state-feedback controller of which the gains are obtained based on an H_2/H_∞ criteria [88].

The rest of this chapter is organized as follows. Section 4.2 presents a reduced linear time-invariant model of the wind turbine system. Section 4.3 proposes the controller combined with a state and disturbance observer. Section 4.4 shows simulation results, including comparison with other previous methods. Section 4.5 provides a summary for this chapter.

4.2 Wind turbine model

The modeling scheme adopted by FAST [87] is employed here, in which the following nonlinear equation of motion describes the wind turbine:

$$\boldsymbol{M}(\boldsymbol{Q}, \boldsymbol{U}, t)\ddot{\boldsymbol{Q}} + \boldsymbol{F}(\boldsymbol{Q}, \dot{\boldsymbol{Q}}, \boldsymbol{U}, \boldsymbol{\Xi}, t) = \boldsymbol{0} \tag{4.1}$$

where $\boldsymbol{M}$ denotes the inertia matrix, $\boldsymbol{F}$ is a nonlinear term, and t is the time. The vector $\boldsymbol{Q}$ represents the displacements of the system's degrees of freedoms (DOFs) including the azimuth angle and the displacements of elastic components such as the

blades, the generator shaft, the drivetrain gearbox, and the tower. For a three-bladed horizontal-axis wind turbine, the full dimension of $\boldsymbol{Q}$ can be set as 24 as accounted in [87], and in such a case, we have $\boldsymbol{M} \in \mathbb{R}^{24\times 24}$ and $\boldsymbol{F} \in \mathbb{R}^{24}$. The vector $\boldsymbol{U}$ is the input to the plant, which may include the pitch angles of the blades, the nacelle yaw angle rate and the electrical torque of the generator. The vector $\boldsymbol{\Xi}$ includes disturbances, such as the hub-height wind speed and the wind share.

4.2.1 Reduced LTI model for controller development

To consider a controller for the plant (4.1), a linear time-invariant (LTI) approximation of (4.1) is needed. The modeling scheme adopted by FAST [87] is followed to derive such an approximation. Considering the nature of wind turbine systems, we can see that the time dependency of the system (4.1) is very small. Moreover, among the many DOFs of the whole system, the rotating motions of the generator and the torsional motion of the drivetrain can be seen as two of the dominant DOFs. The drivetrain here represents the gears and other flexible components that transmit the mechanical power from the rotor shaft to the generator shaft. Thus, we can say that the dominant elements of the vector $\boldsymbol{Q}$ are θ and ϕ, which respectively denote the rotor-shaft angle (rad) and the drivetrain torsional displacement (rad). In addition, it is assumed that the identical pitch angle commands are sent to all blades, and thus the dominant element of $\boldsymbol{U}$ is only one command $\widehat{u} \in \mathbb{R}$, which is referred to as the collective pitch angle (rad). The dominant member of the disturbance vector $\boldsymbol{\Xi}$ is assumed to be the horizontal wind speed $\widehat{\xi} \in \mathbb{R}$ measured in m/s. Then, we can write the reduced time-invariant nonlinear model as follows:

$$\begin{bmatrix} \dot{\theta} \\ \dot{\phi} \end{bmatrix} = \begin{bmatrix} \omega \\ \nu \end{bmatrix} \tag{4.2}$$

$$\begin{bmatrix} \dot{\omega} \\ \dot{\nu} \end{bmatrix} = \boldsymbol{f}\left(\begin{bmatrix} \theta \\ \phi \end{bmatrix}, \begin{bmatrix} \omega \\ \nu \end{bmatrix}, \begin{bmatrix} \widehat{u} \\ \widehat{\xi} \end{bmatrix} \right) \tag{4.3}$$

where ω and ν are the angular velocity (rad/s) of the rotor shaft and the rate-of-change (rad/s) of the drivetrain torsion, respectively. Such a reduced-dimensional model can be obtained by FAST [87] by "disabling" specified DOFs and specifying necessary elements of $\boldsymbol{U}$ and $\boldsymbol{\Xi}$.

Here, let us set the following assumption:

Assumption 1. *With a given angular velocity ω_r of the rotor shaft and a given wind speed $\widehat{\xi}_r$, there exists a collective pitch angle $\widehat{u} = \widehat{u}_f(\widehat{\xi}_r, \omega_r)$ with which the system is in the steady state.*

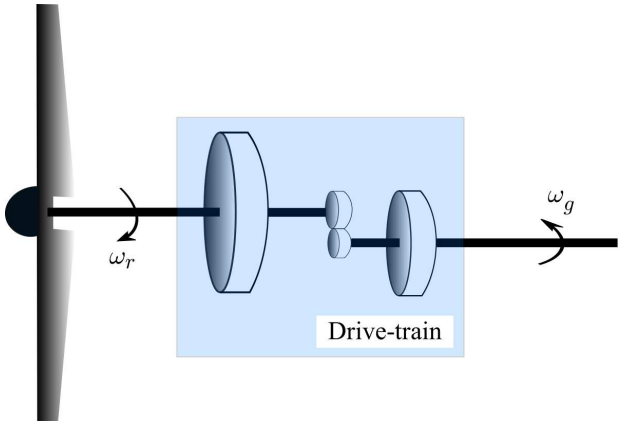

Figure 4.2: Dynamics of 2 DOFs.

The steady state here stands for the situation where ω is constant (at a value ω_r) and ν and ϕ exhibit cyclic behaviors of which each cycle corresponds to the rotation of θ from 0 to 2π. Actually, FAST [87] has a function to find such a steady state and $\widehat{u}_f(\widehat{\xi}_r, \omega_r)$ according to given values of $\widehat{\xi}_r$ and ω_r. In such a situation, $\dot{\omega} = 0$ is satisfied and ϕ, ν and $\dot{\nu}$ are functions of θ. That is, there exist appropriate functions ϕ_f, ν_f and ν_{Df} (where the subscript f stands for a function) with which the following equation is satisfied for all $\theta_0 \in [0, 2\pi)$:

$$\begin{bmatrix} 0 \\ \nu_{Df}(\theta_0, \widehat{\xi}_r, \omega_r) \end{bmatrix} = \boldsymbol{f}\left(\begin{bmatrix} \theta_0 \\ \phi_f(\theta_0, \widehat{\xi}_r, \omega_r) \end{bmatrix}, \begin{bmatrix} \omega_r \\ \nu_f(\theta_0, \widehat{\xi}_r, \omega_r) \end{bmatrix}, \begin{bmatrix} \widehat{u}_f(\widehat{\xi}_r, \omega_r) \\ \widehat{\xi}_r \end{bmatrix} \right). \quad (4.4)$$

Such a situation can be referred to as an "operating point", which can be defined as follows:

$$\begin{aligned} \mathcal{P}(\theta_0, \widehat{\xi}_r, \omega_r) = \ & \big\{ \theta = \theta_0,\ \phi = \phi_f(\theta_0, \widehat{\xi}_r, \omega_r),\ \omega = \omega_r,\ \nu = \nu_f(\theta_0, \widehat{\xi}_r, \omega_r), \\ & \dot{\omega} = 0,\ \dot{\nu} = \nu_{Df}(\theta_0, \widehat{\xi}_r, \omega_r),\ \ \widehat{\xi} = \widehat{\xi}_r,\ \widehat{u} = \widehat{u}_f(\widehat{\xi}_r, \omega_r) \big\}. \end{aligned} \quad (4.5)$$

Around an operating point $\mathcal{P}(\theta_0, \widehat{\xi}_r, \omega_r)$, one can obtain a linear approximation of the system (4.3) as follows:

$$\begin{aligned} \begin{bmatrix} \dot{\theta} - \omega_r \\ \dot{\phi} - \nu_f(\theta_0, \widehat{\xi}_r, \omega_r) \\ \dot{\omega} \\ \dot{\nu} - \nu_{Df}(\theta, \widehat{\xi}_r, \omega_r) \end{bmatrix} = \ & \widehat{\boldsymbol{A}}(\theta_0, \widehat{\xi}_r, \omega_r) \begin{bmatrix} \theta - \theta_0 \\ \phi - \phi_f(\theta_0, \widehat{\xi}_r, \omega_r) \\ \omega - \omega_r \\ \nu - \nu_f(\theta_0, \widehat{\xi}_r, \omega_r) \end{bmatrix} \\ & + \widehat{\boldsymbol{B}}(\theta_0, \widehat{\xi}_r, \omega_r) \begin{bmatrix} \widehat{u} - \widehat{u}_f(\widehat{\xi}_r, \omega_r) \\ \widehat{\xi} - \widehat{\xi}_r \end{bmatrix} \end{aligned} \quad (4.6)$$

where

$$\widehat{\boldsymbol{A}}(\theta_0, \widehat{\xi}_r, \omega_r) \triangleq \left[\begin{array}{cc} \boldsymbol{O}_{2\times 2} & \boldsymbol{I}_2 \\ \partial \boldsymbol{f}/\partial[\theta,\phi]^T & \partial \boldsymbol{f}/\partial[\omega,\nu]^T \end{array} \right]\Bigg|_{\mathcal{P}(\theta_0,\widehat{\xi}_r,\omega_r)} \in \mathbb{R}^{4\times 4} \tag{4.7}$$

$$\widehat{\boldsymbol{B}}(\theta_0, \widehat{\xi}_r, \omega_r) \triangleq \left[\begin{array}{c} \boldsymbol{O}_{2\times 2} \\ \partial \boldsymbol{f}/\partial[\widehat{u},\widehat{\xi}]^T \end{array} \right]\Bigg|_{\mathcal{P}(\theta_0,\widehat{\xi}_r,\omega_r)} \in \mathbb{R}^{4\times 2}. \tag{4.8}$$

Because of the cyclic nature of the behavior and the fact that θ is not of interest for control purposes, one can consider an *averaged* dynamics of the system over $\theta_0 \in [0, 2\pi)$. Let N be a natural number. Averaging over N operating points yields the following:

$$\boldsymbol{A}(\widehat{\xi}_r, \omega_r) \triangleq \frac{1}{N}\sum_{i=1}^{N} \boldsymbol{J}\widehat{\boldsymbol{A}}(2\pi i/N, \widehat{\xi}_r, \omega_r)\boldsymbol{J}^T \in \mathbb{R}^{3\times 3} \tag{4.9}$$

$$\boldsymbol{B}(\widehat{\xi}_r, \omega_r) \triangleq \frac{1}{N}\sum_{i=1}^{N} \boldsymbol{J}\widehat{\boldsymbol{B}}(2\pi i/N, \widehat{\xi}_r, \omega_r) \in \mathbb{R}^{3\times 2} \tag{4.10}$$

$$\bar{\phi}_f(\widehat{\xi}_r, \omega_r) \triangleq \frac{1}{N}\sum_{i=1}^{N} \phi_f(2\pi i/N, \widehat{\xi}_r, \omega_r) \in \mathbb{R}. \tag{4.11}$$

Here, $\boldsymbol{J} \triangleq [\boldsymbol{o}_3, \boldsymbol{I}_3] \in \mathbb{R}^{3\times 4}$ where $\boldsymbol{o}_3$ is the three dimensional zero column vector, and $\boldsymbol{I}_3$ is the three dimensional identity matrix. In addition, the cyclic change of ϕ results in the following:

$$\frac{1}{N}\sum_{i=1}^{N} \nu_f(2\pi i/N, \widehat{\xi}_r, \omega_r) \approx 0 \tag{4.12}$$

$$\frac{1}{N}\sum_{i=1}^{N} \nu_{Df}(2\pi i/N, \widehat{\xi}_r, \omega_r) \approx 0. \tag{4.13}$$

As a result, we can obtain the following reduced system:

$$\left[\begin{array}{c} \dot{\phi} \\ \dot{\omega} \\ \dot{\nu} \end{array} \right] = \boldsymbol{A}(\widehat{\xi}_r, \omega_r) \left[\begin{array}{c} \phi - \bar{\phi}_f(\widehat{\xi}_r, \omega_r) \\ \omega - \omega_r \\ \nu \end{array} \right] + \boldsymbol{B}(\widehat{\xi}_r, \omega_r) \left[\begin{array}{c} \widehat{u} - \widehat{u}_f(\widehat{\xi}_r, \omega_r) \\ \widehat{\xi} - \widehat{\xi}_r \end{array} \right]. \tag{4.14}$$

Next, let us set another assumption and consider using $\widehat{\xi}_m$, which is the wind-speed value measured by a sensor.

Assumption 2. *The changes in $\boldsymbol{A}(\widehat{\xi}, \omega_r)$ and $\boldsymbol{B}(\widehat{\xi}, \omega_r)$ according to the change in $\widehat{\xi}$ are sufficiently small within a certain range of $\widehat{\xi}$ including $\widehat{\xi}_r$ and $\widehat{\xi}_m$.*

This assumption leads to the following approximation of (4.14):

$$\begin{bmatrix} \dot{\phi} \\ \dot{\omega} \\ \dot{\nu} \end{bmatrix} = \boldsymbol{A}(\widehat{\xi}_r, \omega_r) \begin{bmatrix} \phi - \bar{\phi}_f(\widehat{\xi}_m, \omega_r) \\ \omega - \omega_r \\ \nu \end{bmatrix} + \boldsymbol{B}(\widehat{\xi}_r, \omega_r) \begin{bmatrix} \widehat{u} - \widehat{u}_f(\widehat{\xi}_m, \omega_r) \\ \widehat{\xi} - \widehat{\xi}_m \end{bmatrix}. \quad (4.15)$$

With a fixed $\widehat{\xi}_r$ and ω_r and the measured $\widehat{\xi}_m$, let us define

$$\boldsymbol{x} \triangleq \begin{bmatrix} \phi - \bar{\phi}_f(\widehat{\xi}_m, \omega_r) \\ \omega - \omega_r \\ \nu \end{bmatrix} \quad (4.16)$$

$$u \triangleq \widehat{u} - \widehat{u}_f(\widehat{\xi}_m, \omega_r) \quad (4.17)$$

$$\xi \triangleq \widehat{\xi} - \widehat{\xi}_m \quad (4.18)$$

$$\boldsymbol{A} \triangleq \boldsymbol{A}(\widehat{\xi}_r, \omega_r) \quad (4.19)$$

$$[\boldsymbol{b}, \boldsymbol{g}] \triangleq \boldsymbol{B}(\widehat{\xi}_r, \omega_r). \quad (4.20)$$

Then, (4.15) is now described as the following LTI system:

$$\dot{\boldsymbol{x}} = \boldsymbol{A}\boldsymbol{x} + \boldsymbol{b}u + \boldsymbol{g}\xi. \quad (4.21)$$

Such an LTI model, more specifically, the set of matrices $\boldsymbol{A} \in \mathbb{R}^{3\times3}$, $\boldsymbol{b} \in \mathbb{R}^3$ and $\boldsymbol{g} \in \mathbb{R}^3$, can be obtained by utilizing built-in functions of FAST [87]. Linear approximations of the form (4.21) of wind turbine systems have also been used by some previous researchers [36, 88].

In the LTI model (4.21), the state vector $\boldsymbol{x}$ is not available, except the second element being obtained through the rotor tachometer, but the later Section 4.3.2 will introduce a state- and disturbance-observer to estimate it. As for the first element of $\boldsymbol{x}$, its value is directly obtained through the observer, although ϕ is not available and $\bar{\phi}_f(\widehat{\xi}_m, \omega_r)$ does not have to be computed. Although $\widehat{\xi}_m$ is available, the true wind speed $\widehat{\xi}$ is unavailable and the measurement error ξ is to be estimated also through the observer. The control input u is to be provided by a controller designed based on the LTI model (4.21). The actual control input $\widehat{u}$, to be given to the plant, should be obtained as $\widehat{u} = u + \widehat{u}_f(\widehat{\xi}_m, \omega_r)$, as can be seen in (4.17). Here, the function $\widehat{u}_f(\widehat{\xi}_m, \omega_r)$ needs to be given as a lookup table built in advance. It can be built with, for example, FAST [87], which has functions of searching for the steady states.

The output equation of the LTI model (4.21) is as follows:

$$\Delta\omega_g = \boldsymbol{h}^T\boldsymbol{x} \quad (4.22)$$

where

$$\Delta\omega_g \triangleq \omega_g - \omega_{gr} \tag{4.23}$$

and ω_g (rpm) and ω_{gr} (rpm) are the observed and the reference generator speeds. The vector $\boldsymbol{h}$ is defined as $\boldsymbol{h} = [0, h_1, 0]^T$ where h_1 is the product of the gear ratio and the conversion coefficient from rad/s to rpm (i.e., $h_1 = \omega_{gr}$ (rpm)$/\omega_r$ (rad/s)).

Remark 4.2.1. *It should be noted that the LTI model (4.21) is an approximation of the nonlinear system (4.1) neglecting the motions of 22 DOFs, and it does not even include any error terms that may be caused by this approximation. The validity of the proposed controller built on this simplified LTI model (4.21) will be empirically tested with simulation, in which the controller is applied to the fully nonlinear time-variant system (4.1).*

4.2.2 Pitch actuator model

Each blade of the wind turbine has a pitch actuator that receives the control signal $\widehat{u}$ and changes the blade angle accordingly around its longitude axis. Due to its intrinsic mechanical properties, the angle and the angular velocity of the blades are limited, which means that the control signal $\widehat{u}$ needs to satisfy the following conditions:

$$|\widehat{u}| \leq \alpha, \qquad |d\widehat{u}/dt| \leq \beta \tag{4.24}$$

where α and β are positive constants. For example, the pitch actuator of a 5 MW wind turbine discussed in [2] has the following; $\alpha = 1.5$ rad and $\beta = 0.14$ rad/s. We can now divide the limitations (4.24) corresponding to u and $\widehat{u}_f(\widehat{\xi}_m, \omega_r)$ as follows:

$$|u| \leq \alpha_u, \qquad |\dot{u}| \leq \beta_u, \tag{4.25}$$

$$|\widehat{u}_f(\widehat{\xi}_m, \omega_r)| \leq \alpha_{\widehat{u}_f}, \qquad \left|\frac{d\widehat{u}_f(\widehat{\xi}_m, \omega_r)}{dt}\right| \leq \beta_{\widehat{u}_f} \tag{4.26}$$

where $\alpha = \alpha_u + \alpha_{\widehat{u}_f}$ and $\beta = \beta_u + \beta_{\widehat{u}_f}$.

4.3 Colletive Pitch Controller

4.3.1 An amplitude- and rate-saturated controller

This section extends the controller of Chapter 2 to be able to deal with the LTI system (4.21), which approximates the nonlinear plant (4.1). The main part of this controller

has the following form:

$$\dot{u} \in -\beta_u \mathrm{sgn}\left(u + \mathrm{sat}_{\alpha_u}(\boldsymbol{c}^T\boldsymbol{x}/\gamma(\boldsymbol{x}, u))\right) \tag{4.27}$$

where the vector $\boldsymbol{c} \in \mathbb{R}^3$ is a controller parameter that should be chosen appropriately, $\gamma(\boldsymbol{x}, u)$ is a nonlinear function defined later. In almost the same way as in Chapter 2, it can be shown that the controller (4.27) applied to the LTI plant (4.21) is a sliding mode controller of which the sliding surface is $u + \mathrm{sat}_{\alpha_u}(\boldsymbol{c}^T\boldsymbol{x}/\gamma) = 0$ and that the sliding mode takes place when

$$\gamma > \frac{|\boldsymbol{c}^T\boldsymbol{A}\boldsymbol{x} + \boldsymbol{c}^T\boldsymbol{b}u| + |\boldsymbol{c}^T\boldsymbol{g}\xi|}{\beta_u} \tag{4.28}$$

is satisfied. This implies that selecting large γ enlarges the region in which the sliding mode happens. In the sliding mode, the controller (4.27) reduces to a linear controller $u = -\boldsymbol{c}^T\boldsymbol{x}/\gamma$ (see Theorem 2.3.1) and the poles of the closed-loop system coincide with the eigenvalues of the matrix $(\boldsymbol{A} - \boldsymbol{b}\boldsymbol{c}^T/\gamma)$. In such a case, a small value of γ facilitates a high-gain control action, which mitigates the influence of disturbances and attracts the state to a neighborhood of the origin, reducing the size of the finite time attractor.

Chapter 2 employed a particular definition of the nonlinear function $\gamma(\boldsymbol{x}, u)$ to enlarge the region of attraction when the state is far from the origin and to shrink the finite time attractor when the state is near the origin. Because the plant (4.21) is slightly different from the plant considered in (2.1), this chapter proposes a slightly modified definition of $\gamma(\boldsymbol{x}, u)$, which is described as follows:

$$\gamma(\boldsymbol{x}, u) \triangleq \min\left(\gamma_c, \frac{|\boldsymbol{c}^T\boldsymbol{A}\boldsymbol{x}| + \boldsymbol{c}^T\boldsymbol{b}|u| + |\boldsymbol{c}^T\boldsymbol{g}\xi| + \boldsymbol{c}^T\boldsymbol{b}L}{\beta_u}\right) \tag{4.29}$$

where γ_c and L are positive scalars that need to be appropriately chosen. The parameter γ_c should be chosen large to enlarge the region of attraction but should be small enough to set the eigenvalues of the matrix $(\boldsymbol{A} - \boldsymbol{b}\boldsymbol{c}^T/\gamma(\boldsymbol{x}, u))$ within a give subset of the complex plane. As for the choice of the parameter L, we at this time do not have a clear guideline, although in Chapter 2, it was suggested to choose it according to the upperbound of a disturbance superposed to the input u, which is absent in the plant (4.21). It should be noted that $\boldsymbol{c}^T\boldsymbol{b} > 0$ is assumed to be satisfied.

Because the proposed controller (4.27) is to be implemented in discrete-time controllers, we need to avoid the chattering caused by inappropriate treatment of the set-valued sgn function in the discretization. Chapter 2 employed a model-based implicit discretization scheme [54, 55] to obtain a discrete-time algorithm of the controller. In

the same light, the following discrete-time algorithm is proposed as an implementation of the controller (4.27) combined with (4.29):

$$w_{k-1} := \boldsymbol{c}^T(\boldsymbol{I} + h\boldsymbol{A})\boldsymbol{x}_{k-1} \tag{4.30a}$$

$$\gamma_k := \min\left(\gamma_c, \frac{|\boldsymbol{c}^T\boldsymbol{A}\boldsymbol{x}_{k-1}| + \boldsymbol{c}^T\boldsymbol{b}|u_{k-1}| + |\boldsymbol{c}^T\boldsymbol{g}\xi_{k-1}| + \boldsymbol{c}^T\boldsymbol{b}L}{\beta_u}\right) \tag{4.30b}$$

$$u_k := u_{k-1} - \mathrm{sat}_{h\beta_u}\left(u_{k-1} + \mathrm{sat}_{\alpha_u}\left(\frac{w_{k-1}}{\gamma_k + \boldsymbol{c}^T\boldsymbol{b}h}\right)\right) \tag{4.30c}$$

where k is the discrete-time index and h is the sampling interval.

4.3.2 State and disturbance observer

In the controller (4.30), the state $\boldsymbol{x}$ and the residual disturbance ξ cannot be measured directly. One method to estimate them is the use of an observer called an unknown input observer (UIO) [89]. An early version of UIO was introduced by Johnson [90]. He later extended it to be a part of a disturbance accommodation controller (DAC) [79], which has been applied also to wind turbine systems [80, 81].

In the same light as in [80,91], a direct application of an UIO to the plant composed of (4.21) and (4.22) can be obtained as follows:

$$\frac{d}{dt}\begin{bmatrix}\hat{\boldsymbol{x}}\\ \hat{\xi}\end{bmatrix} = \boldsymbol{\mathcal{A}}\begin{bmatrix}\hat{\boldsymbol{x}}\\ \hat{\xi}\end{bmatrix} + \boldsymbol{\mathcal{B}}u + \boldsymbol{K}(\Delta\omega_g - \boldsymbol{h}^T\hat{\boldsymbol{x}}) \tag{4.31}$$

where

$$\boldsymbol{\mathcal{A}} \triangleq \begin{bmatrix}\boldsymbol{A} & \boldsymbol{g}\\ \boldsymbol{o}_3^T & 0\end{bmatrix}, \quad \boldsymbol{\mathcal{B}} \triangleq \begin{bmatrix}\boldsymbol{b}\\ 0\end{bmatrix}. \tag{4.32}$$

Here, the vector $\hat{\boldsymbol{x}}$ is the estimated state vector and $\hat{\xi}$ is the estimated residual disturbance. The observer gain $\boldsymbol{K} \in \mathbb{R}^4$ is calculated via a pole placement problem to assign the eigenvalues of $(\boldsymbol{\mathcal{A}} - \boldsymbol{K}\boldsymbol{\mathcal{H}})$ at desired locations, where $\boldsymbol{\mathcal{H}} = [\boldsymbol{h}^T, 0]$. This observer structure of course requires the observability of the pair $\{\boldsymbol{\mathcal{A}}, \boldsymbol{\mathcal{H}}\}$, which can be easily checked when the linearlized model is obtained. At this time, a strict proof of the observability of wind turbine systems is not derived here, but at least a wind turbine model provided by FAST [87] presented in the next section is indeed observable. The overall control scheme including this observer is shown in Fig. 4.3.

4.3.3 Parameter design

To implement the discrete-time algorithm (4.30), we need to set the values of the parameters $\{\boldsymbol{A}, \boldsymbol{b}, \boldsymbol{g}, \alpha_u, \beta_u, L, \boldsymbol{c}, \gamma_c\}$. Among them, $\{\boldsymbol{A}, \boldsymbol{b}, \boldsymbol{g}, \alpha_u, \beta_u\}$ are determined

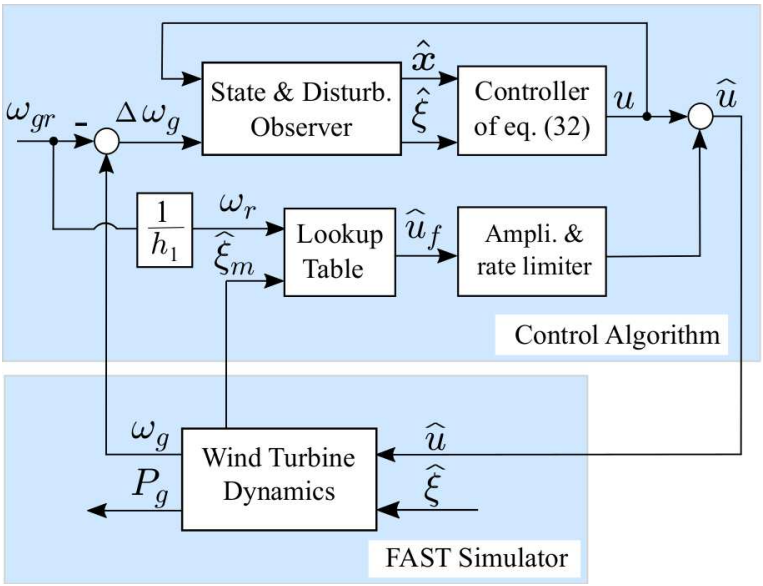

Figure 4.3: Block diagram of the proposed control scheme, where P_g is the generated power.

by the physical properties of the plant (4.21), while the rest ones, $\{L, \boldsymbol{c}, \gamma_c\}$, need to be carefully designed. Chapter 3 proposed a selection procedure for the parameters $\{\boldsymbol{c}, \gamma_c\}$ based on the assumption that L is given in advance. The procedure was based on the following two main objectives. One is to make $\|\boldsymbol{c}/\gamma_c\|$ small to enlarge the region in which the sliding mode occurs, i.e., in which the condition (4.28) is satisfied. The second is to keep all the eigenvalues of $\boldsymbol{A} - \boldsymbol{b}\boldsymbol{c}^T/\gamma(\boldsymbol{x}, u)$ inside a specified region $\mathcal{R}$ in the complex plane. Further discussion and details are found in Section 3.2.

4.4 Simulation setup and results

4.4.1 Simulation setup

The wind turbine simulator FAST [87] is used here to simulate a 5 MW, three-bladed, horizontal-axis wind turbine as specified in Table 4.1. The full 24-DOF nonlinear dynamics model of the turbine is considered in the simulation. The proposed controller (4.30) combined with the state- and disturbance-observer (4.31) and the lookup table $\widehat{u}_f(\widehat{\xi}_m, \omega_r)$ are applied to the FAST simulator, as illustrated in Fig. 4.3, via Simulink interface. In this simulation, a step-like wind speed profile and a stochastic wind speed profile are used.

Table 4.1: Wind Turbine Specifications [2, Table 1-1].

Power rating	5 MW
Number of blades	3
Rotor diameter	126 m
Hub Height	90 m
Cut-in wind speed	3 m/s
Rated wind speed	11.4 m/s
Cut-out wind speed	25 m/s
Cut-in rotor speed	6.9 rpm
Rated rotor speed	12.1 rpm
Gearbox ratio	97:1
Rated generator speed	1173.7 rpm

To determine the matrices $\boldsymbol{A}$, $\boldsymbol{b}$ and $\boldsymbol{g}$ of the plant (4.21), the linearization feature of FAST [87] is applied at a particular operating point of $\mathcal{P}(\widehat{\xi}_r, \omega_r)$. Here, the steady wind speed is selected as $\widehat{\xi}_r = 18$ m/s, while ω_r is set as the rated speed of the turbine, which is 1.27 rad/s (i.e.,12.1 rpm as specified in Table 4.1). The resulted matrices were as follows:

$$\boldsymbol{A} = \begin{bmatrix} 0 & 0 & 1 \\ 172.6 & -2.731 & 1.237 \\ -195 & 2.4555 & -1.6725 \end{bmatrix}, \tag{4.33}$$

$$\boldsymbol{b} = \begin{bmatrix} 0 \\ 0 \\ -1.3265 \end{bmatrix}, \ \boldsymbol{g} = \begin{bmatrix} 0 \\ 0 \\ 0.0308 \end{bmatrix}, \tag{4.34}$$

$$\boldsymbol{h} = \begin{bmatrix} 0 & 926.3 & 0 \end{bmatrix}^T. \tag{4.35}$$

The second element of $\boldsymbol{h}$ is the ratio between the generator speed in rpm and the rotor-shaft speed in rad/s, which is the reduction ratio of the gearbox, as indicated in Table 4.1 by 97, multiplied by $60/(2\pi)$.

The linearization process of FAST was also performed with a set of steady wind speed values $\widehat{\xi}_m$ from 12 m/s to 22 m/s to obtain the corresponding pitch angles $\widehat{u}_f(\widehat{\xi}_m, \omega_r)$. The results data of the linearization process are arranged in a lookup table shown in Table 4.2. In a real implementation, the wind speed is supposed to be measured via proper sensors such as LiDAR [2], or a cup anemometer. The

Table 4.2: The Lookup table that is applied to obtain the pitch angle $\widehat{u}_f(\widehat{\xi}_m, \omega_r)$.

$\widehat{\xi}_m$	$\widehat{u}_f(\widehat{\xi}_m, \omega_r)$
12 m/s	0.077266 rad
13 m/s	0.121026 rad
14 m/s	0.155668 rad
15 m/s	0.185741 rad
16 m/s	0.213168 rad
17 m/s	0.238465 rad
18 m/s	0.262362 rad
19 m/s	0.285104 rad
20 m/s	0.306746 rad
21 m/s	0.327591 rad
22 m/s	0.347891 rad

limitations of u and $\widehat{u}_f(\widehat{\xi}_m, \omega_r)$, which are defined in (4.25) and (4.26), are set as follows; $\alpha_u = 0.5$ rad, $\beta_u = 0.06$ rad/s, $\alpha_{\widehat{u}_f} = 1$ rad and $\beta_{\widehat{u}_f} = 0.08$ rad/s.

The parameters for the controller (4.30) were chosen as $L = 0.05$, $\gamma_c = \infty$ and $\boldsymbol{c} = [-0.2130, -0.0225, -0.0081]^T$, partially through the procedure presented in Section 3.2. Some trial and error were needed for the parameter tuning because the procedure in Section 3.2 was originally for the plant defined in (2.1), which is slightly different from the plant (4.21). Specifically, the parameter L was initially set to be $L = 0.001$ and the procedure was performed to obtain $\boldsymbol{c}$ and γ_c. After that, by observing the preliminary simulation results, L was manually tuned and ended up with $L = 0.05$. In the application of the procedure of Section 3.2, auxiliary inputs were set as: $\mathcal{R}$ = the whole left half plane, $R = 1$, $\boldsymbol{Q} = 10^{-4}\boldsymbol{I}$, $\delta_1 \in [0.01, 1], \delta_2 \in [1, 1000]$, $\gamma_{\min} \in [10^{-7}, 0.01]$. The matrix $\boldsymbol{T} = \mathrm{diag}[-1, -1, -0.7539]$ is also used to transform the system into the equivalent system satisfying $\boldsymbol{Tb} = [\boldsymbol{o}_3^T, 1]^T$, which was necessary for the procedure. As a result, the aforementioned values of $\boldsymbol{c}$ and γ_c are obtained and the auxiliary outputs $\gamma_{\min} = 1.8 \times 10^{-5}$, $\delta_1 = 0.01$, $\delta_2 = 1000$. Fig. 4.4 is the root locus diagram of the matrix $\boldsymbol{A} - \boldsymbol{bc}^T/\gamma$ with varying γ, showing that the eigenvalues are always inside $\mathcal{R}$.

The sampling interval of the discrete-time implementation (4.30) was set as $h = 0.01$. Regarding the UIO, we can see that the pair $\{\boldsymbol{\mathcal{A}}, \boldsymbol{\mathcal{H}}\}$ is observable from the definitions of $\boldsymbol{A}$, $\boldsymbol{g}$, and $\boldsymbol{h}$ in (4.33)-(4.35). The gain vector of the observer was set as

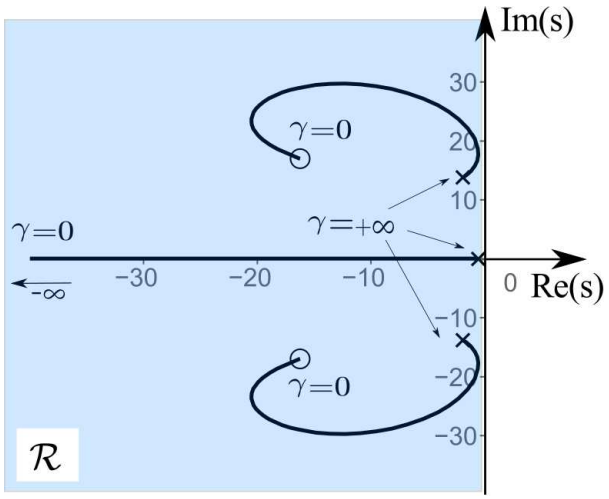

Figure 4.4: The loci of the eigenvalues of the matrix $(\boldsymbol{A} - \boldsymbol{b}\boldsymbol{c}^T/\gamma)$ within the region $\mathcal{R}$.

$\boldsymbol{K} = [0.05, 0.19, 0.86, 200]^T$, with which the eigenvalues of $(\boldsymbol{\mathcal{A}} - \boldsymbol{K}\boldsymbol{\mathcal{H}})$ are placed at -10, -20, -50, and -100.

4.4.2 Simulation results

Here, the proposed controller is compared with two previous controllers. One is a gain-scheduling PI controller described in [2]. This controller employs a gain-correction factor to automatically modify the proportional and integral gains corresponding to the latest value of the collective pitch angle. Further details about the gain-correction factor can be found in [2]. The proportional and integral gains are set as 0.0019 and 0.0008, respectively, while the gain-correction factor is set as $1/(1 + (\widehat{u}/0.11))$.

The other is a controller shown in Fig. 4.5, which is a linear state-feedback controller combined with a linear state observer and a feedforward term $\widehat{u}_f(\widehat{\xi}_m, \omega_r)$. This controller is motivated by the controller of Hassan *et al.* [88], who proposed an optimization method for a linear controller for wind turbines combined with some sophisticated techniques such as Kalman filtering and individual pitch control. In the controller of Fig. 4.5, the gain vector $\boldsymbol{k}$ is particularly chosen as:

$$\boldsymbol{k} = [3.5842, 2.0471, 1.6246]^T, \tag{4.36}$$

which is exactly the result of Hassan *et al.* [88], who applied their H_2/H_∞ optimization technique to the same plant. As for the linear observer in Fig. 4.5, the observer gains are chosen so that its poles were placed at $\{-10, -20, -50\}$.

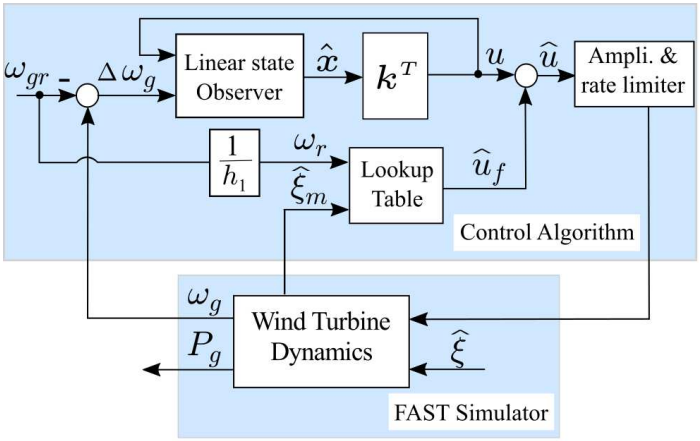

Figure 4.5: Block diagram of the control scheme used for the comparison study including the linear feedback controller (4.36), a linear state observer and the lookup table detailed in Table 4.2. Here, P_g denotes the generated power.

Here, it is needed to point out that both of those previous controllers apply the pitch actuator limitations (4.24) through an amplitude saturation and rate limiter imposed on the total control action $\widehat{u}$, as shown in Fig. 4.5.

Fig. 4.6 shows the results of the simulation in which the wind turbine is subjected to a step-like wind profile. The graphs of the wind speed and γ shows that γ takes larger values when the wind speed changes. Such large values of γ produces low-gain actions, resulting in smaller fluctuations in the generator speed and the generator power than the other controllers.

Fig. 4.7 shows the results of the simulation in which the wind turbine is subjected to a stochastic wind speed profile. Here, the wind speed fluctuation is smaller than that in Fig. 4.6. In this case, γ maintains low values, which result in a high-gain control action in the regulation of the generator speed. The regulation of the generator speed under the proposed controller and the linear controller are almost the same, although a very slight improvement under the proposed controller can be seen in Table 4.3. With both of the linear controller and the proposed controller, the regulation of the generator speed is better than that with the scheduling PI controller. It can be concluded that the main feature of the proposed controller is that it is robust against high variations in the wind speed while achieving almost the same performance as an optimized linear controller under small fluctuation in the wind speed.

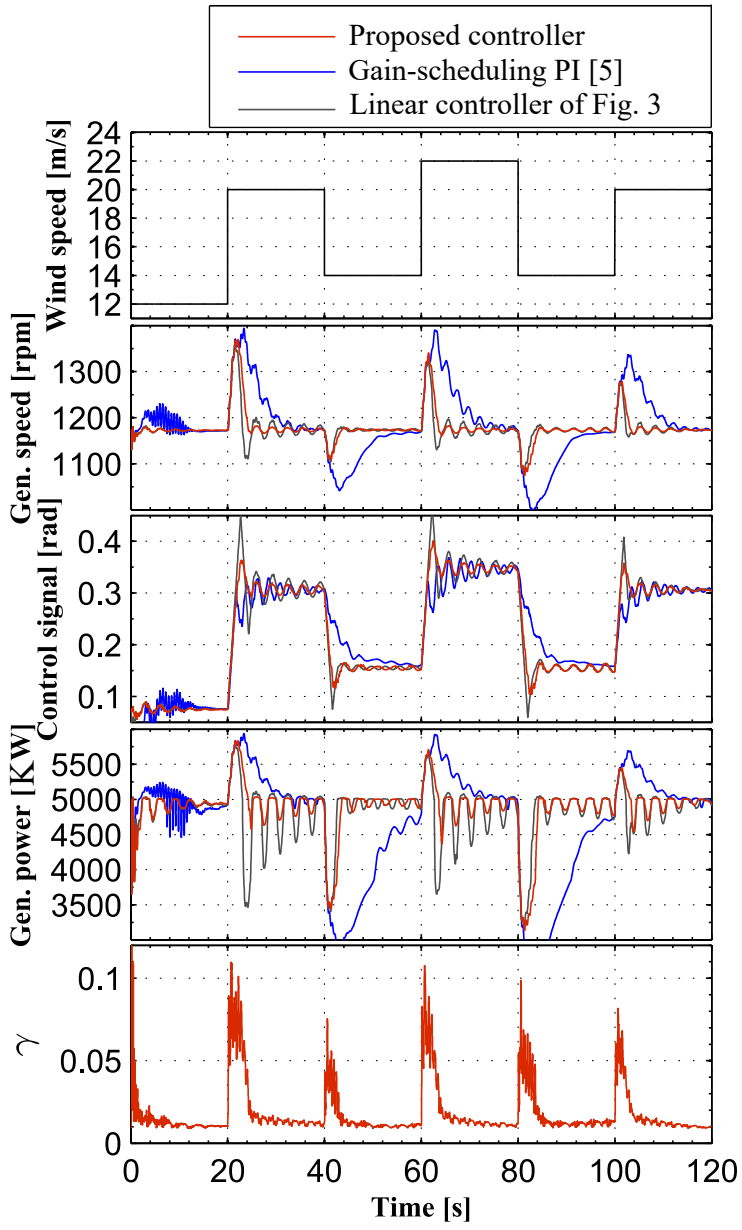

Figure 4.6: Simulation results of the proposed control scheme (red), a gain-scheduling PI controller (blue) [2], and a linear state-feedback controller (dark-gray), detailed in Fig 4.5, with a step-like wind speed profile.

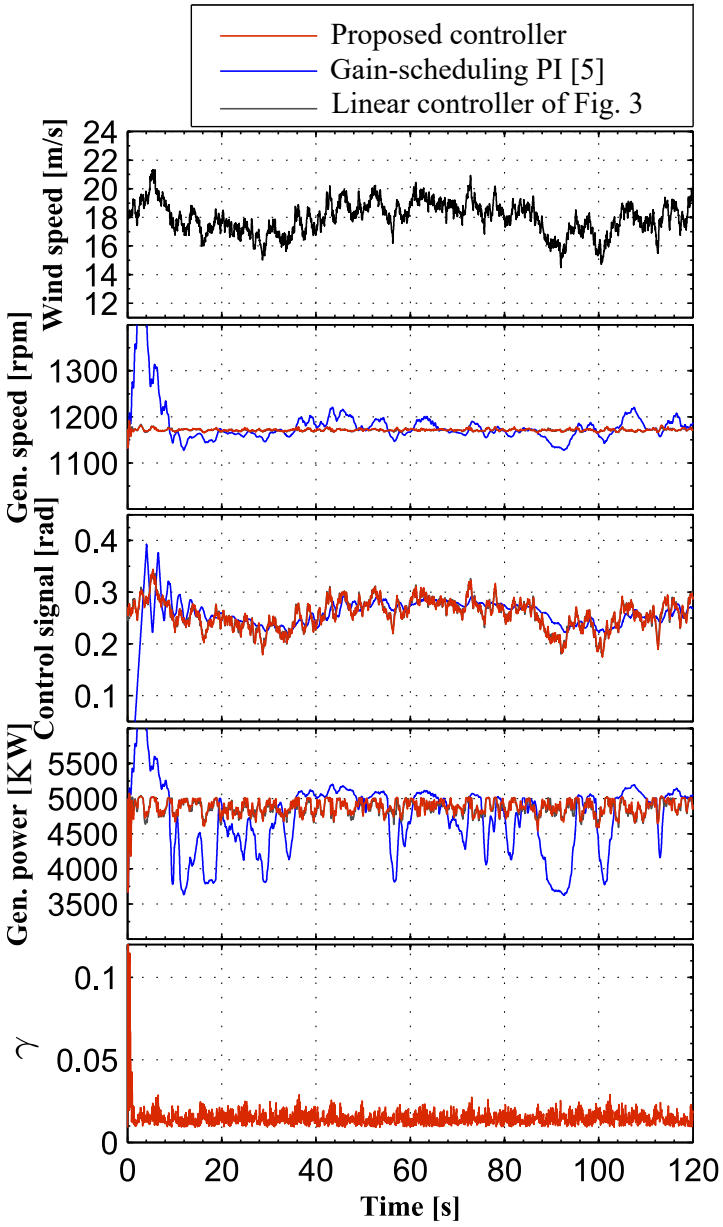

Figure 4.7: Simulation results of the proposed control scheme (red), a gain-scheduling PI controller (blue) [2], and a linear state-feedback controller (dark-gray), detailed in Fig 4.5, with a stochastic wind speed profile.

Table 4.3: Statistic analysis of the simulation results of Fig. 4.7.

		mean	std.
Proposed controller			
	Gen. Speed	1172	2.931
	Gen. Power	4879	112.7
Linear feedback controller			
	Gen. Speed	1171	3.01
	Gen. Power	4867	116.4

4.5 Summary

This chapter has proposed a new collective pitch controller to maintain the generator speed at its rated value in Region 3. The proposed controller, which is an extension of the controller proposed in Chapter 2, respects the limitations of the blade angles by producing control signal with a limited amplitude and a limited rate-of-change. The simulation results have shown that the proposed controller is robust against significant variations in wind speed. Extending the proposed controller for MIMO systems is highly needed in a future study to consider the mechanical fatigue loads [92] on the blades in addition to the regulation of the generator speed.

Chapter 5

Conclusion

5.1 Conclusion remarks

This dissertation has proposed a control technique for the system that has an amplitude- and rate-limitation on its input signal. Chapter 2 has proposed a sliding-mode like controller involving a state-dependent parameter, which influences the feedback gain. In this particular sliding-mode like structure, a higher gain results in a steeper slope of the switching surface, which further results in a smaller sliding patch on the sliding surface and a smaller finite-time attractor. Therefore, the nonlinear function $\gamma(\boldsymbol{x}, u)$ is designed so that the gain is low when the state is far from the origin to enlarge the region of attraction, and is high when the state is close to the origin to set the finite-time attractor smaller. In Chapter 2 also, the controller parameters are designed to place the closed loop eigenvalues in pre-specified locations inside a given region in the complex plane when the state-dependent parameter reaches its minimum. The parameters are also designed to maintain the eigenvalues inside the given complex-region along the different values of the nonlinear function $\gamma(\boldsymbol{x}, u)$.

Chapter 3 has proposed a new design procedure to select the controller parameters. This procedure has been divided into two stages; the first obtains the vector $\boldsymbol{c}$ using an iterative algorithm, which involves a set of LMIs. These LMIs are derived in the case where the state-dependent parameter comes to its minimum for which the asymptotic stability is guaranteed in the absence of disturbance. The second stage is designed to search for a maximum possible value of the upperbound γ_c to achieve low control action when the state goes far from the origin.

Chapter 4 represents a direct application to a real system, which needs an amplitude- and rate-saturated controller. The application system is a nonlinear wind turbine system and the purpose of controlling is to maintain the generated speed constant when the wind speed is above the rated wind speed. Because the controller in Chapter 2 is

mainly proposed considering a linear controlled plant, the linearized model of the wind turbine system was necessary to design the proposed controller in this chapter, and the utilized function $\gamma(\boldsymbol{x}, u)$ has been slightly modified to match with the linearized model. Finally, the controller is applied to a full nonlinear wind turbine plant emulated by a software simulator called "FAST" [87]. The advantage of the proposed controller has been shown by comparing it with another control method. The comparison shows that the proposed controller reduces the fluctuations' amplitude of the generated power, specially in the presence of high wind-speed variations. This reduction is expected to promote better generated-power quality and longer life-time for the mechanical parts of the wind turbine system.

5.2 Future Work

The controller proposed in this dissertation still needs further studies to obtain the controller parameters respecting a specific region of attraction. Moreover, the proposed design procedure of the controller parameters would not be the only method that could be used for the design of the controller. The selection of the controller parameters is an open problem according to the purpose of the design. The following are some of open problems, and suggestions regarding each one.

5.2.1 Stability proofs considering the effects of $\dot{\gamma}$

With the nonlinear function $\gamma(\boldsymbol{x}, u)$, the stability proofs in Section 2.3 do not strictly hold because it will inject additional terms proportional to $\dot{\gamma}$ to the derivatives of $V_s(s(\boldsymbol{\xi}))$ and $V_q(\boldsymbol{x})$. They are still valid if $\dot{\gamma}$ is small enough, although it is still unclear in what regions of the state space $|\dot{\gamma}|$ can be said to be small enough.

5.2.2 Estimating a specific region of attraction

The sliding mode-like controller proposed in Chapter 2 needs further study to estimate a set of initial states that could be attracted to the designed switching surface. On the same context, a future study should address extensions of the parameter designing procedure to choose the parameter values so that a given initial state is included in the region of attraction and so that a given size of the finite-time attractor is realized.

Regarding this open problem, the sliding mode condition (2.27) needs to hold true at an initial state $(\boldsymbol{x}_0, u_0)$. This implies that:

$$\gamma_c > \frac{|\boldsymbol{c}^T \boldsymbol{A}\boldsymbol{x}_0 + \boldsymbol{c}^T \boldsymbol{b} u_0 + \boldsymbol{c}^T \boldsymbol{b}\zeta|}{\beta}. \tag{5.1}$$

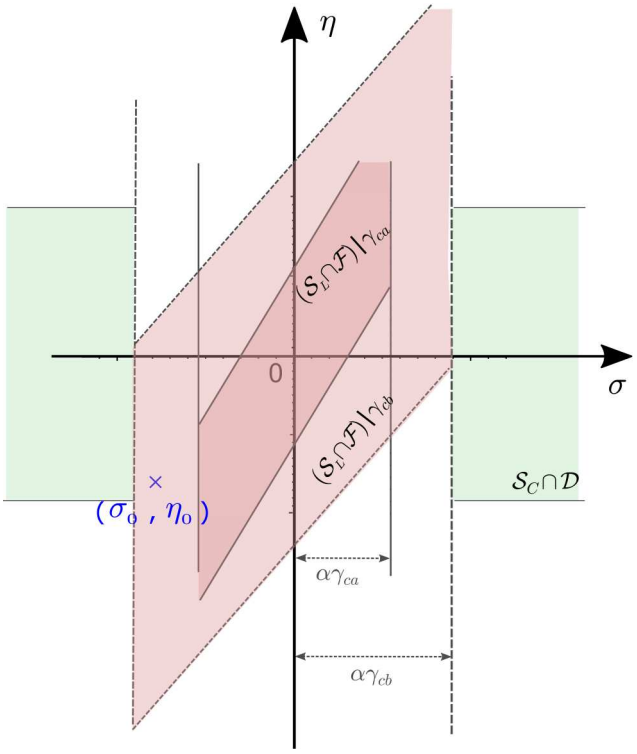

Figure 5.1: Different size of the region $\boldsymbol{\mathcal{S}}_L \cap \boldsymbol{\mathcal{F}}$ corresponding to different γ_c.

Considering the σ-η plane, one can say that the initial point (σ_0, η_0) needs to be inside the region $\boldsymbol{\mathcal{S}}_L \cap \boldsymbol{\mathcal{F}}$.

To obtain the controller parameters $\{\boldsymbol{c}, \gamma_c\}$ respecting the above condition, one possible idea is to use the design procedure of Chapter 3 to find the vector $\boldsymbol{c}$, and then, γ_c could be selected according to the condition (5.1). Fig 5.1 shows the influences of different values of γ_c to include a certain initial condition.

Another possible idea might be inspired from Method B of Sec. 3.2.3, in which the upperbound γ_c is obtained based on the matrices $\{\boldsymbol{E}_1, \boldsymbol{F}_1, \boldsymbol{E}_2, \boldsymbol{F}_2\}$, specifically, γ_c depends on the minimum real eigenvalues of $(\boldsymbol{F}_1\boldsymbol{E}_1^{-1})$ and $(\boldsymbol{F}_2\boldsymbol{E}_2^{-1})$. Because these matrices are functions of $\boldsymbol{c}$, we can develop a new selection method of $\boldsymbol{c}$ to result in $(\boldsymbol{F}_1\boldsymbol{E}_1^{-1})$ and $(\boldsymbol{F}_2\boldsymbol{E}_2^{-1})$ with real eigenvalues as large as possible.

5.2.3 Controller parameter tuning for already-stable plants

With a stable system in the open loop, a significant-low control action keeps the system near the stable open loop. One possible idea here might be setting the parameter γ_c to

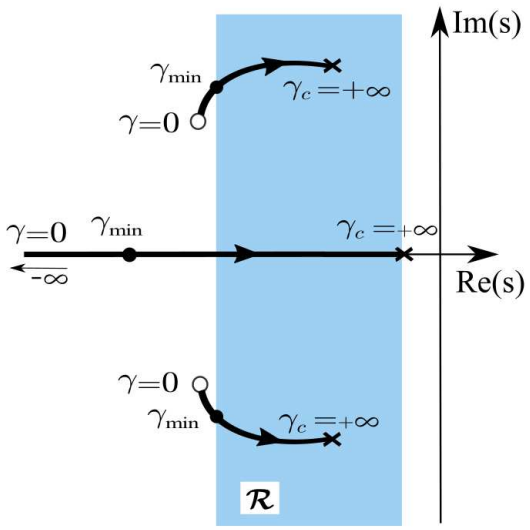

Figure 5.2: An example of the root locus of stable system and the working region $\mathcal{R}$.

be ∞, which is an ideal value for the upperbound of $\gamma(\boldsymbol{x}, u)$ to facilitate a wide region of attraction. In such a case, the selection procedure of the controller parameters will be started by setting $\gamma_c \equiv \infty$, and then, the other controller parameters $\boldsymbol{c}$ will be selected respecting a small size of the finite-time attractor. During the design of $\boldsymbol{c}$, we have to be sure from the system's stability along the changes in γ from ∞ to the designed $\gamma_m in$. This scenario is valid only when there is no conditions on the eigenvalues of the closed loop system when γ holds at γ_c.

5.2.4 Extension for MIMO systems

For multi-input multi-output (MIMO) systems, a MIMO controller is necessary to achieve multi control purposes. For example, the wind turbine system, discussed in Chapter 4, could need an individual pitch angle controller to overcome the fatigue loads on the blades [92]. In such a case, the controlled plant is MIMO systems, in which the measured moment of each blade is required to construct the controller. It would be beneficial to extend the controller proposed in Chapter 2 to be applied to MIMO systems. The selection procedure of the controller parameters in Chapter 3 can also be modified to be compatible with a MIMO version of the proposed controller of this dissertation.

Bibliography

[1] A. H. K. Palmeira, J. M. Gomes da Silva Jr, S. Tarbouriech, and I. M. F. Ghiggi, "Sampled-data control under magnitude and rate saturating actuators," *International Journal of Robust and Nonlinear Control*, vol. 26, no. 15, pp. 3232–3252, 2016.

[2] W. M. J. Jonkman, S. Butterfield and G. Scott, "Definition of a 5-MW reference wind turbine for offshore system development," *NREL, Golden, CO., USA, Tech. Rep.TP-500-38060*, 2009.

[3] V. Kapila and W. M. Haddad, "Fixed-structure controller design for systems with actuator amplitude and rate non-linearities," *International Journal of Control*, vol. 73, no. 6, pp. 520–530, 2000.

[4] R. A. Hess and S. A. Snell, "Flight control system design with rate saturating actuators," *Journal of Guidance, Control, and Dynamics*, vol. 20, no. 1, pp. 90–96, 1997.

[5] C. Fielding and P. K. Flux, "Non-linearities in flight control systems," *The Aeronautical Journal.*, vol. 107, no. 1077, pp. 673–696, 2003.

[6] J. Sofrony, M. C. Turner, I. Postlethwaite, O. Brieger, and D. Leibling, "Anti-windup synthesis for pio avoidance in an experimental aircraft," in *Proceedings of 45th IEEE Conference on Decision and Control*, 2006, pp. 5412–5417.

[7] D. Famularo, D. Martino, and M. Mattei, "Constrained control strategies to improve safety and comfort on aircraft," *Journal of Guidance Control and Dynamics*, vol. 31, no. 6, pp. 1782–1792, 2008.

[8] F. Garelli, P. Camocardi, and R. J. Mantz, "Variable structure strategy to avoid amplitude and rate saturation in pitch control of a wind turbine," *International Journal of Hydrogen Energy*, vol. 35, no. 11, pp. 5869–5875, 2010.

[9] C. Tutivén, Y. Vidal, L. Acho, and J. Rodellar, "Hysteresis-based design of dynamic reference trajectories to avoid saturation in controlled wind turbines," *Asian Journal of Control*, vol. 19, no. 2, pp. 438–449, 2017.

[10] Geng Tao and Zhao Jin, "Generalized predictive control with constraints for ship autopilot," in *Proceedings of 24th Chinese Control and Decision Conference*, 2012, pp. 1548–1551.

[11] Accident and serious incident reports: Loc. SKYbrary. [Online]. Available: www.skybrary.aero/index.php

[12] P. Dvorak. (2016, February 26) Extreme torsional loads damage more than wind turbine gearboxes. [Online]. Available: www.windpowerengineering.com/extreme-torsional-loads-damage-more-than-wind-turbine-gearboxes/

[13] A. Bateman and Z. Lin, "An analysis and design method for linear systems under nested saturation," *Systems & Control Letters*, vol. 48, no. 1, pp. 41–52, 2003.

[14] J. M. Gomes da Silva, S. Tarbouriech, and G. Garcia, "Local stabilization of linear systems under amplitude and rate saturating actuators," *IEEE Transactions on Automatic Control*, vol. 48, no. 5, pp. 842–847, 2003.

[15] A. A. Stoorvogel and A. Saberi, "Output regulation of linear plants with actuators subject to amplitude and rate constraints," *International Journal of Robust and Nonlinear Control*, vol. 9, no. 10, pp. 631–657, 1999.

[16] J. M. Gomes da Silva, D. Limon, T. Alamo, and E. F. Camacho, "Dynamic output feedback for discrete-time systems under amplitude and rate actuator constraints," *IEEE Transactions on Automatic Control*, vol. 53, no. 10, pp. 2367–2372, 2008.

[17] F. A. Bender and J. M. Gomes da Silva, "Output feedback controller design for systems with amplitude and rate control constraints," *Asian Journal of Control*, vol. 14, no. 4, pp. 1113–1117, 2012.

[18] V. Kapila, H. Pan, and M. S. de Queiroz, "LMI-based control of linear systems with actuator amplitude and rate nonlinearities," in *Proceedings of IEEE Conference on Decision and Control*, 1999, pp. 1413–1418.

[19] Z. Lin, "Semi-global stabilization of linear systems with position and rate-limited actuators," *Systems & Control Letters*, vol. 30, no. 1, pp. 1–11, 1997.

[20] S. Galeani, S. Onori, A. Teel, and L. Zaccarian, "A magnitude and rate saturation model and its use in the solution of a static anti-windup problem," *Systems & Control Letters*, vol. 57, no. 1, pp. 1–9, 2008.

[21] J. Macki and A. Strauss, *Introduction to Optimal Control Theory.* Springer, 1982.

[22] S. Tarbouriech, C. Prieur, and J. M. Gomes da Silva, "L_2 performance design problem for systems presenting nested saturations," in *Proceedings of 44th IEEE Conference on Decision and Control*, 2005, pp. 5000–5005.

[23] K. Zhou and J. C. Doyle, "Essentials of robust control," .: Printice Hall, 1997.

[24] W. Reinelt, "Design of optimal control systems with bounded control signals," in *Proceedings of European Control Conference*, Sep. 2001, pp. 348–353.

[25] P. Chen, S. Chen, and C. Hsu, "The H infinity optimal control of linear systems with actuators magnitude and rate saturation," in *Proceedings of Fourth International Conference on Innovative Computing, Information and Control*, 2009, pp. 561–564.

[26] C. Sendi and M. A. Ayoubi, "Robust-optimal fuzzy model-based control of flexible spacecraft with actuator amplitude and rate constraints," in *Proceedings of Dynamic Systems and Control Conference*, vol. 1, 10 2015.

[27] D. S. Bernstein and A. N. Michel, "A chronological bibliography on saturating actuators," *International Journal of Robust and Nonlinear Control*, vol. 5, no. 5, pp. 375–380, 1995.

[28] T. Hu, B. Huang, and Z. Lin, "Absolute stability with a generalized sector condition," *IEEE Transactions on Automatic Control*, vol. 49, no. 4, pp. 535–548, 2004.

[29] F. Forni, S. Galeani, and L. Zaccarian, "Model recovery anti-windup for continuous-time rate and magnitude saturated linear plants," *Automatica*, vol. 48, no. 8, pp. 1502 – 1513, 2012.

[30] M. S. Reineh, S. S. Kia, and F. Jabbari, "Anti-windup designs for systems with amplitude and rate bounded actuators," *IFAC-PapersOnLine*, vol. 50, no. 1, pp. 11 509–11 514, 2017.

[31] C. Barbu, R. Reginatto, A. R. Teel, and L. Zaccarian, "Anti-windup for exponentially unstable linear systems with inputs limited in magnitude and rate," in *Proceedings of American Control Conference*, vol. 2, June 2000, pp. 1230–1234.

[32] H. Michalska and D. Q. Mayne, "Robust receding horizon control of constrained nonlinear systems," *IEEE Transactions on Automatic Control*, vol. 38, no. 11, pp. 1623–1633, 1993.

[33] F. Findeisen and F. Allgower, "An introduction to nonlinear model predictive control," in *Proceedings of 21st Benelux Meeting on Systems and Control, Veldhoven*, 2002.

[34] W. H. Kwon and S. Han, *Receding Horizon Controll: model predictive control for state models*. Springer, London, 2005.

[35] V. Kapila and S. Valluri, "Model predictive control of systems with actuator amplitude and rate saturation," in *Proceedings of 37th IEEE Conference on Decision and Control*, vol. 2, 1998, pp. 1396–1401.

[36] A. Lasheen and A. L. Elshafei, "Wind-turbine collective-pitch control via a fuzzy predictive algorithm," *Renewable Energy*, vol. 87, pp. 298 – 306, 2016.

[37] L. L. Giovanini, "Model predictive control with amplitude and rate actuator saturation," *ISA Transactions*, vol. 42, no. 2, pp. 227 – 240, 2003.

[38] A. Sabanovic, "Variable structure systems with sliding modes in motion control-a survey," *IEEE Transactions on Industrial Informatics*, vol. 7, no. 2, pp. 212–223, 2011.

[39] V. I. Utkin, *Sliding Modes in Control and Optimization*. Berlin, Germany: Springer-Verlag, 1992.

[40] B. Bandyopadhyay et al., *Advances in Sliding Mode Control: Design of Sliding Mode Controller with Actuator Saturation*. Lecture Notes in Control and Information Sciences, Springer, Berlin, Heidelberg, 2013, vol. 440.

[41] H. J. Sussmann, E. D. Sontag, and Y. Yang, "A general result on the stabilization of linear systems using bounded controls," in *Proceedings of 32nd IEEE Conference on Decision and Control*, vol. 2, 1993, pp. 1802–1807.

[42] C.-C. Hsu and I.-K. Fong, "Robust state feedback control through actuators with generalized sector nonlinearities and saturation," *Asian Journal of Control*, vol. 5, no. 3, pp. 382–389, 2003.

[43] Z. Lin and A. Saberi, "Semi-global exponential stabilization of linear discrete-time systems subject to input saturation via linear feedbacks," *Systems & Control Letters*, vol. 24, no. 2, pp. 125 – 132, 1995.

[44] Z. Lin, A. A. Stoorvogel, and A. Saberi, "Output regulation for linear systems subject to input saturation," *Automatica*, vol. 32, no. 1, pp. 29 – 47, 1996.

[45] A. R. Teel, "Semi-global stabilizability of linear null controllable systems with input nonlinearities," *IEEE Transactions on Automatic Control*, vol. 40, no. 1, pp. 96–100, 1995.

[46] K. Kefferpüz, B. Fischer, and J. Adamy, "A nonlinear controller for input amplitude and rate constrained linear systems," *IEEE Transactions on Automatic Control*, vol. 58, no. 10, pp. 2693–2697, 2013.

[47] F. A. Miranda-Villatoro, F. Castaños, and B. Brogliato, "A set-valued nested sliding-mode controller," *International Federation of Automatic Control*, vol. 50, no. 1, pp. 2971–2976, 2017.

[48] A. Nemirovski, J. Alan, Laub., M. Chilali., and P. Gahinet., "LMI control toolbox user's guide." 1995.

[49] N. Baiomy and R. Kikuuwe, "An amplitude- and rate-saturated controller for linear systems," *Asian Journal of Control*, vol. 21, no. 6, p. , 2019.

[50] H. K. Khalil, *Nonlinear Systems*, 3rd ed. Upper Saddle River: Prentice Hall, 2002.

[51] K.-K. Young, P. Kokotovic, and V. Utkin, "A singular perturbation analysis of high-gain feedback systems," *IEEE Transactions on Automatic Control*, vol. 22, no. 6, pp. 931–938, 1977.

[52] V. Utkin and Hoon Lee, "Chattering problem in sliding mode control systems," in *Proceedings of International Workshop on Variable Structure Systems*, 2006, pp. 346–350.

[53] H. Lee and V. I. Utkin, "Chattering suppression methods in sliding mode control systems," *Annual Reviews in Control*, vol. 31, no. 2, pp. 179 – 188, 2007.

[54] V. Acary and B. Brogliato, "Implicit euler numerical scheme and chattering-free implementation of sliding mode systems," *Systems & Control Letters*, vol. 59, no. 5, pp. 284–293, 2010.

[55] O. Huber, V. Acary, and B. Brogliato, "Lyapunov stability and performance analysis of the implicit discrete sliding mode control," *IEEE Transactions on Automatic Control*, vol. 61, no. 10, pp. 3016–3030, 2016.

[56] R. Kikuuwe, S. Yasukouchi, H. Fujimoto, and M. Yamamoto, "Proxy-based sliding mode control: A safer extension of PID position control," *IEEE Transactions on Robotics*, vol. 26, no. 4, pp. 670–683, 2010.

[57] N. Baiomy and R. Kikuuwe, "Parameter selection procedure for an amplitude- and rate-saturated controller," *International Journal of Control, Automation and Systems*, vol. 17, no. 4, pp. 926–935, 2019.

[58] J. Wilkinson, *The Algebraic Eigenvalue Problem*. Oxford University Press, 1965.

[59] A. Pandey, R. Schmid, T. Nguyen, Y. Yang, V. Sima, and A. L. Tits, "Performance survey of robust pole placement methods," in *Proceedings of 53rd IEEE Conference on Decision and Control*, 2014, pp. 3186–3191.

[60] Y. Li, J. L. Wang, and G.-H. Yang, "Sub-optimal linear quadratic control for singularly perturbed systems," in *Proceedings of 40th IEEE Conference on Decision and Control*, vol. 4, 2001, pp. 3698–3703.

[61] Y. Li, J. L. Wang, and G.-H. Yang, "Linear quadratic control for singularly perturbed systems," *Dynamics of Continuous, Discrete and Impulsive Systems Series B: Applications and Algorithms*, vol. 12, no. 1, pp. 29–39, 2005.

[62] S. Boyd, L. El Ghaoui, E. Feron, and V. Balakrishnan, *Linear Matrix Inequalities in System and Control Theory*. SIAM, Philadelphia, 1994.

[63] M. Chilali and P. Gahinet, "H_∞ design with pole placement constraints: an LMI approach," *IEEE Transactions on Automatic Control*, vol. 41, no. 3, pp. 358–367, 1996.

[64] M. Chilali, P. Gahinet, and P. Apkarian, "Robust pole placement in LMI regions," *IEEE Transactions on Automatic Control*, vol. 44, no. 12, pp. 2257–2270, 1999.

[65] A. Fuller, "Conditions for a matrix to have only characteristic roots with negative real parts," *Journal of Mathematical Analysis and Applications*, vol. 23, no. 1, pp. 71–98, 1968.

[66] M. Tobias, *Matrices in Engineering Problems*, S. L. Steven G. Krantz, Washington University, Ed. Morgan & Claypool, 2011.

[67] S. Sen and K. Datta, "Stability bounds of singularity perturbed systems," *IEEE Transactions on Automatic Control*, vol. 38, no. 2, pp. 302–304, 1993.

[68] N. Baiomy and Ryo Kikuuwe, "An LMI-based parameter selection procedure for an amplitude- and rate-saturated controller," in *Proceedings of SICE International Symposium on Control Systems*, 2018, pp. 54–60.

[69] E. C. Navarrete, M. Trejo Perea, J. C. Jáuregui Correa, R. V. Carrillo Serrano, and G. J. R. Moreno, "Expert control systems implemented in a pitch control of wind turbine: a review," *IEEE Access*, vol. 7, pp. 13 241–13 259, 2019.

[70] N. J. T. Burton, D. Sharpe and E. Bossanyi, *The Controller, in Wind Energy Handbook*. John Wiley & Sons, 2001, ch. 8, sec. 8.3, p. 484.

[71] V. Court, "Energy capture, technological change, and economic growth: An evolutionary perspective," *BioPhysical Economics and Resource Quality*, vol. 3, pp. 1–27, 2018.

[72] N. Lior, "Energy resources and use: The present situation and possible paths to the future," *Energy*, vol. 33, no. 6, pp. 842 – 857, 2008.

[73] L. Y. Pao and K. E. Johnson, "Control of wind turbines," *IEEE Control Systems Magazine*, vol. 31, no. 2, pp. 44–62, 2011.

[74] W. E. Leithead and B. Connor, "Control of variable speed wind turbines: Design task," *International Journal of Control*, vol. 73, no. 13, pp. 1189–1212, 2000.

[75] J. G. Njiri and D. Söffker, "State-of-the-art in wind turbine control: Trends and challenges," *Renewable and Sustainable Energy Reviews*, vol. 60, pp. 77–393, 2016.

[76] E. Muljadi and C. P. Butterfield, "Pitch-controlled variable-speed wind turbine generation," *IEEE Transactions on Industry Applications*, vol. 37, no. 1, pp. 240–246, 2001.

[77] D. C. Vega, J. A. Marin, and R. T. Sánchez, "Pitch angle controllers design for a horizontal axis wind turbine," in *Proceedings of IEEE International Autumn Meeting on Power, Electronics and Computing*, 2015, pp. 1–6.

[78] H. Takaai, Y. Chida, K. Sakurai, and T. Isobe, "Pitch angle control of wind turbine generator using less conservative robust control," pp. 542–547, July 2009.

[79] C. D. Johnson, "Theory of disturbance-accommodating controllers," *Control and Dynamic Systems*, vol. 12, pp. 387–489, 1976.

[80] M. Balas, Y. Lee, and L. Kendall, "Disturbance tracking control theory with application to horizontal axis wind turbines," *American Institute of Aeronautics and Astronautics*, pp. 95–99, Jan. 1998.

[81] I. P. Girsang and J. S. Dhupia, "Collective pitch control of wind turbines using stochastic disturbance accommodating control," *Wind Energy*, vol. 37, no. 5, pp. 517–534, Oct. 2013.

[82] S. H. Lee, Y. J. Joo, J. Back, and J. H. Seo, "Sliding mode controller for torque and pitch control of wind power system based on PMSG," in *Proceedings of International Conference on Control, Automation and Systems*, Oct 2010, pp. 1079–1084.

[83] B. Beltran, T. Ahmed-Ali, and M. E. H. Benbouzid, "Sliding mode power control of variable-speed wind energy conversion systems," *IEEE Transactions on Energy Conversion*, vol. 23, no. 2, pp. 551–558, June 2008.

[84] H. De Battista, R. J. Mantz, and C. F. Christiansen, "Dynamical sliding mode power control of wind driven induction generators," *Power Engineering Society Summer Meeting, Seattle, WA, USA*, July 2000.

[85] B. Beltran, T. Ahmed-Ali, and M. E. H. Benbouzid, "High-order sliding-mode control of variable-speed wind turbines," *IEEE Transactions on Industrial Electronics*, vol. 56, no. 9, pp. 3314–3321, Sep. 2009.

[86] L. Colombo, M. Corradini, G. Ippoliti, and G. Orlando, "Pitch angle control of a wind turbine operating above the rated wind speed: A sliding mode control approach," *ISA Transactions*, 2019.

[87] J. M. Jonkman and M. L. Buhl, Jr., "FAST user's guide," National Renewable Energy Laboratory, Tech. Rep. NREL/EL-500-38230, 2005.

[88] H. Hassan, A. ElShafei, W. Farag, and M. Saad, "A robust lmi-based pitch controller for large wind turbines," *Renewable Energy*, vol. 44, pp. 63–71, 2012.

[89] L. G. W. Chen, J. Yang and S. Li, "Disturbance-observer-based control and related methods−an overview," *IEEE Transactions on Industrial Electronics*, vol. 63, no. 2, pp. 1083–1095, Feb. 2016.

[90] C. D. Johnson, "Optimal control of the linear regulator with constant disturbances," *IEEE Transactions on Automatic Control*, vol. 13, no. 4, pp. 416–421, Aug. 1968.

[91] K. T. Magar, M. Balas, S. Frost, and N. Li, "Adaptive state feedback-theory and application for wind turbine control," *Energies*, vol. 10, no. 12, pp. 1–15, Dec. 2017.

[92] E. A. Bossanyi, "Wind turbine control for load reduction," *Wind Energy*, vol. 6, no. 3, pp. 229–244, 2003.

[93] Creative commons. [Online]. Available: https://creativecommons.org/licenses/

Appendix A

FAST files

A.1 Linearization file

The linearized model of the wind turbine system is obtained via FAST [87] after carrying out some steps as follows;

- Inside a file called "primary" file, we adjust FAST task to linearization, and we enable the desired DOFs.
- Other flags in the "primary" file such as PCMode, YCMode, GenTiStr, GenTiStp, TimGenOn, THSSBrDp, TiDynBrk, TTpBrDpi, TYawManS, TPitManSi and TBDepISpi, must be adjusted as described in the guide manual of FAST [87].
- The wind profile in a file with extension " .hh" must be steady.

Now, after setting the aforementioned steps, we run "FAST.exe" directly or via the "Command Prompt" to trace errors, which could be happened during the execution of the linearization process. The generated file that contains the linearization data has an extension ".lin", and it appears as follows:

This linearized model file was generated by FAST (v7.00.00a-bjj, 31-Mar-2010) on 03-Apr-2019 at 13:15:28.
The aerodynamic calculations were made by AeroDyn (v13.00.00a-bjj, 31-Mar-2010).

NREL 5.0 MW Baseline Wind Turbine for Use in Offshore Analysis.

Some Useful Information:

Type of steady state solution found Trimmed collective blade pitch (TrimCase = 3)
Azimuth-average rotor speed, RotSpeed (rad/s) 1.26711E+00
Period of steady state solution (sec) 4.95868E+00
Iterations needed to find steady state solution 39
Displacement 2-norm of steady state solution (rad) 9.60374E-03
Velocity 2-norm of steady state solution (rad/s) 1.81437E-04
Number of equally-speced azimuth steps, NAzimStep 12
Order of linearized model, MdlOrder 1
Number of active (enabled) DOFs 2 (4 states)
Number of control inputs, NInputs 1
Number of input wind disturbances, NDisturbs 1
Number of output measurements 1

Order of States in Linearized State Matrices:

Row/column 1 = Variable speed generator DOF (internal DOF index = DOF_GeAz)
Row/column 2 = Drivetrain rotational-flexibility DOF (internal DOF index = DOF_DrTr)
Row/column 3 to 4 = First derivatives of row/column 1 to 2.

Order of Control Inputs in Linearized State Matrices:

Column 1 = rotor collective blade pitch (rad) 2.62362E-01 op

Order of Input Wind Disturbances in Linearized State Matrices:

Column 1 = horizontal hub-height wind speed (m/s) 0.00000E+00 op*

Order of Output Measurements in Linearized State Matrices:

Row 1 = HSShftV (rpm)

Linearized State Matrices:

* This value is not the practical value of the wind speed. Although it is printed by zero, the exact value is supported in the file of the wind profile.

```
------- Azimuth =   0.00 deg (with respect to AzimB1Up =   0.00 deg) ---------
op State   | op        | A - State                          | B - Input  | Bd - Dstrb
Derivativs | States    | Matrix                             | Matrix     | Matrix
 1.265E+00 |  4.708E+00 |  0.000E+00  0.000E+00  1.000E+00  0.000E+00 |  0.000E+00 |  0.000E+00
 6.442E-06 |  4.740E-03 |  0.000E+00  0.000E+00  0.000E+00  1.000E+00 |  0.000E+00 |  0.000E+00
 2.039E-04 |  1.265E+00 | -1.251E-09  1.726E+02 -2.731E+00  1.237E+00 |  6.045E-08 |  2.183E-10
-2.017E-05 |  6.442E-06 |  1.927E-05 -1.950E+02  2.453E+00 -1.675E+00 | -1.338E+00 |  3.107E-02

op Output  | This colmn | C - Output                         | D - Trnsmt | Dd - DTsmt
Measurmnts | is blank   | Matrix                             | Matrix     | Matrix
 1.172E+03 |            |  0.000E+00  0.000E+00  9.263E+02  0.000E+00 |  0.000E+00 |  0.000E+00

--------- Azimuth =  30.00 deg (with respect to AzimB1Up =   0.00 deg) ---------
op State   | op        | A - State                          | B - Input  | Bd - Dstrb
Derivativs | States    | Matrix                             | Matrix     | Matrix
 1.265E+00 |  5.231E+00 |  0.000E+00  0.000E+00  1.000E+00  0.000E+00 |  0.000E+00 |  0.000E+00
-3.390E-06 |  4.742E-03 |  0.000E+00  0.000E+00  0.000E+00  1.000E+00 |  0.000E+00 |  0.000E+00
 5.571E-05 |  1.265E+00 | -5.211E-11  1.726E+02 -2.730E+00  1.237E+00 |  6.826E-08 | -1.122E-08
-7.076E-05 | -3.390E-06 | -8.605E-04 -1.950E+02  2.455E+00 -1.672E+00 | -1.322E+00 |  3.078E-02

op Output  | This colmn | C - Output                         | D - Trnsmt | Dd - DTsmt
Measurmnts | is blank   | Matrix                             | Matrix     | Matrix
 1.172E+03 |            |  0.000E+00  0.000E+00  9.263E+02  0.000E+00 |  0.000E+00 |  0.000E+00


--------- Azimuth =  60.00 deg (with respect to AzimB1Up =   0.00 deg) ---------
op State   | op        | A - State                          | B - Input  | Bd - Dstrb
Derivativs | States    | Matrix                             | Matrix     | Matrix
 1.265E+00 |  5.755E+00 |  0.000E+00  0.000E+00  1.000E+00  0.000E+00 |  0.000E+00 |  0.000E+00
-1.441E-05 |  4.736E-03 |  0.000E+00  0.000E+00  0.000E+00  1.000E+00 |  0.000E+00 |  0.000E+00
-3.386E-04 |  1.265E+00 | -4.169E-10  1.726E+02 -2.731E+00  1.237E+00 |  5.586E-07 |  3.347E-09
 3.939E-05 | -1.441E-05 | -4.160E-05 -1.950E+02  2.457E+00 -1.671E+00 | -1.324E+00 |  3.076E-02

op Output  | This colmn | C - Output                         | D - Trnsmt | Dd - DTsmt
Measurmnts | is blank   | Matrix                             | Matrix     | Matrix
 1.172E+03 |            |  0.000E+00  0.000E+00  9.263E+02  0.000E+00 |  0.000E+00 |  0.000E+00


-------- Azimuth =  90.00 deg (with respect to AzimB1Up =   0.00 deg) ---------
op State   | op        | A - State                          | B - Input  | Bd - Dstrb
Derivativs | States    | Matrix                             | Matrix     | Matrix
 1.265E+00 |  6.278E+00 |  0.000E+00  0.000E+00  1.000E+00  0.000E+00 |  0.000E+00 |  0.000E+00
 1.061E-05 |  4.735E-03 |  0.000E+00  0.000E+00  0.000E+00  1.000E+00 |  0.000E+00 |  0.000E+00
 8.335E-05 |  1.265E+00 |  1.042E-10  1.726E+02 -2.732E+00  1.237E+00 | -4.794E-08 | -2.219E-09
 3.684E-05 |  1.061E-05 |  8.544E-04 -1.950E+02  2.457E+00 -1.672E+00 | -1.322E+00 |  3.077E-02

op Output  | This colmn | C - Output                         | D - Trnsmt | Dd - DTsmt
Measurmnts | is blank   | Matrix                             | Matrix     | Matrix
 1.172E+03 |            |  0.000E+00  0.000E+00  9.263E+02  0.000E+00 |  0.000E+00 |  0.000E+00


--------- Azimuth = 120.00 deg (with respect to AzimB1Up =   0.00 deg) ---------
op State   | op        | A - State                          | B - Input  | Bd - Dstrb
Derivativs | States    | Matrix                             | Matrix     | Matrix
 1.265E+00 |  5.189E-01 |  0.000E+00  0.000E+00  1.000E+00  0.000E+00 |  0.000E+00 |  0.000E+00
 6.484E-06 |  4.740E-03 |  0.000E+00  0.000E+00  0.000E+00  1.000E+00 |  0.000E+00 |  0.000E+00
 2.040E-04 |  1.265E+00 |  6.253E-10  1.726E+02 -2.731E+00  1.237E+00 | -5.086E-07 | -9.240E-09
-1.857E-05 |  6.484E-06 |  1.963E-05 -1.950E+02  2.453E+00 -1.675E+00 | -1.338E+00 |  3.107E-02

op Output  | This colmn | C - Output                         | D - Trnsmt | Dd - DTsmt
Measurmnts | is blank   | Matrix                             | Matrix     | Matrix
 1.172E+03 |            |  0.000E+00  0.000E+00  9.263E+02  0.000E+00 |  0.000E+00 |  0.000E+00


--------- Azimuth = 150.00 deg (with respect to AzimB1Up =   0.00 deg) ---------
op State   | op        | A - State                          | B - Input  | Bd - Dstrb
Derivativs | States    | Matrix                             | Matrix     | Matrix
 1.265E+00 |  1.042E+00 |  0.000E+00  0.000E+00  1.000E+00  0.000E+00 |  0.000E+00 |  0.000E+00
-3.322E-06 |  4.742E-03 |  0.000E+00  0.000E+00  0.000E+00  1.000E+00 |  0.000E+00 |  0.000E+00
 5.561E-05 |  1.265E+00 |  5.211E-11  1.726E+02 -2.730E+00  1.237E+00 |  2.835E-07 | -6.130E-09
-7.763E-05 | -3.322E-06 | -8.610E-04 -1.950E+02  2.455E+00 -1.672E+00 | -1.322E+00 |  3.078E-02

op Output  | This colmn | C - Output                         | D - Trnsmt | Dd - DTsmt
Measurmnts | is blank   | Matrix                             | Matrix     | Matrix
 1.172E+03 |            |  0.000E+00  0.000E+00  9.263E+02  0.000E+00 |  0.000E+00 |  0.000E+00
```

```
--------- Azimuth = 180.00 deg (with respect to AzimB1Up =   0.00 deg) ---------
op State   | op        | A - State                          | B - Input  | Bd - Dstrb
Derivativs | States    | Matrix                             | Matrix     | Matrix
 1.265E+00 |  1.566E+00 |  0.000E+00  0.000E+00  1.000E+00  0.000E+00 |  0.000E+00 |  0.000E+00
-1.432E-05 |  4.736E-03 |  0.000E+00  0.000E+00  0.000E+00  1.000E+00 |  0.000E+00 |  0.000E+00
-3.385E-04 |  1.265E+00 | -1.251E-09  1.726E+02 -2.731E+00  1.237E+00 | -2.876E-07 |  3.201E-09
 3.927E-05 | -1.432E-05 | -4.199E-05 -1.950E+02  2.457E+00 -1.671E+00 | -1.324E+00 |  3.076E-02

op Output  | This colmn | C - Output                         | D - Trnsmt | Dd - DTsmt
Measurmnts | is blank   | Matrix                             | Matrix     | Matrix
 1.172E+03 |            |  0.000E+00  0.000E+00  9.263E+02  0.000E+00 |  0.000E+00 |  0.000E+00


--------- Azimuth = 210.00 deg (with respect to AzimB1Up =   0.00 deg) ---------
op State   | op        | A - State                          | B - Input  | Bd - Dstrb
Derivativs | States    | Matrix                             | Matrix     | Matrix
 1.265E+00 |  2.090E+00 |  0.000E+00  0.000E+00  1.000E+00  0.000E+00 |  0.000E+00 |  0.000E+00
 1.057E-05 |  4.735E-03 |  0.000E+00  0.000E+00  0.000E+00  1.000E+00 |  0.000E+00 |  0.000E+00
 8.286E-05 |  1.265E+00 | -3.127E-10  1.726E+02 -2.732E+00  1.237E+00 | -2.647E-07 |  1.048E-08
 3.929E-05 |  1.057E-05 |  8.541E-04 -1.950E+02  2.457E+00 -1.672E+00 | -1.322E+00 |  3.077E-02

op Output  | This colmn | C - Output                         | D - Trnsmt | Dd - DTsmt
Measurmnts | is blank   | Matrix                             | Matrix     | Matrix
 1.172E+03 |            |  0.000E+00  0.000E+00  9.263E+02  0.000E+00 |  0.000E+00 |  0.000E+00


--------- Azimuth = 240.00 deg (with respect to AzimB1Up =   0.00 deg) ---------
op State   | op        | A - State                          | B - Input  | Bd - Dstrb
Derivativs | States    | Matrix                             | Matrix     | Matrix
 1.265E+00 |  2.613E+00 |  0.000E+00  0.000E+00  1.000E+00  0.000E+00 |  0.000E+00 |  0.000E+00
 6.530E-06 |  4.740E-03 |  0.000E+00  0.000E+00  0.000E+00  1.000E+00 |  0.000E+00 |  0.000E+00
 2.052E-04 |  1.265E+00 |  0.000E+00  1.726E+02 -2.731E+00  1.237E+00 |  4.148E-07 |  7.276E-11
-1.969E-05 |  6.530E-06 |  1.876E-05 -1.950E+02  2.453E+00 -1.675E+00 | -1.338E+00 |  3.107E-02

op Output  | This colmn | C - Output                         | D - Trnsmt | Dd - DTsmt
Measurmnts | is blank   | Matrix                             | Matrix     | Matrix
 1.172E+03 |            |  0.000E+00  0.000E+00  9.263E+02  0.000E+00 |  0.000E+00 |  0.000E+00


--------- Azimuth = 270.00 deg (with respect to AzimB1Up =   0.00 deg) ---------
op State   | op        | A - State                          | B - Input  | Bd - Dstrb
Derivativs | States    | Matrix                             | Matrix     | Matrix
 1.265E+00 |  3.137E+00 |  0.000E+00  0.000E+00  1.000E+00  0.000E+00 |  0.000E+00 |  0.000E+00
-3.294E-06 |  4.742E-03 |  0.000E+00  0.000E+00  0.000E+00  1.000E+00 |  0.000E+00 |  0.000E+00
 5.572E-05 |  1.265E+00 |  2.606E-10  1.726E+02 -2.730E+00  1.237E+00 |  7.921E-08 | -3.329E-09
-6.630E-05 | -3.294E-06 | -8.609E-04 -1.950E+02  2.455E+00 -1.672E+00 | -1.322E+00 |  3.078E-02

op Output  | This colmn | C - Output                         | D - Trnsmt | Dd - DTsmt
Measurmnts | is blank   | Matrix                             | Matrix     | Matrix
 1.172E+03 |            |  0.000E+00  0.000E+00  9.263E+02  0.000E+00 |  0.000E+00 |  0.000E+00


--------- Azimuth = 300.00 deg (with respect to AzimB1Up =   0.00 deg) ---------
op State   | op        | A - State                          | B - Input  | Bd - Dstrb
Derivativs | States    | Matrix                             | Matrix     | Matrix
 1.265E+00 |  3.660E+00 |  0.000E+00  0.000E+00  1.000E+00  0.000E+00 |  0.000E+00 |  0.000E+00
-1.434E-05 |  4.736E-03 |  0.000E+00  0.000E+00  0.000E+00  1.000E+00 |  0.000E+00 |  0.000E+00
-3.385E-04 |  1.265E+00 |  0.000E+00  1.726E+02 -2.731E+00  1.237E+00 | -9.171E-08 | -3.201E-09
 3.963E-05 | -1.434E-05 | -4.208E-05 -1.950E+02  2.457E+00 -1.671E+00 | -1.324E+00 |  3.076E-02

op Output  | This colmn | C - Output                         | D - Trnsmt | Dd - DTsmt
Measurmnts | is blank   | Matrix                             | Matrix     | Matrix
 1.172E+03 |            |  0.000E+00  0.000E+00  9.263E+02  0.000E+00 |  0.000E+00 |  0.000E+00


--------- Azimuth = 330.00 deg (with respect to AzimB1Up =   0.00 deg) ---------
op State   | op        | A - State                          | B - Input  | Bd - Dstrb
Derivativs | States    | Matrix                             | Matrix     | Matrix
 1.265E+00 |  4.184E+00 |  0.000E+00  0.000E+00  1.000E+00  0.000E+00 |  0.000E+00 |  0.000E+00
 1.061E-05 |  4.735E-03 |  0.000E+00  0.000E+00  0.000E+00  1.000E+00 |  0.000E+00 |  0.000E+00
 8.321E-05 |  1.265E+00 | -3.127E-10  1.726E+02 -2.732E+00  1.237E+00 |  3.106E-07 | -3.347E-09
 2.942E-05 |  1.061E-05 |  8.541E-04 -1.950E+02  2.457E+00 -1.672E+00 | -1.322E+00 |  3.077E-02

op Output  | This colmn | C - Output                         | D - Trnsmt | Dd - DTsmt
Measurmnts | is blank   | Matrix                             | Matrix     | Matrix
 1.172E+03 |            |  0.000E+00  0.000E+00  9.263E+02  0.000E+00 |  0.000E+00 |  0.000E+00
```

Appendix B

MATLAB codes

The following is an example of the implementation of the discrete-time controller proposed in this thesis.

```
%%%system dynamics in Continuous time %%%
%% Example_1%%
A=[0 -.5;1 1.5]; B=[0;-1];C=[1 -1];L=0.125;gamma_c=1/3.62;
x( :,2)= [0.0;0.4]; u(1)=0;beta=2.5;alpha=1;

 %-----------------------------------------------------
[n,n]=size(A);                  % system order
h=.01 ;                         % time step
T=8;                            % simulation time
k=T/h ;                         % time index
t=0;                            % initial time

%%%%%%%%  SGN-SAT CONTROLLER IN DISCRET TIME %%%%%%%%%%
%-----------------------------------------------------
for k=2:1:(T/h);
t=t+h  ;
Z(k)=z*sin(1*t);
% ---------------------- gamma-law --------------
J=(abs(C*A*x(:,k))+abs(C*B*u(k-1))+C*B*L)/beta;
gamma(k)=min(gamma_c,J);

%------------------------ Internal Sat ------------------------
w(k)= (C*(eye(n,n)+h*A)*x(:,k));              % sigma(k-1)+CAhx(k-1)
w_star(k)=w(k)/((gamma(k)+C*B*h));         % (\frac{w_{k-1}}{\alpha ( \gamma_k  + C Bh)})
    if  w_star(k) > alpha ;
      M(k)= -alpha;
    elseif  w_star(k) < -alpha;
      M(k)=  alpha;
    else
      M(k)=-1*w_star(k);
    end

%--------------------  External Sat function ----------------------
   if (u(k-1)-M(k))/(beta*h)<-1;
       u(k)=u(k-1)-(h*beta)*(-1);
   elseif (u(k-1)-M(k))/(beta*h)>1;
       u(k)=u(k-1)-(h*beta);
   else
       u(k)=u(k-1)-(u(k-1)-M(k)) ;
   end

%----------------  (The discrete time representation of the system)  -------------
-------------Calculation of A_dis & B_dis -----------
g1=0;
   for i=0:150
   N=((A^i)*(h^(i+1)))/factorial(i+1);
   g1=g1+N;
   end
   B_dis=g1*B
   A_dis= expm(A*h)
-----------------------
x(: ,k+1)= A_dis*x(: ,k) + B_dis*(u(k)+Z(k));      % system in discrete form
end
```

Appendix C

Copyright permissions

C.1 Copyright permission for Chapter 2

The content of Chapter 2 is partially published in [49], namely, N. Baiomy, R. Kikuuwe. An amplitude- and rate-saturated controller for linear systems. Asian Journal of Control, vol. 21, no. 6, 2019. This paper is under the "OnlineOpen" license, and by contacting Copyright Clearance Center, it is founded that paper mentioned above is under the terms of the Creative Commons Attribution License (CC BY) [93], which permits use, distribution and reproduction in any medium, provided that the Contribution is properly cited. Due to this, permission is not required to reuse the content from the paper [49] in this doctoral dissertation.

C.2 Copyright permission for Chapter 3

The content of Chapter 3 is partially published in [57], namely, N. Baiomy and R. Kikuuwe. Parameter selection procedure for an amplitude- and rate-saturated controller. International Journal of Control, Automation and Systems, vol. 17, no. 4, pp. 926-935, 2019. By contacting Copyright Clearance Center, it is founded that the reuse of the material [57] in the author's Ph.D. dissertation is granted. However, the author has to cite the published paper in his dissertation.

Request for reuse permission

journal@ijcas.com <journal@ijcas.com> Fri, Nov 15, 2019 at 10:50 AM
To: "Nehal M.Khames" <eng.nehal90@gmail.com>
Cc: "제어로봇시스템학회(ICROS)" <icros@icros.org>

Dear Mr. Nehal Baiomy,

We have received your email below.

We would like to inform you that the reuse of the material in your Ph.D. dissertat on is granted.

However, you have to cite the published paper in your dissertat on.

Thank you for your inquiry and if you have further quest on, please send us an email.

Best regards,

Kaeun Choi

IJCAS Secretariat

Internat onal Journal of Control, Automat on, and Systems (IJCAS) Secretariat
Suseo Hyundai-Ventureville 723, Bamgogae-ro 1-gil 10
Gangnam-gu, Seoul 06349, Korea
Tel: +82-2-6949-5806 Fax: +82-2-6949-5807
Homepage: http://www.ijcas.com E-mail: journal@ijcas.com

From: Nehal M.Khames <eng.nehal90@gmail.com>
Sent: Wednesday, November 13, 2019 11:35 AM
To: IJCAS <journal@ijcas.com>
Subject: Request for reuse permission

Dear Mr./Ms.

This is Nehal Baiomy on of authors who published a paper named ``Parameter Selection Procedure for an Amplitude- and Rate-saturated Controller" in International Journal of Control, Automation and Systems under the following Doi: 10.1007/s12555-018-0450-x, cited as

``Baiomy, N. & Kikuuwe, R. Int. J. Control Autom. Syst. (2019) 17: 926. https://doi.org/10.1007/s12555-018-0450-x"

I am writing regarding my request to reuse any part or all of the aforementioned paper in my doctoral dissertation entitled ``A Sliding Mode-Based Amplitude- and Rate-Saturated Controller and Its Application to Wind Turbine Systems" to be published by Kyushu University, Japan.

I would appreciate sending me permission regarding my above request.

Best Regards,

Nehal

Nehal M. Khames M. Baiomy

Doctoral student

Department of Mechanical Engineering

Faculty of Engineering

Kyushu University, Japan

Tel: +8180-4277-4991